FFI-rapport 2008/02329

Comparison of sound propagation codes: Milstøy, BNoise and a PE-method

Michelle Swearingen, Morten Huseby and Reza Rahimi

Norwegian Defence Research Establishment (FFI)

25 February 2009

FFI-rapport 2008/02329

3533

P: ISBN 978-82-464-1529-1
E: ISBN 978-82-464-1530-7

Keywords

måling

støy

beregning

C4

detonasjon

Approved by

Jan Ivar Botnan Director

Summary

Ranges for military training must ensure that noise reaching neighbors is kept at an acceptable level. In Norway, strict noise limits are set by the authorities. To comply with these regulations, the Norwegian Defence and the Norwegian Defence Estates Agency needs accurate tools for calculating the noise propagation from noisy activity out to the neighbors of the training field.

The goal of the study documented in this report was to compare four different prediction methods to an experimental data set, and see which method provided the most accurate results. The prediction methods, in order of complexity, were:

1. Industry Noise (IN) model in Milstøy (current Norwegian standard method)
2. Nord2000road (N2R), a "quick" ray-tracing kernel included in Milstøy and currently under investigation as a possible upgrade
3. Fast Field Program (FFP) as implemented in the US noise assessment software, BNoise
4. Generalized Terrain Parabolic Equation (GT-PE), a research model utilizing the parabolic equation approximation to the acoustic wave equation.

The predictions were compared to selected data from the Nortrial data set, with the specific data physically recorded at Finnskogen, Norway.

In the US, noise maps for large weapons are made with BNoise. BNoise is a tool with the same functionality as Milstøy. With regards to the basic assumptions, the propagation model in BNoise seems to be more advanced than both IN and N2R (in Milstøy). One difference between MS and BNoise is that BNoise pre-calculates noise propagation and stores it in lookup tables, while MS performs “instantaneous” calculations.

The PE method can handle horizontal range-dependence, allowing the inclusion of terrain and horizontally-varying meteorology and ground type. Refinements of the PE are frequently addressed at professional conferences and the PE is generally considered state of the art. This report describes experiences with a recent implementation of the PE method to predict military shooting noise.

Choosing between FFP and PE it seems that the advantage with the FFP is that it is proven to work, and is in use. Typically more advanced models seem to have a tendency to become unstable for realistic conditions. The PE could have computational advantages, and be

more oriented towards the future due to its higher degree of flexibility. To be able to make a decision about which direction to take, we here try to evaluate some properties of the different computational methods.

The results of the study are not conclusive, but much was learned. One of the propagation conditions in BNoise consistently gave the best results, but other propagation conditions in that method were no better than any other method. The GTPE gave reasonable results in many cases, but the choice of which propagation condition parameters provide the best results, i.e. included terrain and type of meteorological profile used, varied from case to case. Both the IN and N2R methods did not perform as well and had a strong tendency to overpredict the received noise levels.

This report provides details on the data set used, overviews of each of the computational methods, and results of all trials. Further analysis is needed to determine which method best serves the needs of the Norwegian Defence.

Sammendrag

Nær skytefelt er Forsvaret ansvarlig for å overholde støygrensene som er satt av SFT. Forsvarsbygg trenger derfor nøyaktige beregningsverktøy for å kunne beregne støyutbredelsen ut til naboene.

Målet med denne rapporten er å sammenligne fire forskjellige beregningsmetoder for utbredelse av støy

1. Industristøy metoden (IN) i Milstøy (den nåværende norske standardmetoden)
2. Nord2000road (N2R), en "rask" ray-tracing kjerne inkludert i Milstøy, under uttesting
3. Fast Field Program (FFP) som implementert i US noise assessment software, BNoise
4. Generalized Terrain Parabolic Equation (GT-PE), en forskningsmodell

I USA lages støykart med BNoise, som har samme funksjonalitet som Milstøy. En forskjell er at BNoise forhåndskalkulerer transmisjonstap, mens Milstøy beregner støyutbredelsen “instantant”.

Når man skal velge mellom FFP og PE har FFP den fordelen at den er operativ og beviselig har en god ytelse. PE har en del ekstra fordeler, og er mer orientert mot fremtiden, men er ikke garantert å virke. For å kunne gjøre et valg har vi forsøkt å evaluere noen egenskaper ved disse metodene.

Det blir ikke trukket noen endelig konklusjon i denne rapporten. Likevel har vi lært mye om egenskapene til de forskjellige metodene. For en type utbredelsesbetingelser ga BNoise best resultater. For andre betingelser var BNoise ikke bedre enn de andre metodene. Både IN og N2R viste relativt dårligere ytelse, og hadde en sterk tendens til å overpredikere støynivået.

Denne rapporten gir detaljer om datasettet som ble benyttet, oversikt over beregningsmetodene og resultater for alle målingene. Mer forskning er nødvendig for å kunne avgjøre hvilken metode som best vil oppfylle behovene til Forsvaret.

Contents

1 Introduction

One of the authors, Michelle Swearingen, wrote this report during her one year stay (2008) as a visting scientist at FFI. Her stay was part of the ESEP-program (US Army Engineer & Scientist Exchange Program). January 2009 Swearingen returned to her work at ERDC-CERL (US Army Engineer Research and Development Center - Construction Engineering Research Laboratory).

Ranges for military training must ensure that noise reaching neighbors is kept at an acceptable level. In Norway strict noise limits are set by the authorities, e.g. for heavy guns and detonations L_{CE} must be below 95 dB at the neighbors (100 dB if less than 100 shots a year exceeds 90 dB). To comply with these regulations, the Norwegian Defence needs accurate tools for calculating the noise propagation from noisy activity out to the neighbors of the training field.

The Norwegian Defence Estates Agency (FB) is responsible for building training ranges and communicating with the environmental authorities. At present FB uses the program Milstøy (MS) to do area planing connected to noise and as an aid when controlling noisy activity.

The calculations in MS, as currently used by FB, are made by the "industry noise" (IN) computational kernel, which is a fairly simple semi-empirical formulation that does not take weather data as input. An obvious evolution is to look for a computational kernel that is more accurate. We then have many options. Four of these are:

1. "Quick" ray-tracing
2. Ray-tracing
3. FFP (Fast Field Program)
4. PE (Parabolic Equation)

These four options are listed by their computational speed, PE being the slowest. All of these methods are slower than the IN-method.

The term "quick" ray-tracing refers to what is implemented in the Nord2000road (N2R) computational kernel (in MS)[1, 2]. N2R takes the weather into account, and is a much more complicated method than IN. The performance of N2R compared to IN and measured

data has been evaluated for detonations of C4 explosives over realistic terrain [3, 4, 5]. At present N2R has not been tested enough to validate a significant performance improvement over IN for realistic conditions. An overview of the performance of newly developed modules in MS is described in [6].

There exist several codes from other fields that use ray-tracing. Swedish Defence Research Agency has produced such a method and applied it to some introductory testing [7]. Ray-tracing relies on the infinitesimal wavelength, infinite frequency assumption. Much of the energy in military noise, e.g. for artillery and detonation of large amounts of explosives, is low frequency, with frequencies on the order of 5-50 Hz. Because of this, empirical corrections to the ray tracing are frequently required.

In the US, noise maps for large weapons are made with BNoise [8]. BNoise is a tool with the same functionality as MS. It was made many years ago at ERDC-CERL, with a major update in the late 1990's. With regards to the basic assumptions, the propagation model in BNoise seems to be more advanced than both MS and N2R (in MS). One difference between MS and BNoise is that BNoise pre-calculates noise propagation and stores it in lookup tables, while MS performs "instantaneous" calculations.

In BNoise, an FFP method calculates the sound propagation in horizontal homogeneous layers of the atmosphere. This full-wave method can accurately model low frequencies. However, it assumes a medium that does not vary with range. Therefore, terrain and horizontally-dependent microclimates and ground types cannot be addressed.

In the PE method the sound propagation is calculated by solving a parabolic equation using an assumption that neglects sound waves with a large elevation angle. This full-wave method can also accurately model low frequencies. In addition, it can handle horizontal range-dependence, allowing the inclusion of terrain and horizontally-varying meteorology and ground type. Refinements of the PE are frequently addressed at professional conferences and the PE is generally considered state of the art. Systems that apply continuous weather data in PE-systems for calculating noise from weapons (and traffic) are reported to be undergoing development by several groups. At present the authors have not seen evidence of the existence of stable operating versions of such a system for realistic conditions. This report describes experiences with a recent implementation of the PE method to predict military shooting noise.

Choosing between FFP and PE it seems that the advantage with the FFP is that it is proven to work, and is in use. Typically more advanced models seem to have a tendency to become unstable for realistic conditions, i.e. non-idealized terrain, temperature and wind conditions. The PE could have computational advantages, and be more oriented towards

the future due to its higher degree of flexibility. The downside is that it is not guaranteed to work. To be able to make a decision about which direction to take, we here try to evaluate some properties of the different computational methods.

We test four codes against full scale field measurements of detonations of C4 explosives at Finnskogen in Norway.

2 Description of the measurements

In 1994 a large set of full scale measurements of detonation of C4 explosives was conducted at Finnskogen in Norway. The database containing the measurements is called NORTRIAL, is implemented in the Matlab environment, and comes with supporting functions to aid in data extraction, manipulation and processing. The existence of NORTRIAL and its public availability was announced at [9]. The database can be obtained by contacting NGI (Norwegian Geotechnical institute) from http://nortrial.ngi.no. An example the functionality of NORTRIAL is given in [3].

We selected measurements along the north-south axis. It is between 1 and 8 km between source and sensor. We only consider detonations with $L_{\mathrm{CE}} > 75$ dB. In this report sound pressure level (L_{CE}) is the indicator used to describe the loudness of the noise. Before we continue we will go through some basic expressions for sound exposure level.

2.1 Sound exposure level

Sound exposure level (L_{E}) indicates the noise level relative to the reference pressure $p_0 = 2 \cdot 10^{-5}$Pa, and can be defined as [10]

$$L_{\mathrm{E}} = 10 \log \left(\frac{1}{T_0 p_0^2} \int_0^{\tau} p(t)^2 \, dt \right) = 10 \log \left(\frac{\tau}{T_0 p_0^2} \sum_{n=0}^{N-1} p_n^2 \right), \tag{2.1}$$

where $T_0 = 1$s, p_n are the (N) samples of the pressure and τ is the sampling period. In the frequency domain this may be expressed

$$L_{\mathrm{E}} = 10 \log \left(\frac{\tau}{T_0 p_0^2 N} \sum_{n=0}^{N-1} |P_n|^2 \right), \tag{2.2}$$

where a FFT (Fast Fourier Transform) may give you

$$P_k = \sum_{n=0}^{N-1} p_n e^{-j(2\pi/N)kn}. \tag{2.3}$$

Assuming that all energy is captured inside L number of 1/3-octave bands [11],

$$L_{\mathrm{E}} = 10 \log \left(\frac{1}{T_0 p_0^2} \sum_{l=1}^{L} SE_l \right) = 10 \log \left(\frac{2\tau^2}{T_0 p_0^2} \sum_{l=1}^{L} \int_{f_1^{(l)}}^{f_2^{(l)}} |P(\omega)|^2 \, df \right), \tag{2.4}$$

where SE_l is the sound exposure of band number l, the edge frequencies [12] of band l is given by $f_1^{(l)}$ and $f_2^{(l)}$ and $\omega = 2\pi f$. The Fourier transform (discrete time, continuous frequency) is defined by

$$P(\omega) = \sum_{n=-\infty}^{\infty} p_n e^{-j\omega n}. \tag{2.5}$$

If we are going to use a FFT it is useful to note that $|P_k| = |P(\omega_k)|$, where $\omega_k = k\omega_0$ and $\omega_0 = 2\pi/N$. Some choice of interpolation may give us $P(\omega)$ between the points $w = w_k$. When L_{E}-spectrum is calculated a C-weighting [10] is applied to arrive at the L_{CE}-spectrum.

2.2 Measurements

During the measurements at Finnskogen, we had microphones at positions 0 and 306, and detonations at 101, 302, 304 and 308. It is approximately 2 km between 304 and 306.

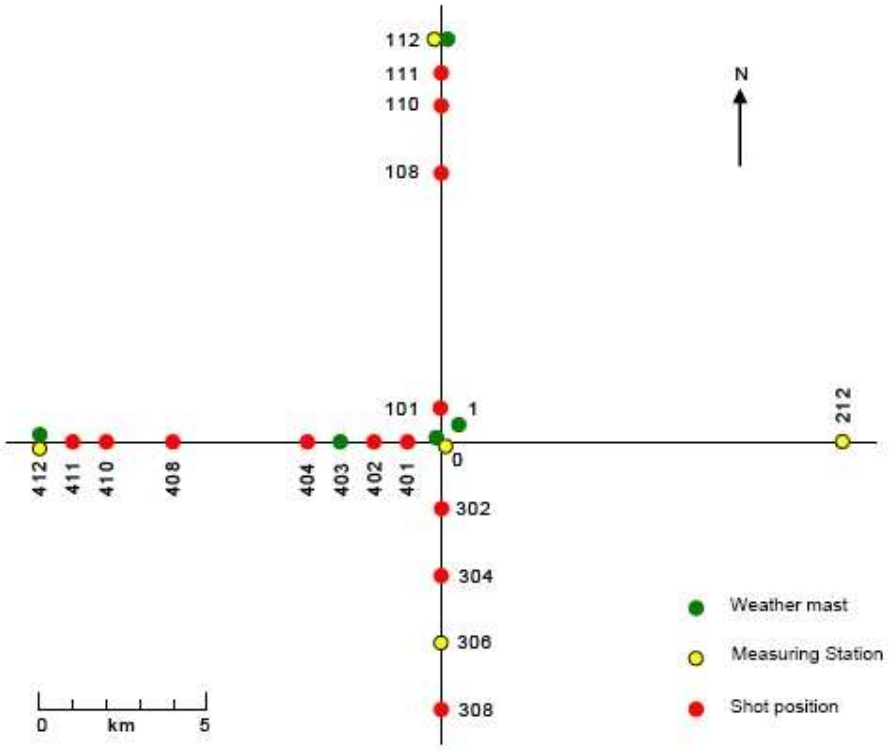

Figure 2.1: Layout of the measurement area.

2.3 Timeseries of the pressure

In Table 2.1 we list the 44 timeseries. A 'fileno' is the unique number of a detonation. The timeseries was measured at two measurement masts, at position 0 and 306. Thus, we may get two timeseries from one detonation. This set of timeseries will be referred to as C3 (Case 3) in the following text. Earlier C1 and C2 was defined in [3, 5]. In all of this set of 44 timeseries, the source and receiver heights are each 2 m above the ground.

Fileno	Met-data	Source		Sensor 306	Sensor 0	Date	Time
		Pos	Weight [kg]	L_{CE} [dB]	L_{CE} [dB]		
63	63	302	1		92.0	13-Sep-1994	14:00:00
69	69	302	1		90.9	13-Sep-1994	14:53:00
70	69	304	1	83.8	83.2	13-Sep-1994	14:56:00
75	69	302	1		89.3	13-Sep-1994	15:23:00
76	69	304	1	87.8	80.6	13-Sep-1994	15:26:00
81	81	302	8		88.3	14-Sep-1994	09:22:00
87	87	302	8		93.6	14-Sep-1994	10:12:00
93	93	302	8		92.5	14-Sep-1994	10:52:00
135	135	302	1	79.8		16-Sep-1994	13:22:00
136	135	304	1	89.9		16-Sep-1994	13:25:00
142	142	101	1		98.9	19-Sep-1994	10:58:59
144	142	304	1	85.9		19-Sep-1994	11:04:59
148	142	101	1		97.7	19-Sep-1994	11:51:59
154	142	101	1		99.7	19-Sep-1994	12:21:59
161	161	302	1	85.8	92.7	21-Sep-1994	07:17:00
167	167	302	1	84.2	80.1	21-Sep-1994	08:11:59
168	167	304	1	100.1	83.6	21-Sep-1994	08:15:00
172	172	101	1	76.6		21-Sep-1994	08:53:59
173	172	302	1	88.5	85.1	21-Sep-1994	08:56:59
174	172	304	1	97.2		21-Sep-1994	09:00:00
178	178	101	1	77.7	102.9	21-Sep-1994	09:53:59
179	178	302	1		93.0	21-Sep-1994	09:56:59
180	178	304	1	87.3		21-Sep-1994	10:00:00
184	184	308	1	80.6		21-Sep-1994	13:28:59
185	184	308	8	92.1	78.3	21-Sep-1994	13:31:59
186	184	308	64	96.1	86.2	21-Sep-1994	13:34:59
190	184	308	1	80.3		21-Sep-1994	14:08:59
191	184	308	8	92.3	80.3	21-Sep-1994	14:11:59
192	184	308	64	96.8	88.8	21-Sep-1994	14:14:59
196	184	308	1	86.0		21-Sep-1994	14:51:59
197	184	308	8	97.7	81.7	21-Sep-1994	14:54:59
198	184	308	64		88.8	21-Sep-1994	14:57:59

Table 2.1: Overview of all 44 measurements for 32 shots (fileno), which share 12 sets of meteorology data.

2.4 Meteorological data

The meteorological data is from a tethersonde going up and down about every 25 min. As we see in Table 2.1 several detonations share the same met-data. There are 12 met-profiles. The met-profiles are truncated at 290 m for consistency. The figures in Appendix A include measurements (blue lines) and linear fits (red lines) for temperature, wind speed, wind direction, and effective wind speed. The lines are linear fits to obtain the Milstøy parameters in Table 2.2. The effective wind speed equals measured wind speed times the cosine of the angle between the propagation direction and the wind vector.

2.5 Terrain

In Figure 2.2 we have plotted the terrain profile from source to sensor for the different combinations of source and sensor positions.

2.6 Milstøy-parameters

We have compiled some parameters for use in MS, as seen in Table 2.2. These parameters can also be found in the Figures in Appendix A.

Fileno	A	B	Wind	Wind dir	Wind gradient
	°C	°C/100 m	m/s	degrees	m/s/(100 m)
63	10.20	-0.91	0.99	94	1.30
69	9.68	-0.72	3.85	89	0.66
81	9.43	-0.81	0.54	30	2.39
87	9.74	-0.91	1.86	44	1.66
93	9.89	-0.80	2.43	54	1.91
135	7.05	-0.81	3.67	46	2.91
142	4.78	-0.26	0.13	143	1.40
161	-3.28	2.98	0.61	21	0.41
167	-1.79	2.47	0.92	359	0.73
172	-0.91	2.35	0.58	59	1.38
178	0.28	1.45	0.06	3	1.15
184	11.22	-1.00	2.58	305	-0.30

Table 2.2: Met-data for the 12 different meteorology conditions. Here 0 degrees means that the wind is coming from the north. A and B are parameters used by Milstøy. A is the temperature at 10 m above ground. B is the temperature gradient per 100 m.

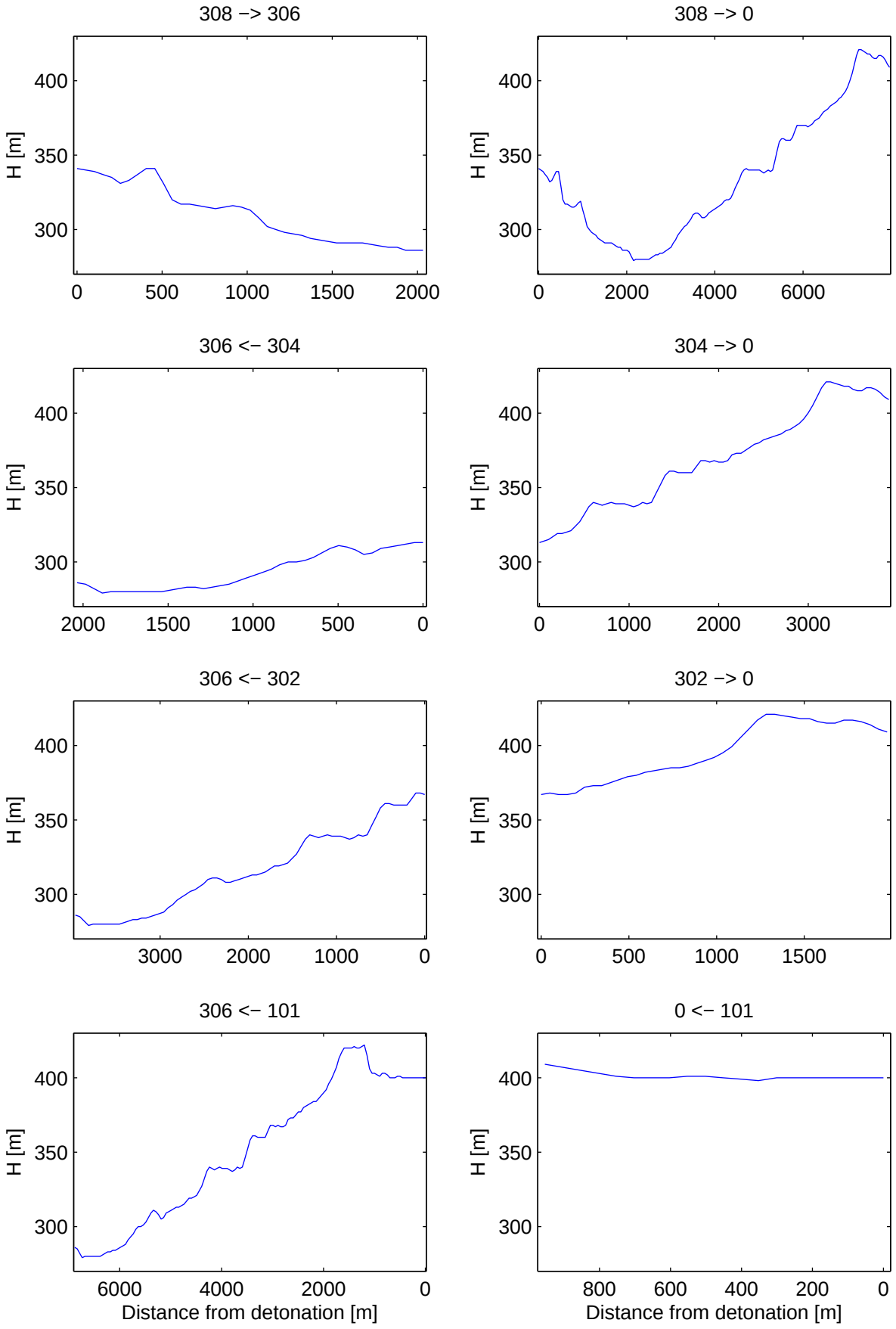

Figure 2.2: Ground profile (height above sea level) from source to receiver.

3 Milstøy results

A Milstøy (version 2.4) database has been developed for case 3 (C3). The corresponding coordinates of the detonation sources and the measurement points are used in the terrain file. The meteorological data in table 2.2 is considered for each event, based on the date and time for that event. Both prediction methods, Industry Noise and Nord2000Road (N2R), have been used for the calculations. The frequency interval for both methods is 12.5 Hz-10 kHz. All noise levels are L_{1s-C} in dB (here equivalent to L_{CE}). Milstøy prediction results and the measurements are summarized in Table 3.1.

Fileno	Met-data	Source		Sensor 306			Sensor 0		
		Pos	Weight [kg]	Measur.	IN	N2R	Measur.	IN	N2R
63	63	302	1				92.0	94.6	87.9
69	69	302	1				90.9	94.6	87.8
70	69	304	1	83.8	98.8	96.6	83.2	87.6	79.2
75	69	302	1				89.3	94.6	87.8
76	69	304	1	87.8	101.8	99.6	80.6	87.6	82.2
81	81	302	8				88.3	100.7	92.3
87	87	302	8				93.6	100.7	93.5
93	93	302	8				92.5	100.7	93.4
135	135	302	1	79.8	94.1	91.7			
136	135	304	1	89.9	98.8	103.4			
142	142	101	1				98.9	107.4	103.4
144	142	304	1	85.9	98.8	96.6			
148	142	101	1				97.7	104.7	103.4
154	142	101	1				99.7	104.7	103.4
161	161	302	1	85.8	94.0	89.8	92.7	94.6	89.9
167	167	302	1	84.2	94.0	89.8	80.1	94.6	94.0
168	167	304	1	100.1	98.8	103.6	83.6	87.5	83.4
172	172	101	1	76.6	91.6	84.0			
173	172	302	1	88.5	94.0	91.4	85.1	94.6	89.7
174	172	304	1	97.2	98.8	104.7			
178	178	101	1	77.7	91.6	83.9	102.9	104.6	104.4
179	178	302	1				93.0	94.6	89.3
180	178	304	1	87.3	98.8	101.6			
184	184	308	1	80.6	98.4	94.3			
185	184	308	8	92.1	104.5	98.9	78.3	91.4	74.1
186	184	308	64	96.1	110.0	104.9	86.2	96.8	80.1
190	184	308	1	80.3	98.4	94.3			
191	184	308	8	92.3	104.5	98.9	80.3	91.4	74.1
192	184	308	64	96.8	110.0	104.9	88.8	96.8	80.1
196	184	308	1	86.0	98.4	94.3			
197	184	308	8	97.7	104.5	98.9	81.7	91.4	74.1
198	184	308	64				88.8	96.8	80.1

Table 3.1: Comparing Milstøy prediction methods, Industry Noise (IN) and Nord2000Road (N2R), with the measurements for 32 shots (fileno). All the values are L_{CE} in dB.

4 BNoise

BNoise is a blast noise prediction model developed by USACERL. It has been in existence since the 1970's, and received a major overhaul in the late 1990's. The current version utilizes transfer function matrices to predict 1/3-octave band propagation through different meteorological classes. These transfer function matrices are pre-calculated using an FFP algorithm. A user chooses the appropriate installation map, firing and target locations, number of shots and the percentage of day and night shots, the noise source and munition type (where applicable), and a weather condition. The weather conditions are rather basic, but cover average categorical meteorological conditions. Most cases assume propagation over a grass-like surface, although there are also options for vegetation and desert, which are based on ANSI S12.17. The algorithm can calculate propagation over water and land-water interfaces when a land-water map is specified. BNoise also has the ability to calculate terrain effects. However, terrain maps require a very specific format and are difficult to create. Therefore, the decision was made not to include terrain in the BNoise runs. BNoise has two operating modes, one that creates noise maps and the other that gives more detailed information on a point to point propagation. The latter operating mode is called OneShot. OneShot provides the results for the specified parameter set (source and receiver location, source type, meteorological condition, desired frequency weighting) as a table of mean value, $\pm\sigma$ and $\pm 2\sigma$, where σ is the standard deviation.

4.1 Comparisons

BNoise comparisons were performed using the OneShot function. OneShot does not take terrain into account. For each propagation distance, the appropriate charge weight of C4 was used for each of the possible weather profile cases in BNoise. Values for CSEL and peak were recorded in a spreadsheet. Mean values and mean $\pm n\sigma$ are all recorded. For comparison purposes, only the mean $+1\sigma$ values were actually considered. This value was chosen because it is the value used in US noise assessments.

4.2 BNoise outputs

Interestingly, the "ANSI Mixed Vegetation" propagation condition, taken at $+1\sigma$ above the mean gives reasonably good results for almost all of the data, see Table 4.1. Choosing other propagation conditions based on inadequate knowledge of the profiles used in BNoise and a determination of the general propagation condition based on the Nortrial meteorology profiles results in poorer results. The "ANSI Mixed Vegetation" is based on data taken in

the 1987 Ft. Leonardwood trials, and subsequently incorporated into ANSI S12.17. Data were only recorded in overall levels (SEL, CSEL, peak). Since no spectral information is available, the attenuation values are applied equally to all frequency bands to attain the correct overall CSEL. It is interesting that this propagation condition provides the best fit to the Finnskogen data. It is possible that the choice of using only levels that exceed 75 dB influences the match to $+1\sigma$ above the mean. Examining other data would be interesting, but beyond the scope of this comparative study.

Fileno	Met-data	Source		Sensor 306		Sensor 0	
		Pos	Weight [kg]	Measur.	BNoise	Measur.	BNoise
63	63	302	1			92.0	91.0
69	69	302	1			90.9	91.0
70	69	304	1	83.8	90.5	83.2	83.0
75	69	302	1			89.3	91.0
76	69	304	1	87.8	90.5	80.6	83.0
81	81	302	8			88.3	98.0
87	87	302	8			93.6	98.0
93	93	302	8			92.5	98.0
135	135	302	1	79.8	82.5		
136	135	304	1	89.9	90.5		
142	142	101	1			98.9	100.0
144	142	304	1	85.9	90.5		
148	142	101	1			97.7	100.0
154	142	101	1			99.7	100.0
161	161	302	1	85.8	82.5	92.7	91.0
167	167	302	1	84.2	82.5	80.1	91.0
168	167	304	1	100.1	90.5	83.6	83.0
172	172	101	1	76.6	76.0		
173	172	302	1	88.5	82.5	85.1	91.0
174	172	304	1	97.2	90.5		
178	178	101	1	77.7	76.0	102.9	100.0
179	178	302	1			93.0	91.0
180	178	304	1	87.3	90.5		
184	184	308	1	80.6	90.5		
185	184	308	8	92.1	98.0	78.3	81.5
186	184	308	64	96.1	104.5	86.2	88.0
190	184	308	1	80.3	90.5		
191	184	308	8	92.3	98.0	80.3	81.5
192	184	308	64	96.8	104.5	88.8	88.0
196	184	308	1	86.0	90.5		
197	184	308	8	97.7	98.0	81.7	81.5
198	184	308	64			88.8	88.0

Table 4.1: Comparing BNoise output using the ANSI Mixed Vegetation profile at $mean+1\sigma$ setting with the measurements for 32 shots (fileno). All the values are L_{CE} in dB.

5 PE

Here we describe the how the PE-method is implemented. We then analyze the comparison between the simulations and measurements from the Finnskogen data (C3).

The data from Finnskogen is given as timeseries of the pressure. This is transformed to 1/3-octave band spectra for comparison with the PE-method (Section 2.1). A function provided with the Nortrial database was used for these calculations.

The basis for the evaluation is that we know L_{CE} both close to the source and several km away. We can then evaluate the performance of the PE-code against this known transmission loss.

5.1 Simulation method

The simulation method used is a Crank-Nicholson Parabolic Equation method, following the Generalized Terrain method by Sack and West (GT-PE) [13]. This method utilizes the first and second derivatives of the height function to perform a coordinate transformation into the terrain-following coordinates. The number and spacing of vertical grid points remains static throughout the horizontal range. This method differs from one that rotates the coordinate system to follow a slope, and eliminates the need for approximating the field each time the slope changes. In the simulations for this project, terrain is modeled as piecewise linear segments with the specified slope, rather than as a continuously varying function of distance. This approximation significantly reduces the computation time, since the propagation matrix only has to be changed at fixed distances instead of at each range step. The approximation has been shown to be as accurate as the continuously varying function [14]. Additionally, the terrain information is only available in segmented format in the Nortrial database, and so any continuous function would also be an approximation.

For completeness, the derivation and nomenclature of the GT-PE method are shown here. The description follows Salomons [15] and Sack and West [13].

The derivation of the parabolic equation starts with the two-dimensional Helmholtz equation:

$$\frac{\delta^2 q}{\delta x^2} + \frac{\delta^2 q}{\delta z^2} + k^2 q = 0 \tag{5.1}$$

where $q = p\sqrt{x}$. with p as the complex pressure amplitude. However, we are really interested in solving this in a terrain-following $\xi\eta$ coordinate system, defined as

$$\begin{aligned} \xi &= x \\ \eta &= z - H(x) \end{aligned} \tag{5.2}$$

where $H(x)$ is the terrain profile. In order to accomplish the coordinate transformation, we first need to find the derivatives with respect to x and z in terms of ξ and η. Using the chain rule and the notation $\delta_x = \delta/\delta x$ and $\delta_x^2 = \delta^2/\delta x^2$, we find:

$$\begin{aligned}
\delta_z &= \delta_\eta \\
\delta_z^2 &= \delta_\eta^2 \\
\delta_x &= \delta_\xi - H'\delta_\eta \\
\delta_x^2 &= \delta_\xi^2 - 2H'\delta_{\xi\eta}^2 - H''\delta_\eta + H'^2\delta_\eta^2.
\end{aligned} \tag{5.3}$$

Now the Helmholtz equation looks like this:

$$\delta_\xi^2 - 2H'\delta_{\xi\eta}^2 - H''\delta_\eta q + (H'^2+1)\delta_\eta^2 q + k^2 q = 0. \tag{5.4}$$

To improve the numerical accuracy of the calculations, it is common to choose $q(\xi,\eta) = \psi(\xi,\eta)\exp(ik_0\xi)$, with k_0 chosen to be the wave number at some average height. Substituting this into Eq. 5.4 gives

$$\delta_\xi^2\psi + 2ik_0\delta_\xi\psi - 2H'(\delta_{\xi\eta}^2\psi + ik_0\delta_\eta\psi) - H''\delta_\eta\psi + (H'^2+1)\delta_\eta^2\psi + (k^2-k_0^2)\psi = 0. \tag{5.5}$$

Now that the basic equation is set up, it is time to make some approximations. A first-order approximation will be made first. This is an inadequate approximation numerically, but the results are needed to simplify solving the second-order approximation.

If we neglect the terms δ_ξ^2 and $\delta_{\xi\eta}^2$ in the equation above, we find

$$\delta_\xi\psi + \frac{i}{2k_0}L_1(\psi) \tag{5.6}$$

where the operator L_1 is given by

$$L_1 + \alpha\delta_\eta^2 - \beta\delta_\eta + \gamma \tag{5.7}$$

with

$$\begin{aligned}
\alpha(\xi) &= H'^2 + 1 \\
\beta(\xi) &= 2ik_0H' + H'' \\
\gamma(\xi) &= k^2(\eta) - k_0^2.
\end{aligned} \tag{5.8}$$

For a flat ground surface we have $\alpha = 1$ and $\beta = 0$, and the Eq. 5.7 reduces to the narrow-angle PE.

The second-order GTPE is obtained by integrating Eq. 5.5 over one range step, from $\xi = a$ to $\xi = b$, where $b = a + \Delta\xi$. Using the first-order solution, $\delta_\xi\psi$ as the integral of the term $\delta_\xi^2\psi$, and integrating the $\delta_{\xi\eta}^2$ term by parts results in the second-order GTPE:

$$\left[\frac{i}{2k_0}L_1(\psi) + 2ik_0\psi - 2H'\delta_\eta\psi\right]_a^b + I_\alpha + I_\chi + I_\gamma = 0 \tag{5.9}$$

with

$$\begin{aligned} I_\alpha &= \int_a^b \alpha(\xi)\delta_\eta^2 d\xi \\ I_\chi &= \int_a^b \chi(\xi)\delta_\eta \psi d\xi \\ I_\gamma &= \int_a^b \gamma(\eta)\psi d\xi \end{aligned} \tag{5.10}$$

where α and γ are given by Eq. 5.8, and χ is given by

$$\chi(\eta) = H'' - 2ik_0 H' \tag{5.11}$$

For convenience, the three integrals above can be written as:

$$I_R = \int_a^b R(\xi)\delta_\eta^n \psi d\xi \tag{5.12}$$

with $n = 2$ for $R = \alpha$, $n = 1$ for $R = \chi$, and $n = 0$ for $R = \gamma$. We can, in most cases, assume a linear variation of $\delta_\eta^n \psi$ with ξ over the range step from $\xi = a$ to $\xi = b$, we can approximate the integrals I_R with

$$\delta_\eta^n \psi(\xi) = \frac{b-\xi}{\Delta\xi}\delta_\eta^n \psi(a) = \frac{\xi - a}{\Delta\xi}\delta_\eta^n \psi(b). \tag{5.13}$$

Substituting this result back into the expression for I_R gives

$$I_R = A_R \delta_\eta^n \psi(a) + B_R \delta_\eta^n \psi(b) \tag{5.14}$$

with

$$\begin{aligned} A_R &= \frac{1}{\Delta\xi}\int_a^b (b-\xi)R(\xi)d\xi \\ B_R &= \frac{1}{\Delta\xi}\int_a^b (\xi - a)R(\xi)d\xi. \end{aligned} \tag{5.15}$$

These integrals can be approximated assuming a linear variation of R with ξ over the range step from $\xi = a$ to $\xi = b$. For the case of the piecewise linear approximation of terrain, this is always true. A_R and B_R can thus be written as

$$\begin{aligned} A_R &= \Delta\xi\left[\frac{1}{3}R(a) + \frac{1}{6}R(b)\right] \\ B_R &= \Delta\xi\left[\frac{1}{6}R(a) + \frac{1}{3}R(b)\right]. \end{aligned} \tag{5.16}$$

Using a Finite Difference approximation, Eq. 5.9 can be solved using a Crank-Nicholson method. The reader is referred to Salomons' book [15] for details.

Boundary condition at the ground is determined by using the local reaction boundary condition in the direction normal to the ground.

$$\left(\frac{p}{v_n}\right)_{\eta=0} = Z\rho c \tag{5.17}$$

where Z is the normalized ground impedance, ρc is the impedance of air, p is the complex pressure amplitude, and v_n is the component of the complex velocity amplitude normal to the ground surface, in the downward direction. At the top of the grid, $Z = 1$, the normal velocity component is in the upward direction, and an absorbing layer of some form is utilized to eliminate spurious reflections. The actual implementation of the boundary conditions is somewhat complex, and the reader is referred again to Salomons [15] for an excellent, detailed description.

5.2 Simulation setup

Simulations are run with four frequencies per 1/3-octave band. A 1/3-octave band spectrum is generated by averaging the pressures over these four frequencies. This minimizes frequency-specific interference dips while maintaining the overall spectral characteristics. The minimum frequency calculated is 1 Hz in all simulations. The maximum frequency band to be calculated is determined by propagation distance. The following values were used: 4000 Hz @ 1km, 2500 Hz @ 2km, 2000 Hz @ 4 km, and 1250 Hz @ 7 km and 8 km. Distances are approximate. Actual measurement distances are used to find the proper spectrum at the receiver location. These frequencies are the point above which the attenuation drops to more than 60 dB than the least amount of attenuation at that distance. This is largely due to atmospheric absorption. Therefore, it is no surprise that the maximum frequencies decrease with distance.

5.3 Meteorology profiles

Five scenarios were run for each of the 27 distinct cases (meteorology, propagation direction, terrain profile). These scenarios were:

1. log-lin meteorology profile fit and terrain
2. linear meteorology fit and terrain
3. log-lin meteorology fit and flat earth
4. linear meteorology fit and flat earth

Case	Met-data	Src. Pos.	Rec. Pos.
1	142	101	0
2	178	101	0
3	63	302	0
4	69	302	0
5	81	302	0
6	87	302	0
7	93	302	0
8	161	302	0
9	167	302	0
10	172	302	0
11	178	302	0
12	69	304	0
13	167	304	0
14	184	308	0
15	172	101	306
16	178	101	306
17	135	302	306
18	161	302	306
19	167	302	306
20	172	302	306
21	69	304	306
22	135	304	306
23	142	304	306
24	167	304	306
25	172	304	306
26	178	304	306
27	184	308	306

Table 5.1: Case definitions for the GT-PE simulations.

5. Milstøy fit (linear) and terrain

The cases are defined by the meteorology profile and the source and receiver positions. Types 1-4 above take the height-dependent wind direction into account. Type 5 assumes a constant wind direction with height. Terrain is defined by the source and receiver locations. Charge size is not considered, as this effect is added to the simulations as an emission spectrum just prior to comparisons to the C3 data set. Definitions are in Table 5.1. In all cases, the ground impedance was determined using the Delany-Bazley [16] model down to 315 Hz and the Darcy-Taraldsen model [17] below, and range-dependent effective flow resistivities as provided in the Nortrial database.

5.4 Source formulation in the PE

In many cases it is sufficient to use a simplification of the point source over a finite-impedance ground, as given by

$$q(0,z) = q_0(z - z_s) + Cq_0(z + z_s) \tag{5.18}$$

where $q(0,z)$ is the starting field, z is the height above the ground, z_s is the source height, q_0 is given by

$$q_0 = \sqrt{ik_0}\exp\left(-\frac{1}{2}k_0^2 z^2\right) \tag{5.19}$$

with k_0 as the reference wavenumber, and C is the plane wave reflection coefficient as defined by

$$C = \frac{Z_g - 1}{Z_g + 1} \tag{5.20}$$

where Z_g is the normalized ground impedance.

This definition of the source is the most commonly used, but it unfortunately fails to provide the correct result to the simple test of checking the geometric decay with distance over rigid ground in a homogeneous atmosphere for low frequencies. This issue was uncovered while all properties of the simulation were investigated as an attempt to determine the reason for the low-frequency discrepancies between the simulations and the measurements. Because the benchmark testing cases for the terrain contributions of the GT-PE were all for frequencies above 300 Hz, this issue did not surface until this time. It was determined that a more exact point source was required, and a Laplace transform version [18]was used instead. The source must be placed at a distance of either λ or 1 m from the source point (r=0), whichever is further. The calculation method for the ground impedance value was also called into question. There are known issues with the Delany-Bazley model below approximately 50 Hz. Because of this, the Darcy-Taraldsen [17] model was chosen instead.

This model matches the Delany-Bazley model within the D-B model's range of applicability, and then provides more correct results at lower frequencies. The source term and ground impedance model were updated and frequencies below 315 Hz were re-run, and the results of this change are shown in Figure 5.4. The authors have found no mention of this issue in any of the literature.

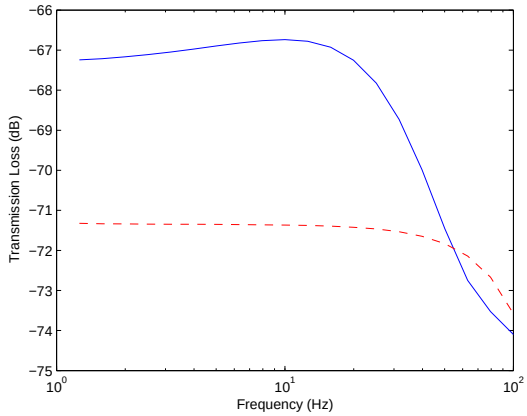

Figure 5.1: Homogeneous atmosphere with rigid ground case showing that the geometric attenuation is incorrect with the simple approximation to the point source. For a propagation distance of 8 km over rigid ground, the attenuation should be approximately -72 dB.

5.5 Source emission spectrum

A FOFT spectrum [19] for the appropriate charge weight is used to simulate the source. In the FOFT-model (FOFT: Danish Defence Research Establishment) a parametric model is proposed for time series of the sound pressure around a spherical detonation. This model consists of two parts. First, a simple function is fitted to the measured data from Baker's book [20], to describe the way the peak-pressure and the positive phase duration of a detonation depends on the mass of explosives and the distance from the source. Then, this peak-pressure and positive phase duration are used as input to Reed's formula for the time series of the pressure [21].

Then 1/3-octave band spectra are generated from the time series for each charge weight at the distance where the propagation becomes linear (pressure = 1 kPa). These spectra are then linearly scaled back to a distance of 1 m (or actually the largest of λ and 1 m from the source), and added to the appropriate simulated transmission loss spectra in dB to correspond to the measurement set. This method allows direct comparisons between measurements and simulations, and also facilitates finding the overall CSEL. A plot of the

FOFT spectrum, linearly scaled back to 1 m distance, for each of the three charge sizes is in Fig. 5.5.

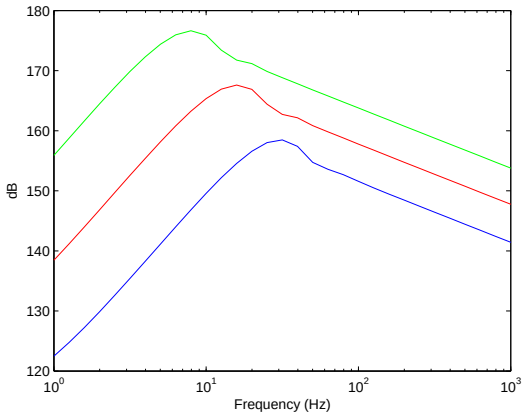

Figure 5.2: FOFT spectra for each of the three charge sizes. Levels are calculated at the linear range and scaled back to 1 m. Line color indicates charge size as follows: Blue = 1 kg, Red = 8 kg, Green = 64 kg.

The Friedlander method was also attempted, but there was too much confusion about how to actually use the emission spectrum (unsure of the location at which it is calculated). However, the Friedlander spectrum and the FOFT-method give results that are in good correspondence, where a comparison can be made.

5.6 Turbulent loss threshold

Because the upward refracting cases in particular have what could easily be deemed as excessive predicted attenuation, a turbulent loss threshold was put in place. The excess attenuation (attenuation over and above that obtained by geometric spreading and atmospheric absorption) was set to be no greater than 30 dB. Salomons [15] states in his book that 20 dB is a good threshold for an unstable atmosphere and 30 dB for a stable atmosphere. The 30 dB value was used, as it appears to be appropriate for the higher frequencies when compared to the data. There are cases where the 30 dB threshold is still cutting off potentially real effects.

5.7 Analysis, general notes

In general, the simulations (weighted with the FOFT spectrum) are nearly as likely to over-predict as under-predict the received values in overall L_{CE} (dB). Much more discrepancy

lies in the low frequency predictions, particularly below 10 Hz. This tendency is masked when looking at overall L_{CE} but appears when looking at individual 1/3-octave band level differences. The simulations do not generally attenuate enough at very low frequencies. This causes the combination of simulation and FOFT to show a lower frequency peak than is present in much of the data. The low frequencies do not drop off as sharply in the simulations as they do in the measurements. Levels are generally over-predicted when looking at the spectra. Upward refracting cases for types 1, 2, 3, and 5 are over-predicted at a ratio of 9 over to 5 under. Type 4 has a ratio of 8 to 6. Downward refracting cases for types 2, 3, and 5 have an over- to under-prediction ratio of 12 to 2, while type 1 has a ratio of 11 to 3 and type 4 has a ratio of 13 to 1. The two near-neutral profiles under-predict the spectrum in types 1, 2, and 5, but split evenly for types 3 and 4. Note that these assessments of over prediction and under prediction are based primarily on frequencies greater than 10 Hz. This is because, in nearly all cases, below 10 Hz is badly overpredicted. The best fit to data is not consistently any one of the five scenarios simulated for a given measurement. Plots of all data and simulations are in the appendix.

Plots of the difference between predicted level - measured level by 1/3-octave band in dB are in Fig. 5.3. These difference spectra must be interpreted on the background of where in the spectra we have the dominant energy. In Fig. 5.5 we see that the energy peak for 1 kg C4 is around 30 Hz.

The results are quite interesting, but not terribly illuminating. If looking at all comparisons together, regardless of the general direction of refraction, it appears that the log-lin profiles with terrain (type 1) provide the best spectral fits overall. In descending order of apparent goodness of fit, the types are 1, 2, 5, 4, and 3. In general, simulations with terrain are slightly better than flat earth simulations. All simulations badly overpredict the levels below 10 Hz.

If the band level differences are partitioned into direction of refraction, the results become less clear. In near-neutral conditions (Fig. 5.4), a linear profile without terrain (type 4) provides the best fits. Between 70 Hz and 1 kHz, all five types give almost exactly the same answer. The lower frequency error is smaller in type 4 than in the others. In all the difference is within 10 dB near the ground dip frequency and nearly zero above. In upward refracting conditions (Fig. 5.5 and Fig. 5.6), the results are much less clear. With the exception of the errors between below 10 Hz and between 30 and 50 Hz, everything is within $\pm$10 dB. Types 2 and 4 are nearly equivalent in output to type 1. Types 3 and 5 have the most outliers. In the downward refracting case (Fig. 5.7 and Fig. 5.8), types 1 and 2 give better fits than types 3, 4, and 5. Overall, these fits are not very good. In order from best to worst, they are 1, 2, 5, 4, and 3. It is possible that some of the high frequency outliers are due to the turbulent threshold approximation. It is important to note that the

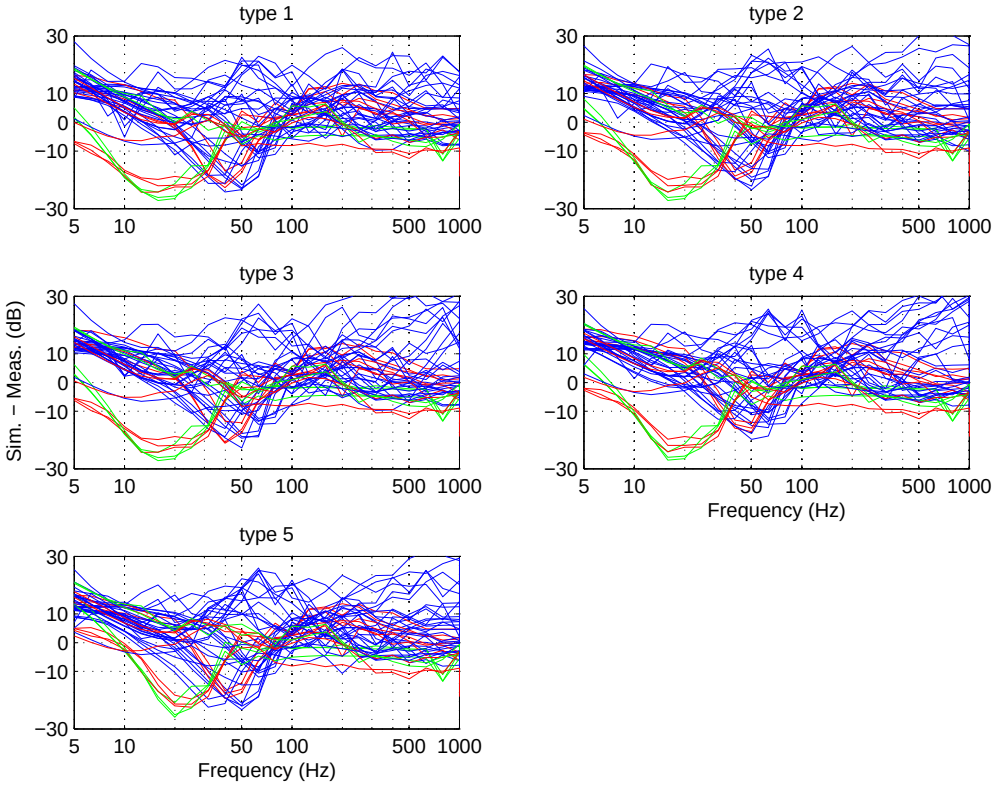

Figure 5.3: Difference between simulated levels and measured levels by 1/3-octave band in dB. All refraction conditions are present. Colors indicate charge weight: Blue = 1 kg, Red = 8 kg, Green = 64 kg.

energy actually present at the lowest and highest frequencies is much lower than for the mid-range, and so differences at those frequencies have a much less significant effect on the overall level. Because this analysis looks at all iterations of a given refraction type, it is impossible to look at whether any of the fits are actually excellent for an individual shot. As it turns out, there are a small number of excellent fits to data, and some with the right shape but the wrong magnitude. Conversely, there are some cases that are obviously not doing an adequate job, although in general the broad features are correct. Plots of each simulation compared to the data are found in Appendix B. When examining only the L_{CE} values, the results are also quite interesting. When partitioning only by propagation type and looking for the number of samples out of the 44 shots within ± 6 dB of the measurement, the following is found: type 1 has 24, type 2 has 21, type 3 has 25, type 4 has 23, and type 5 has 22. This indicates that there is not a huge difference between the various propagation conditions. The results of partitioning the L_{CE} values further into refraction classes is found in Table 5.2. Note that the total numbers match those in the text for the unpartitioned set. There are 26 shots in upward refracting conditions, 14 shots in downward refraction conditions, and 4 in near-neutral conditions.

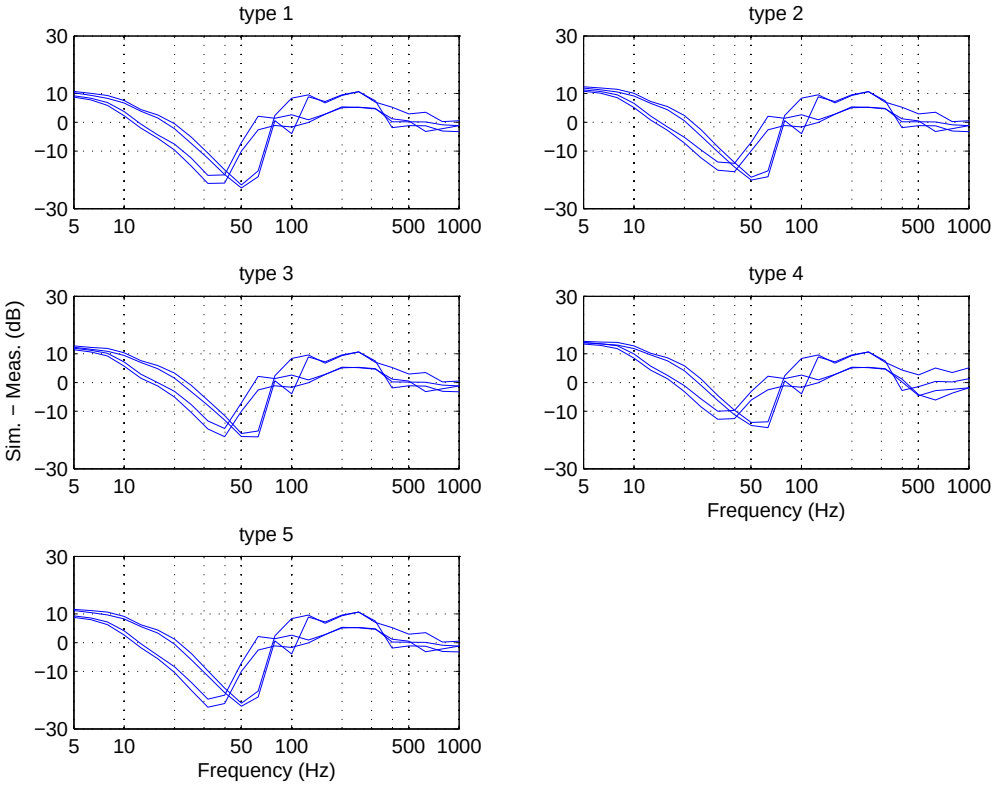

Figure 5.4: Difference between simulated levels and measured levels by 1/3-octave band in dB for neutral refraction conditions. Propagation direction is North. Colors indicate charge weight: Blue = 1 kg, Red = 8 kg, Green = 64 kg.

For completeness, all of the overall L_{CE} values are reported in Table 5.3 and Table 5.4, which contain results at receiver location 0 and 306, respectively.

5.8 Summary and some possible sources of error

Some of the simulations do a good job of predicting the received values and some of them do not. Possible sources of error are the source emission spectrum used (FOFT), approximations to the meteorological profile, absence of turbulence in the simulations and the subsequent introduction of the turbulent threshold, accuracy of the ground properties and model, and accuracy of the terrain profiles. It is also likely that there is some low-frequency effect that is not being adequately captured in the simulations. This could be some additional physical absorption or could be related to range-dependent microclimates. Questions always arise about the formulation of the ground impedance model. In a partially forested environment, it may be more accurate to use an extended reacting approximation instead of the locally reacting approximation. This has not been examined. The meteorological mea-

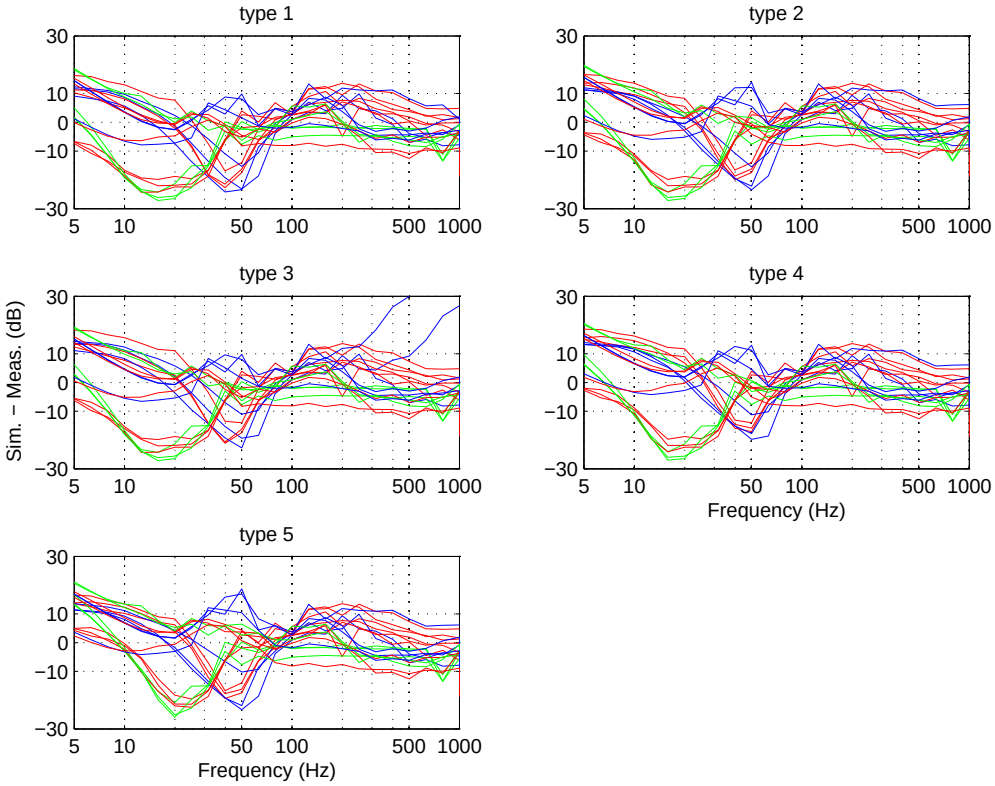

Figure 5.5: Difference between simulated levels and measured levels by 1/3-octave band in dB for upward refracting conditions. Propagation direction is North. Colors indicate charge weight: Blue = 1 kg, Red = 8 kg, Green = 64 kg.

surements that the profiles are based on were taken in the open, while at least some of the propagation was through forest. Forest has a significantly different meteorological profile than an open field. Turbulence can cause large differences in the measured values. Since the turbulence has been neglected, the simulations predict a value based on the averaged microclimate instead of the instantaneous, range-dependent environment that the impulsive signal actually passed through. The actual received value of the measured signal is equally likely (assuming a Gaussian distribution) to be greater than or less than the mean. However, the standard deviation is unknown, due to the small number of measured signals. The expected standard deviation is a topic of current research interest, and could very likely be site-dependent or at least overall environment dependent (hilly, forested, grassy, desert, flat, etc). This particular test site has previously been called challenging in terms of matching simulations to the data because of its variable terrain and ground cover types.

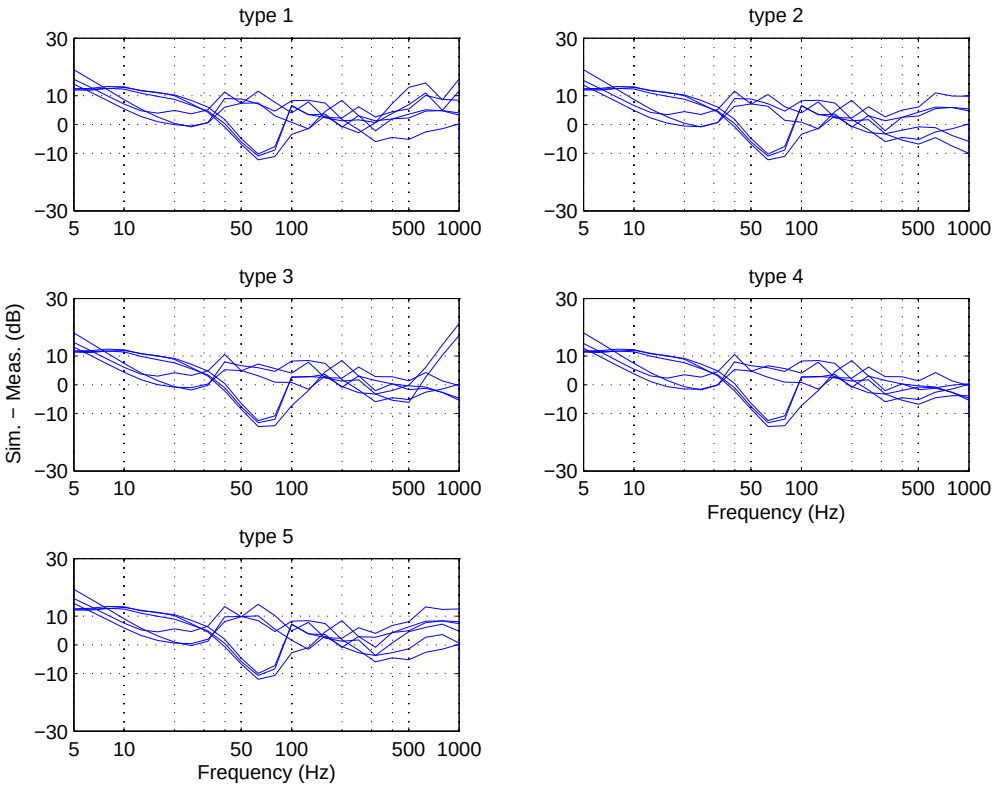

Figure 5.6: Difference between simulated levels and measured levels by 1/3-octave band in dB for upward refracting conditions. Propagation direction is South. Colors indicate charge weight: Blue = 1 kg, Red = 8 kg, Green = 64 kg.

type	upward	downward	neutral	total
1	18	6	0	24
2	16	4	1	21
3	17	6	2	25
4	15	5	3	23
5	16	6	0	22

Table 5.2: Number of shots where the simulated L_{CE} - measured L_{CE} was less than $\pm$ 6 dB, partitioned by direction of refraction.

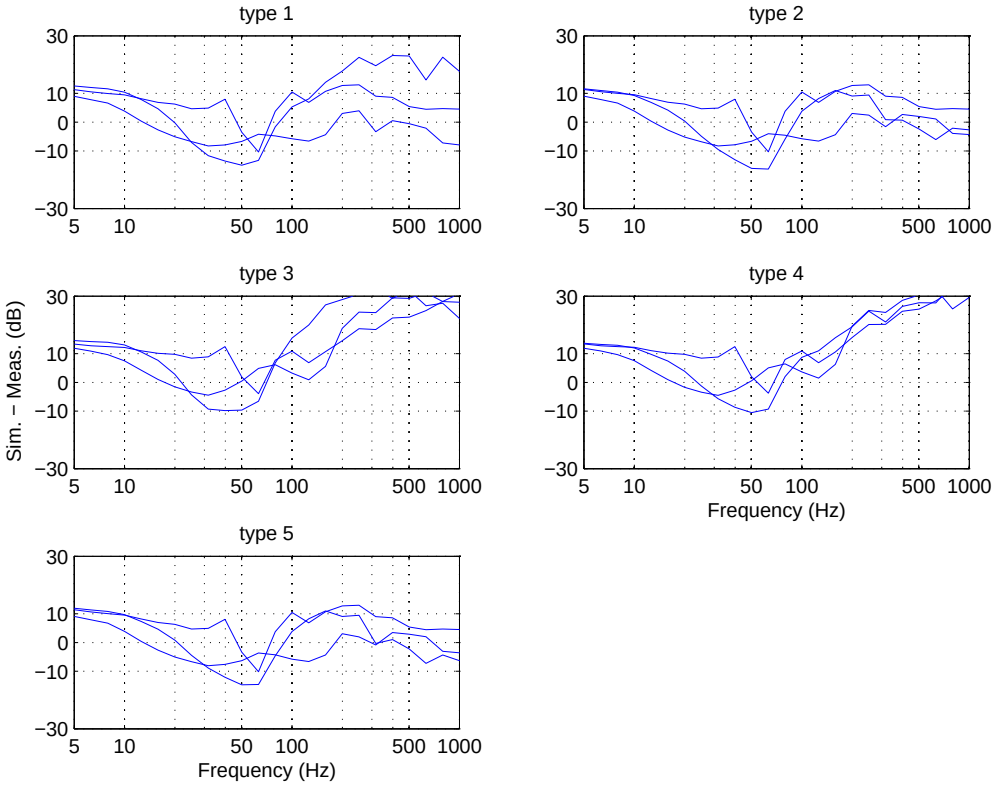

Figure 5.7: Difference between simulated levels and measured levels by 1/3-octave band in dB for downward refracting conditions. Propagation direction is North. Colors indicate charge weight: Blue = 1 kg, Red = 8 kg, Green = 64 kg.

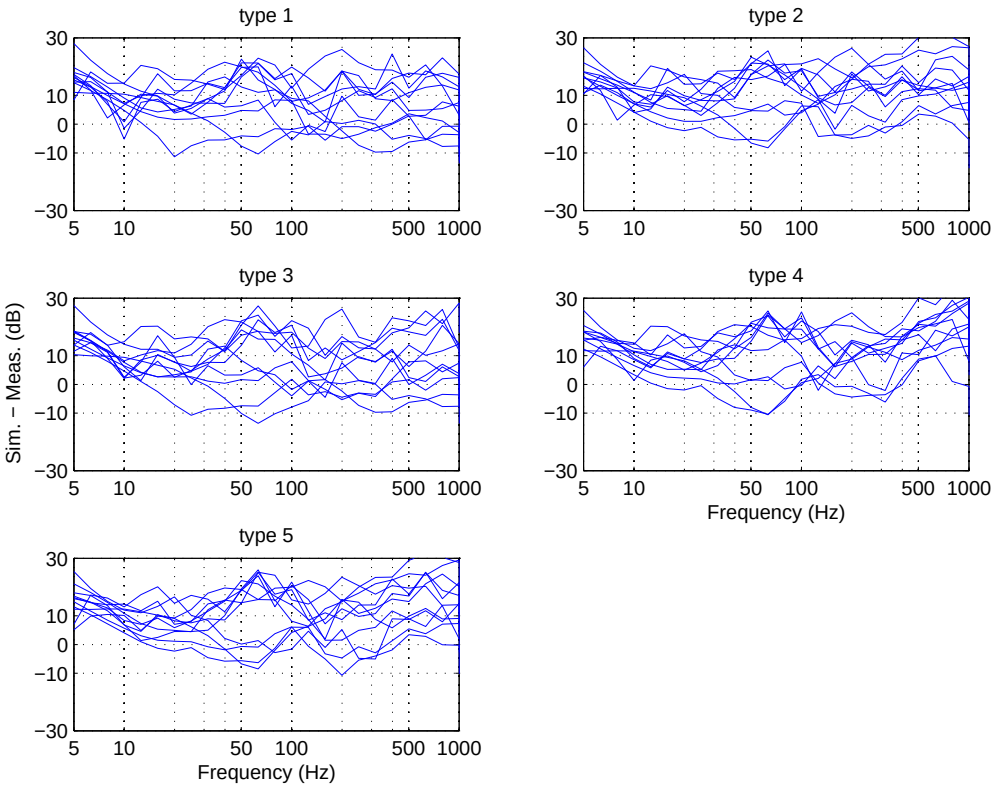

Figure 5.8: Difference between simulated levels and measured levels by 1/3-octave band in dB for downward refracting conditions. Propagation direction is South. Colors indicate charge weight: Blue = 1 kg, Red = 8 kg, Green = 64 kg.

Fileno	Met-data	Source		Sensor 0					
		Pos	Weight [kg]	Measur.	Type 1	Type 2	Type 3	Type 4	Type 5
63	63	302	1	92.0	82.8	82.4	87.8	85.8	82.5
69	69	302	1	90.9	81.4	84.0	85.2	87.5	82.9
70	69	304	1	83.2	70.0	72.7	74.0	76.4	69.7
75	69	302	1	89.3	81.4	84.0	85.2	87.5	82.9
76	69	304	1	80.6	70.0	72.7	74.0	76.4	69.7
81	81	302	8	88.3	91.0	91.6	94.1	94.7	91.5
87	87	302	8	93.6	87.9	92.7	91.1	95.9	93.1
93	93	302	8	92.5	87.0	92.8	90.2	96.0	93.4
135	135	302	1						
136	135	304	1						
142	142	101	1	98.9	100.7	100.8	99.5	99.5	100.9
144	142	304	1						
148	142	101	1	97.7	100.7	100.8	99.5	99.5	100.9
154	142	101	1	99.7	100.7	100.8	99.5	99.5	100.9
161	161	302	1	92.7	86.8	86.2	92.0	92.7	86.7
167	167	302	1	80.1	85.2	85.2	89.7	90.5	85.3
168	167	304	1	83.6	77.5	77.5	84.2	84.4	77.6
172	172	101	1						
173	172	302	1	85.1	83.1	82.8	89.6	86.3	85.2
174	172	304	1						
178	178	101	1	102.9	101.7	104.6	99.9	103.7	104.5
179	178	302	1	93.0	78.7	82.8	82.4	86.3	83.1
180	178	304	1						
184	184	308	1						
185	184	308	8	78.3	63.3	63.5	63.3	63.8	67.2
186	184	308	64	86.2	69.8	71.1	70.0	72.2	78.4
190	184	308	1						
191	184	308	8	80.3	63.3	63.5	63.3	63.8	67.2
192	184	308	64	88.8	69.8	71.1	70.0	72.2	78.4
196	184	308	1						
197	184	308	8	81.7	63.3	63.5	63.3	63.8	67.2
198	184	308	64	88.8	69.8	71.1	70.0	72.2	78.4

Table 5.3: Comparing simulation output using the FOFT source as an emission spectrum and for all five propagation types. All the values are L_{CE} in dB. Only receiver location 0 is shown in this table.

Fileno	Met-data	Source		Sensor306					
		Pos	Weight [kg]	Measur.	Type 1	Type 2	Type 3	Type 4	Type 5
63	63	302	1						
69	69	302	1						
70	69	304	1	83.8	88.4	88.0	88.0	87.1	89.3
75	69	302	1						
76	69	304	1	87.8	88.4	88.0	88.0	87.1	89.3
81	81	302	8						
87	87	302	8						
93	93	302	8						
135	135	302	1	79.8	93.3	95.9	92.1	95.6	93.3
136	135	304	1	89.9	95.4	96.9	93.7	96.4	94.6
142	142	101	1						
144	142	304	1	85.9	86.7	86.8	85.7	85.7	87.3
148	142	101	1						
154	142	101	1						
161	161	302	1	85.8	95.3	96.2	94.6	96.1	95.8
167	167	302	1	84.2	93.8	96.0	92.6	95.7	95.8
168	167	304	1	100.1	95.5	96.9	93.9	96.7	96.7
172	172	101	1	76.6	91.1	90.6	92.2	91.5	91.7
173	172	302	1	88.5	97.2	97.1	97.6	97.3	95.7
174	172	304	1	97.2	99.5	99.2	98.9	98.5	96.4
178	178	101	1	77.7	93.2	91.5	94.0	92.3	91.7
179	178	302	1						
180	178	304	1	87.3	95.4	96.6	92.9	96.3	96.2
184	184	308	1	80.6	80.2	82.3	81.8	84.3	84.8
185	184	308	8	92.1	92.8	94.8	94.4	96.8	96.9
186	184	308	64	96.1	101.6	103.5	102.9	105.1	105.3
190	184	308	1	80.3	80.2	82.3	81.8	84.3	84.8
191	184	308	8	92.3	92.8	94.8	94.4	96.8	96.9
192	184	308	64	96.8	101.6	103.5	102.9	105.1	105.3
196	184	308	1	86.0	80.2	82.3	81.8	84.3	84.8
197	184	308	8	97.7	92.8	94.8	94.4	96.8	96.9
198	184	308	64						

Table 5.4: Comparing simulation output using the FOFT source as an emission spectrum and for all five propagation types. All the values are L_{CE} in dB. Only receiver location 306 is shown in this table.

6 Conclusions

The following tables (6.1-6.4) gather up the L_{CE} data from measurements, Milstoy, BNoise, and the PE simulations for easy side-by-side comparison. Blanks within the tables are used when a particular sensor (0 or 306) either did not record the signal, the signal-to-noise ratio was too low, or the received level was below 75 dB L_{CE}. These lines are left in the tables to facilitate easy comparisons with the other tables in the report.

It is interesting to look at the number of shots that each model predicted the received value to within $\pm 1\ dB$, $\pm 3\ dB$, and $\pm 6\ dB$. This is in Table 6.5. BNoise comes within these tolerances the highest number of times. This is particularly notable because only one propagation condition is considered in this set. As was mentioned in the BNoise section, changing the meteorology significantly reduced the accuracy of the predictions.

To get a better feel for whether the models generally over- or under-predict the measurements, it is interesting to look at the number of times the difference between the simulation and the measurement is greater than zero. Both of the Milstøy methods have a strong tendency to overpredict the level (43 out of 44 times for Industry Noise and 30 out of 44 times for the Nord2000Road). BNoise overpredicts the level 28 out of 44 times. The five PE simulations range from 21 to 25 out of 44 times.

The results of this study have not been strongly conclusive. However, many things have been learned. In working with the PE, we have developed a stable version. Changing the propagation condition does not necessitate a change in the basic parameters. The results are reasonable and within the expected bounds. There appears to be potential for further use of pre-calculated PE output in future noise mapping systems. Real-time calculations are not feasible due to the time needed for each calculation. It appears that BNoise is producing the most reliable results for the propagation case that was selected.

Fileno	Met-data	Source		Sensor 0	Milstøy		BNoise	PE				
		Pos	Wgt [kg]	Measur.	IN	N2R		Type 1	Type 2	Type 3	Type 4	Type 5
63	63	302	1	92.0	94.6	87.9	91.0	82.8	82.4	87.8	85.8	82.5
69	69	302	1	90.9	94.6	87.8	91.0	81.4	84.0	85.2	87.5	82.9
70	69	304	1	83.2	87.6	79.2	83.0	70.0	72.7	74.0	76.4	69.7
75	69	302	1	89.3	94.6	87.8	91.0	81.4	84.0	85.2	87.5	82.9
76	69	304	1	80.6	87.6	82.2	83.0	70.0	72.7	74.0	76.4	69.7
81	81	302	8	88.3	100.7	92.3	98.0	91.0	91.6	94.1	94.7	91.5
87	87	302	8	93.6	100.7	93.5	98.0	87.9	92.7	91.1	95.9	93.1
93	93	302	8	92.5	100.7	93.4	98.0	87.0	92.8	90.2	96.0	93.4
135	135	302	1									
136	135	304	1									
142	142	101	1	98.9	107.4	103.4	100.0	100.7	100.8	99.5	99.5	100.9
144	142	304	1									
148	142	101	1	97.7	104.7	103.4	100.0	100.7	100.8	99.5	99.5	100.9
154	142	101	1	99.7	104.7	103.4	100.0	100.7	100.8	99.5	99.5	100.9
161	161	302	1	92.7	94.6	89.9	91.0	86.8	86.2	92.0	92.7	86.7
167	167	302	1	80.1	94.6	94.0	91.0	85.2	85.2	89.7	90.5	85.3
168	167	304	1	83.6	87.5	83.4	83.0	77.5	77.5	84.2	84.4	77.6
172	172	101	1									
173	172	302	1	85.1	94.6	89.7	91.0	83.1	82.8	89.6	86.3	85.2
174	172	304	1									
178	178	101	1	102.9	104.6	104.4	100.0	101.7	104.6	99.9	103.7	104.5
179	178	302	1	93.0	94.6	89.3	91.0	78.7	82.8	82.4	86.3	83.1
180	178	304	1									

Table 6.1: Comparing simulation output using the FOFT source as an emission spectrum and for all five propagation types. All the values are L_{CE} in dB. Only receiver location 0 is shown in this table. Continued on next table.

Fileno	Met-data	Source		Sensor 0	Milstøy		BNoise	PE				
		Pos	Wgt [kg]	Measur.	IN	N2R		Type 1	Type 2	Type 3	Type 4	Type 5
184	184	308	1									
185	184	308	8	78.3	91.4	74.1	81.5	63.3	63.5	63.3	63.8	67.2
186	184	308	64	86.2	96.8	80.1	88.0	69.8	71.1	70.0	72.2	78.4
190	184	308	1									
191	184	308	8	80.3	91.4	74.1	81.5	63.3	63.5	63.3	63.8	67.2
192	184	308	64	88.8	96.8	80.1	88.0	69.8	71.1	70.0	72.2	78.4
196	184	308	1									
197	184	308	8	81.7	91.4	74.1	81.5	63.3	63.5	63.3	63.8	67.2
198	184	308	64	88.8	96.8	80.1	88.0	69.8	71.1	70.0	72.2	78.4

Table 6.2: Comparing simulation output using the FOFT source as an emission spectrum and for all five propagation types. All the values are L_{CE} in dB. Only receiver location 0 is shown in this table. Continued from previous table.

Fileno	Met-data	Source		Sensor 306	Milstøy		BNoise	PE				
		Pos	Wgt [kg]	Measur.	IN	N2R		Type 1	Type 2	Type 3	Type 4	Type 5
63	63	302	1									
69	69	302	1									
70	69	304	1	83.8	98.8	96.6	90.5	88.4	88.0	88.0	87.1	89.3
75	69	302	1									
76	69	304	1	87.8	101.8	99.6	90.5	88.4	88.0	88.0	87.1	89.3
81	81	302	8									
87	87	302	8									
93	93	302	8									
135	135	302	1	79.8	94.1	91.7	82.5	93.3	95.9	92.1	95.6	93.3
136	135	304	1	89.9	98.8	103.4	90.5	95.4	96.9	93.7	96.4	94.6
142	142	101	1									
144	142	304	1	85.9	98.8	96.6	90.5	86.7	86.8	85.7	85.7	87.3
148	142	101	1									
154	142	101	1									
161	161	302	1	85.8	94.0	89.8	82.5	95.3	96.2	94.6	96.1	95.8
167	167	302	1	84.2	94.0	89.8	82.5	93.8	96.0	92.6	95.7	95.8
168	167	304	1	100.1	98.8	103.6	90.5	95.5	96.9	93.9	96.7	96.7
172	172	101	1	76.6	91.6	84.0	76.0	91.1	90.6	92.2	91.5	91.7
173	172	302	1	88.5	94.0	91.4	82.5	97.2	97.1	97.6	97.3	95.7
174	172	304	1	97.2	98.8	104.7	90.5	99.5	99.2	98.9	98.5	96.4
178	178	101	1	77.7	91.6	83.9	76.0	93.2	91.5	94.0	92.3	91.7
179	178	302	1									
180	178	304	1	87.3	98.8	101.6	90.5	95.4	96.6	92.9	96.3	96.2

Table 6.3: Comparing simulation output using the FOFT source as an emission spectrum and for all five propagation types. All the values are L_{CE} in dB. Only receiver location 306 is shown in this table. Continued on next table.

Fileno	Met-data	Source		Sensor 306	Milstøy		BNoise	PE				
		Pos	Wgt [kg]	Measur.	IN	N2R		Type 1	Type 2	Type 3	Type 4	Type 5
184	184	308	1	80.6	98.4	94.3	90.5	80.2	82.3	81.8	84.3	84.8
185	184	308	8	92.1	104.5	98.9	98.0	92.8	94.8	94.4	96.8	96.9
186	184	308	64	96.1	110.0	104.9	104.5	101.6	103.5	102.9	105.1	105.3
190	184	308	1	80.3	98.4	94.3	90.5	80.2	82.3	81.8	84.3	84.8
191	184	308	8	92.3	104.5	98.9	98.0	92.8	94.8	94.4	96.8	96.9
192	184	308	64	96.8	110.0	104.9	104.5	101.6	103.5	102.9	105.1	105.3
196	184	308	1	86.0	98.4	94.3	90.5	80.2	82.3	81.8	84.3	84.8
197	184	308	8	97.7	104.5	98.9	98.0	92.8	94.8	94.4	96.8	96.9
198	184	308	64									

Table 6.4: Comparing simulation output using the FOFT source as an emission spectrum and for all five propagation types. All the values are L_{CE} in dB. Only receiver location 306 is shown in this table. Continued from previous table.

	within $\pm 1\ dB$	within $\pm 3\ dB$	within$\pm 6\ dB$
IN	0	6	12
N2R	3	9	22
BNoise	11	24	35
PE Type 1	7	13	24
PE Type 2	4	14	21
PE Type 3	6	15	25
PE Type 4	8	14	23
PE Type 5	5	11	23

Table 6.5: Number of occurrences where the specified model predicted the measured level to within $\pm 1\ dB$, $\pm 3\ dB$, and $\pm 6\ dB$. There are a total of 44 possible.

Appendix A Meterology plots

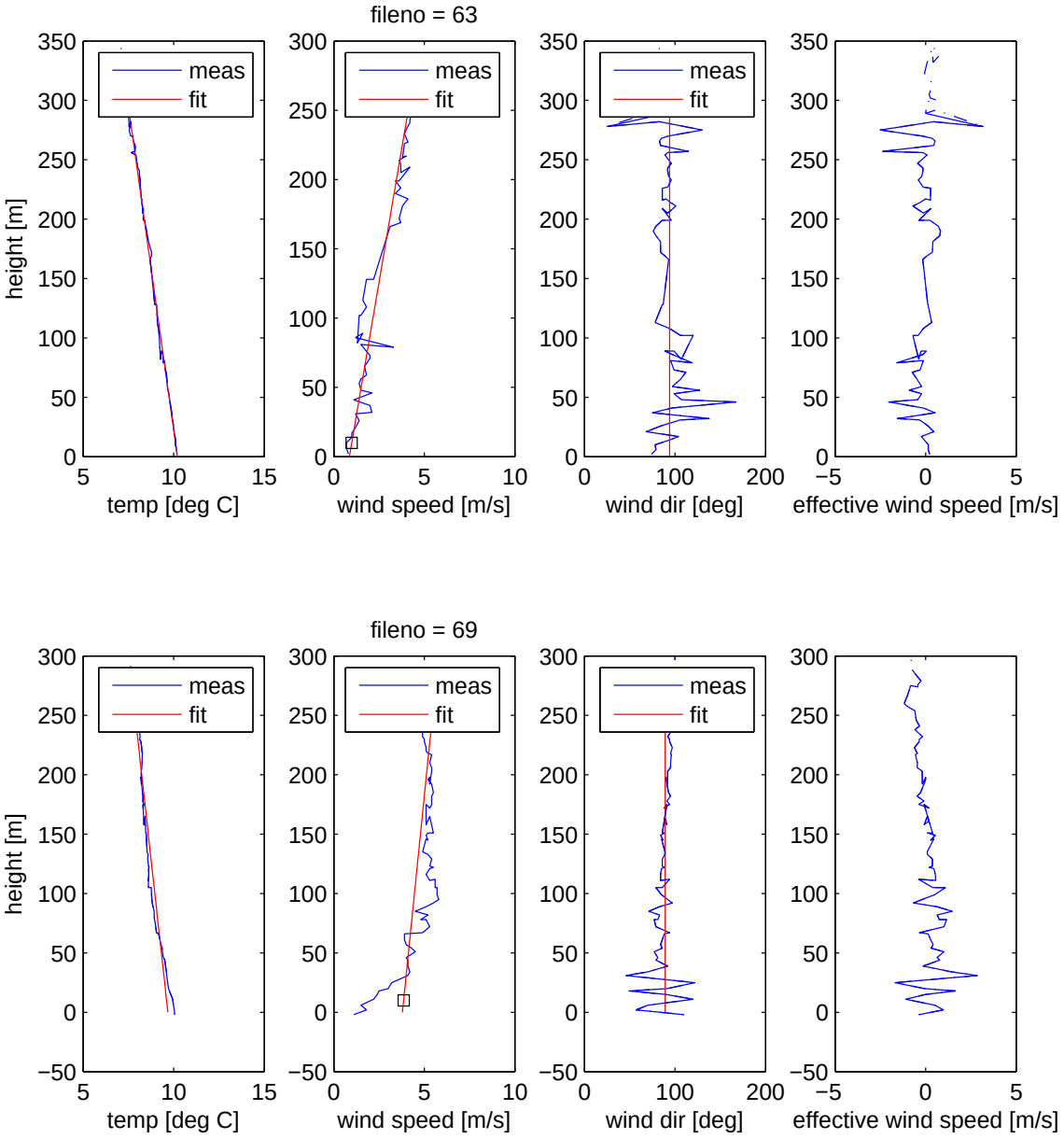

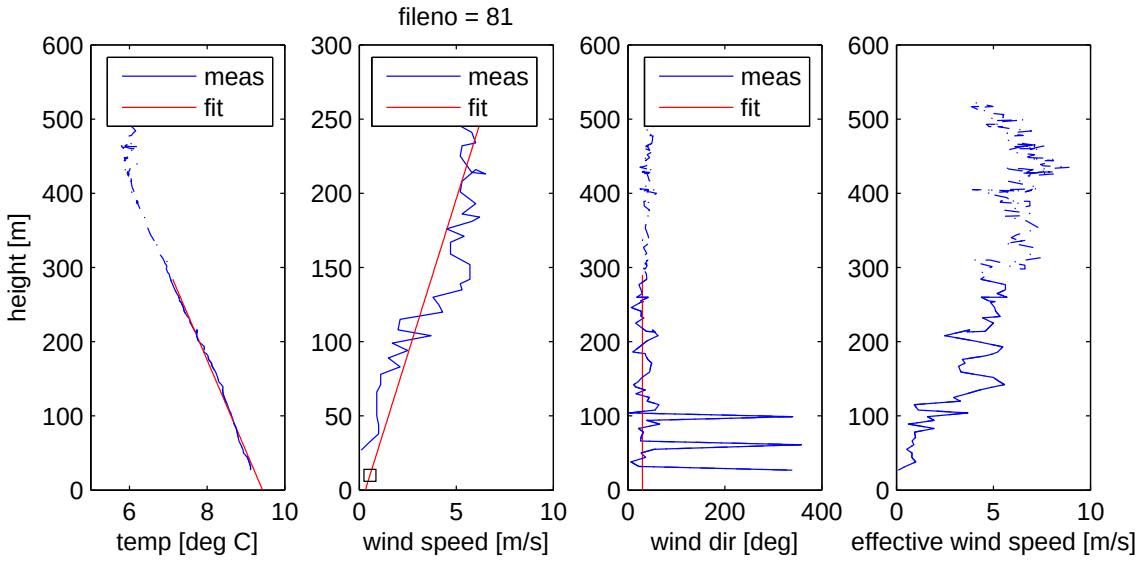
fileno = 81
meas
fit
height [m]
temp [deg C]
wind speed [m/s]
wind dir [deg]
effective wind speed [m/s]

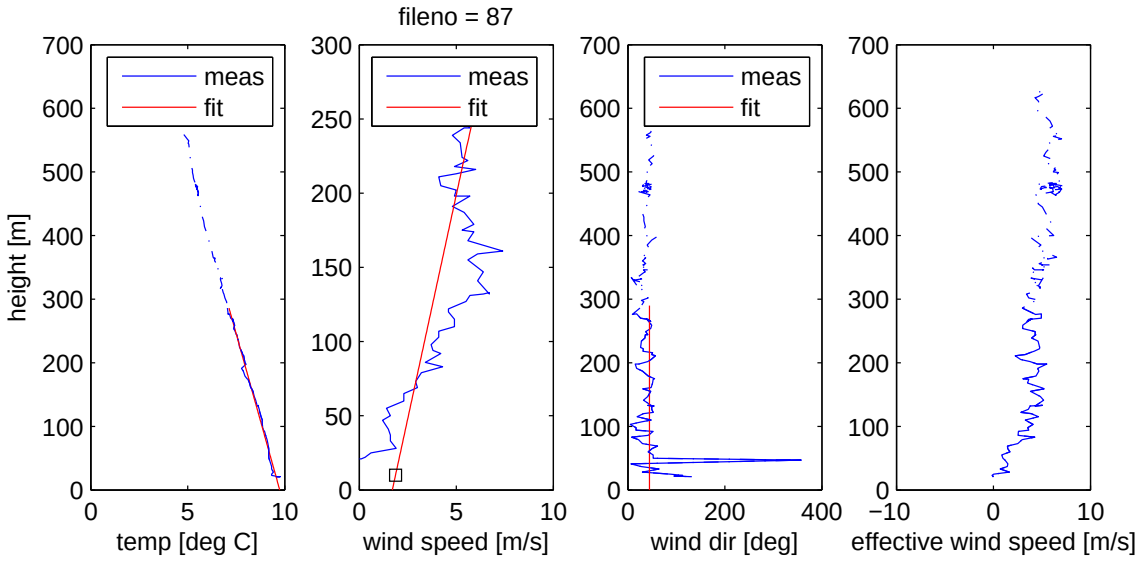
fileno = 87
meas
fit
height [m]
temp [deg C]
wind speed [m/s]
wind dir [deg]
effective wind speed [m/s]

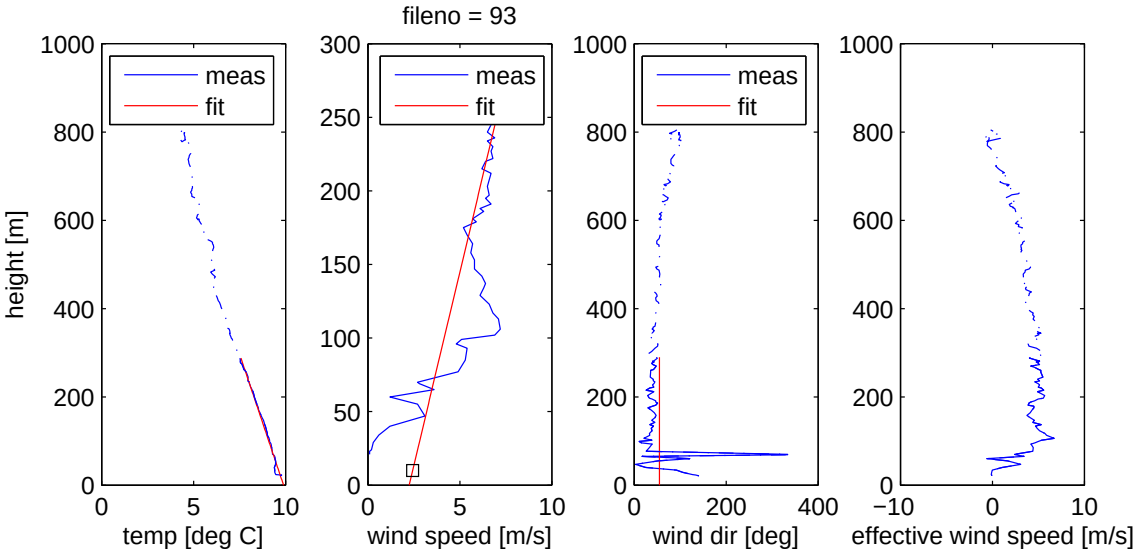
fileno = 93
height [m]
meas
fit
temp [deg C]
wind speed [m/s]
wind dir [deg]
effective wind speed [m/s]

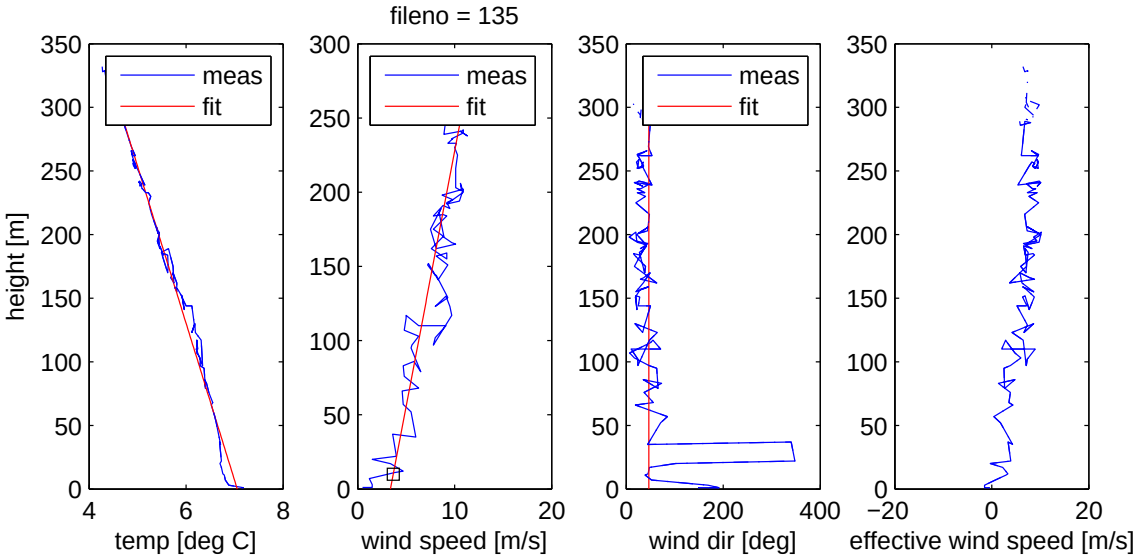
fileno = 135
height [m]
meas
fit
temp [deg C]
wind speed [m/s]
wind dir [deg]
effective wind speed [m/s]

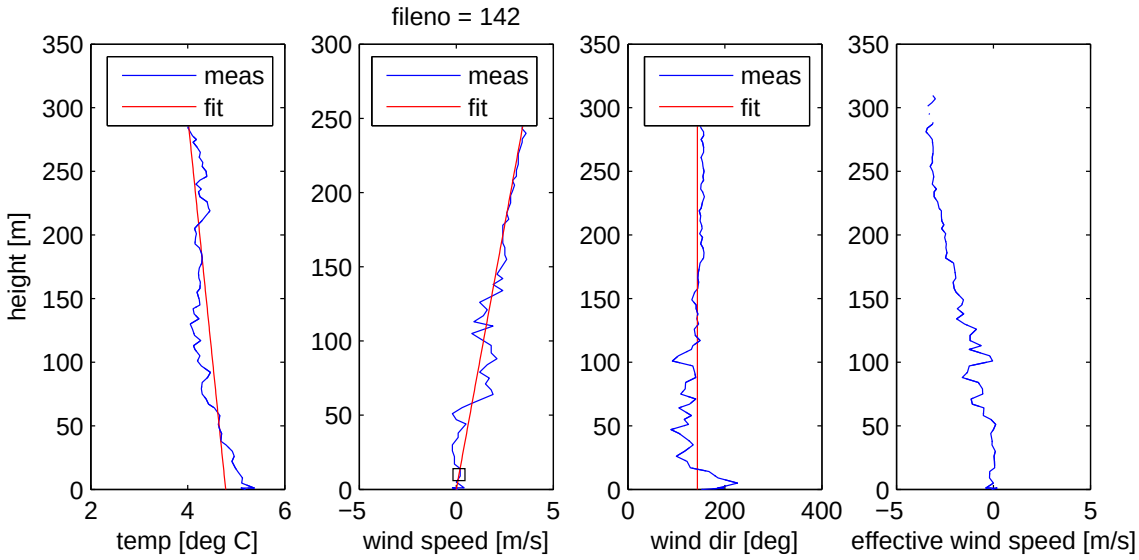
fileno = 142
meas
fit
height [m]
temp [deg C]
wind speed [m/s]
wind dir [deg]
effective wind speed [m/s]

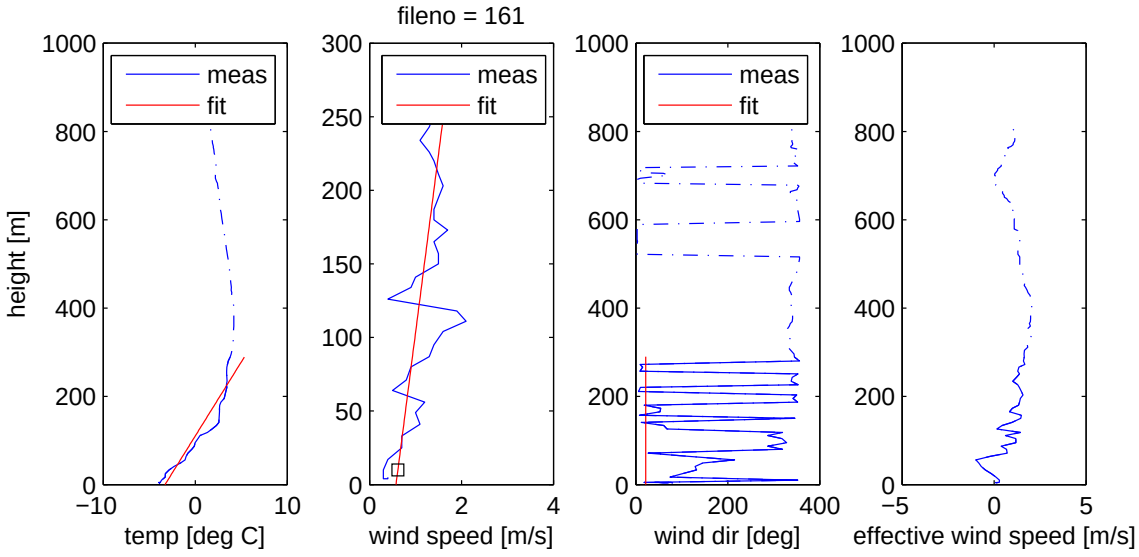
fileno = 161
meas
fit
height [m]
temp [deg C]
wind speed [m/s]
wind dir [deg]
effective wind speed [m/s]

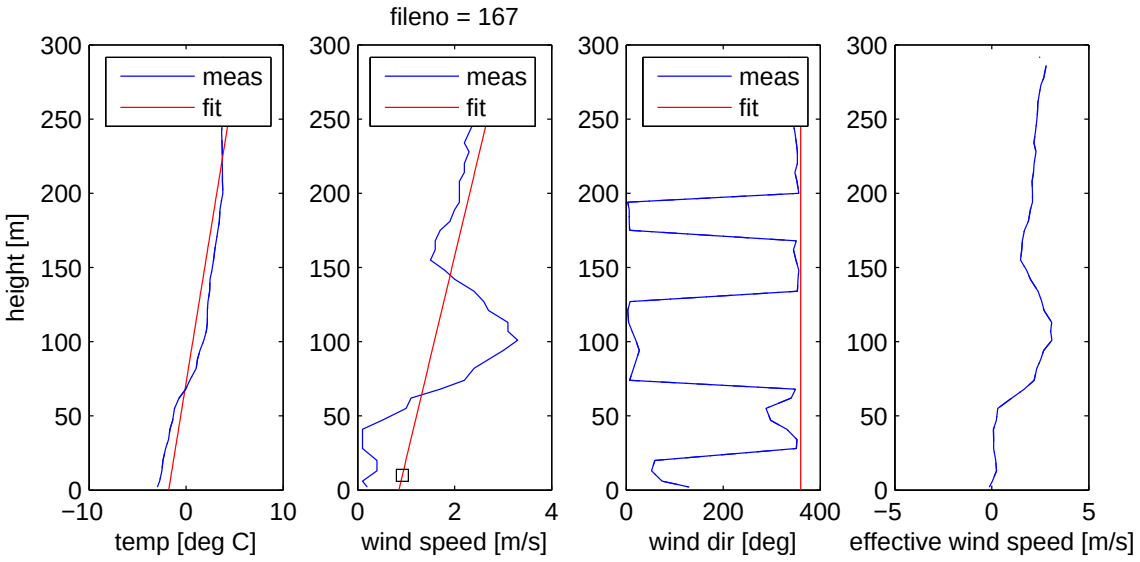
fileno = 167
meas
fit
height [m]
temp [deg C]
wind speed [m/s]
wind dir [deg]
effective wind speed [m/s]

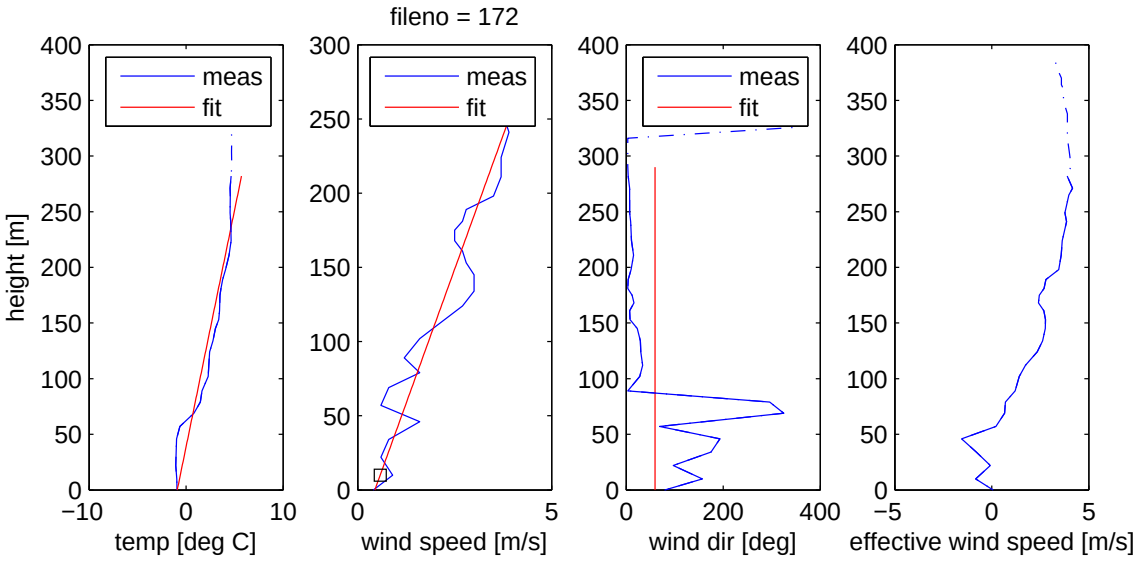
fileno = 172
meas
fit
height [m]
temp [deg C]
wind speed [m/s]
wind dir [deg]
effective wind speed [m/s]

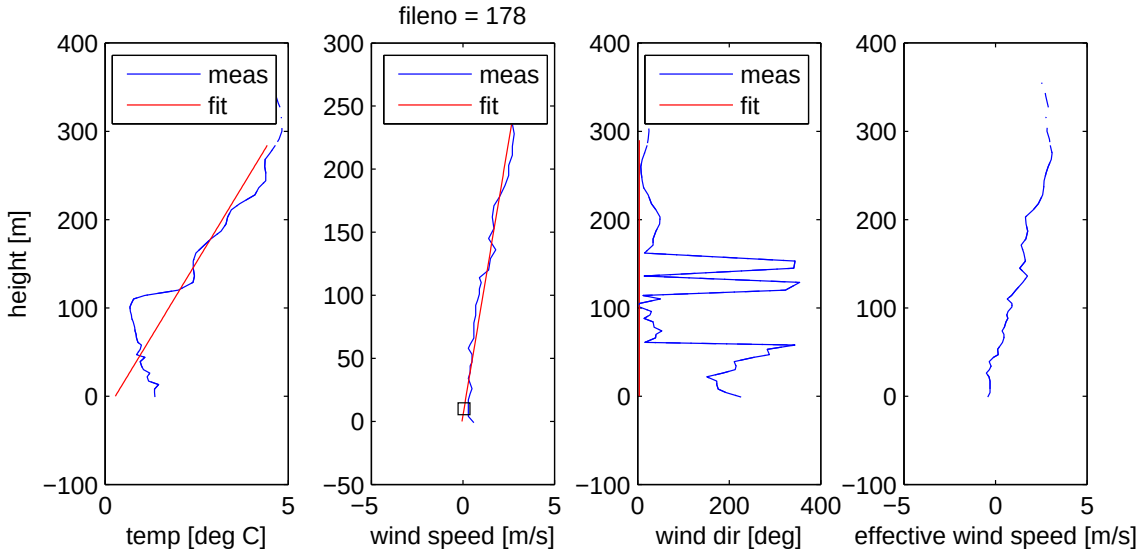
fileno = 178
meas
fit
height [m]
temp [deg C]
wind speed [m/s]
wind dir [deg]
effective wind speed [m/s]

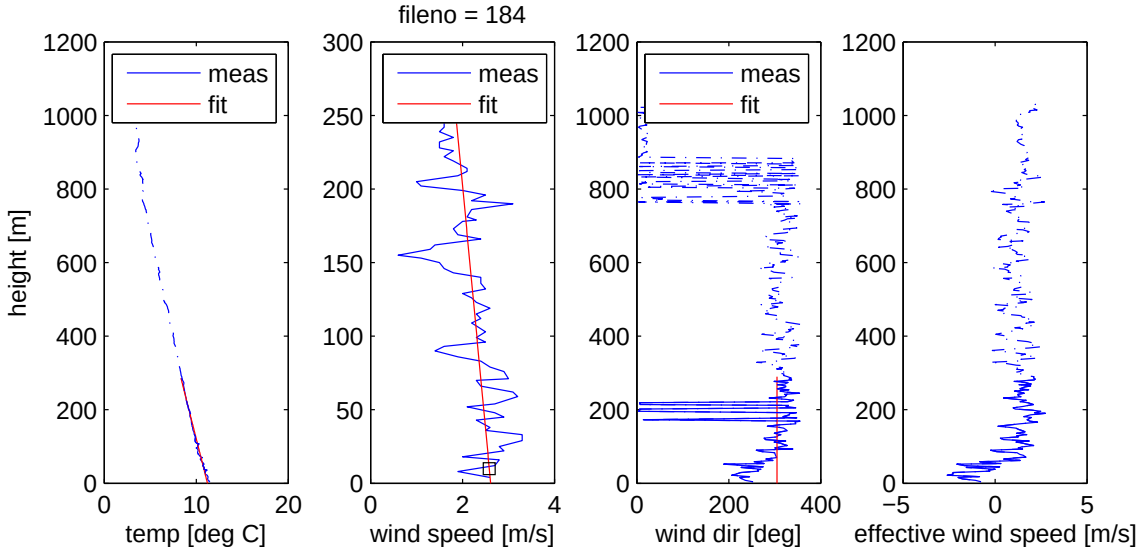
fileno = 184
meas
fit
height [m]
temp [deg C]
wind speed [m/s]
wind dir [deg]
effective wind speed [m/s]

Appendix B Simulation Plots

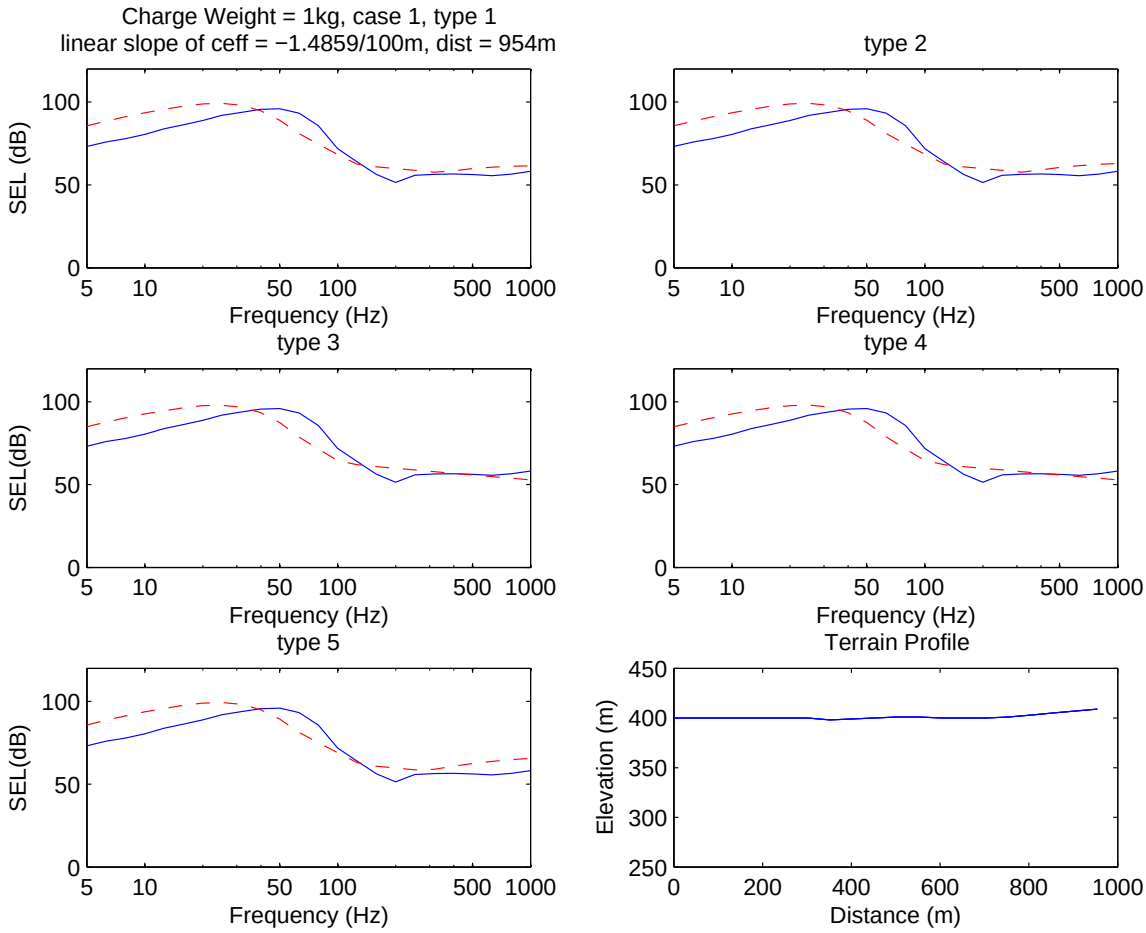

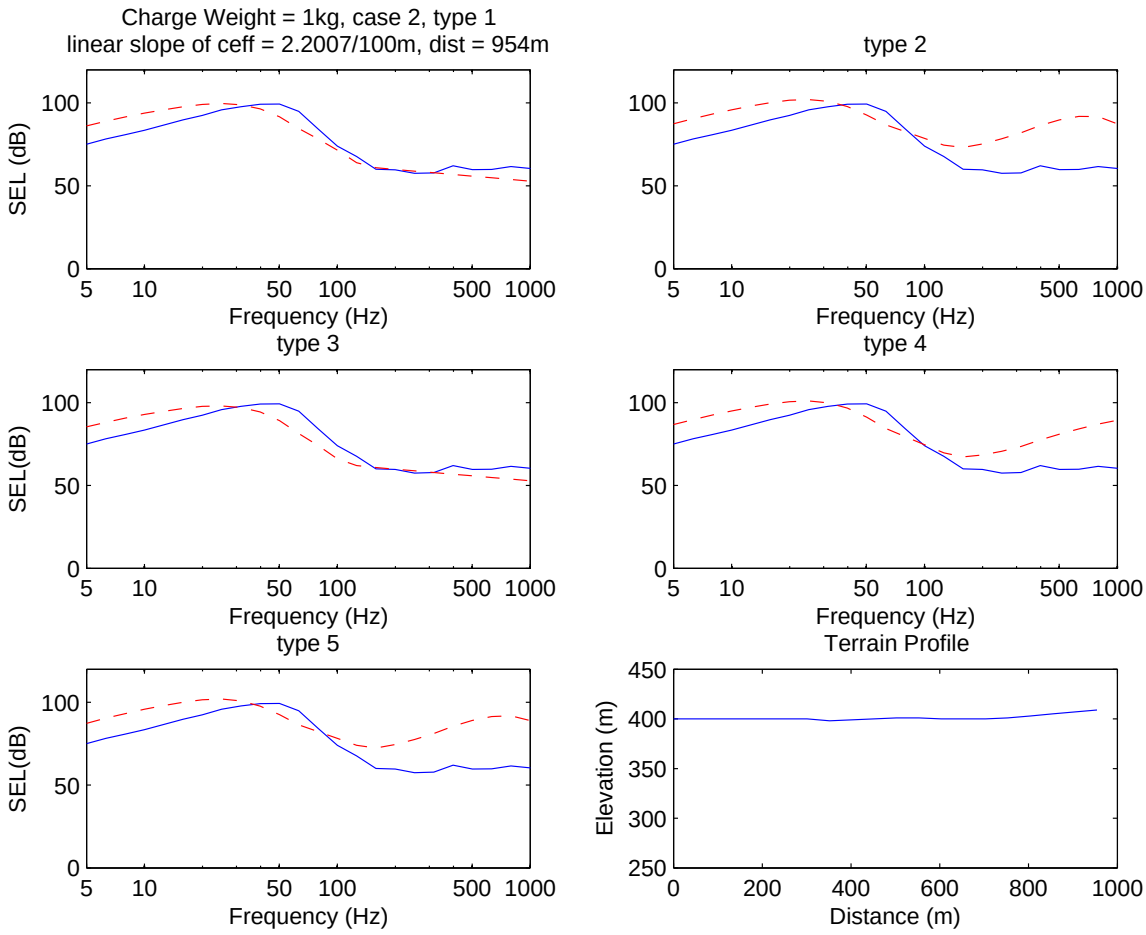
Charge Weight = 1kg, case 2, type 1
linear slope of ceff = 2.2007/100m, dist = 954m
SEL (dB)
Frequency (Hz)
type 2
type 3
SEL(dB)
type 4
type 5
Terrain Profile
Elevation (m)
Distance (m)

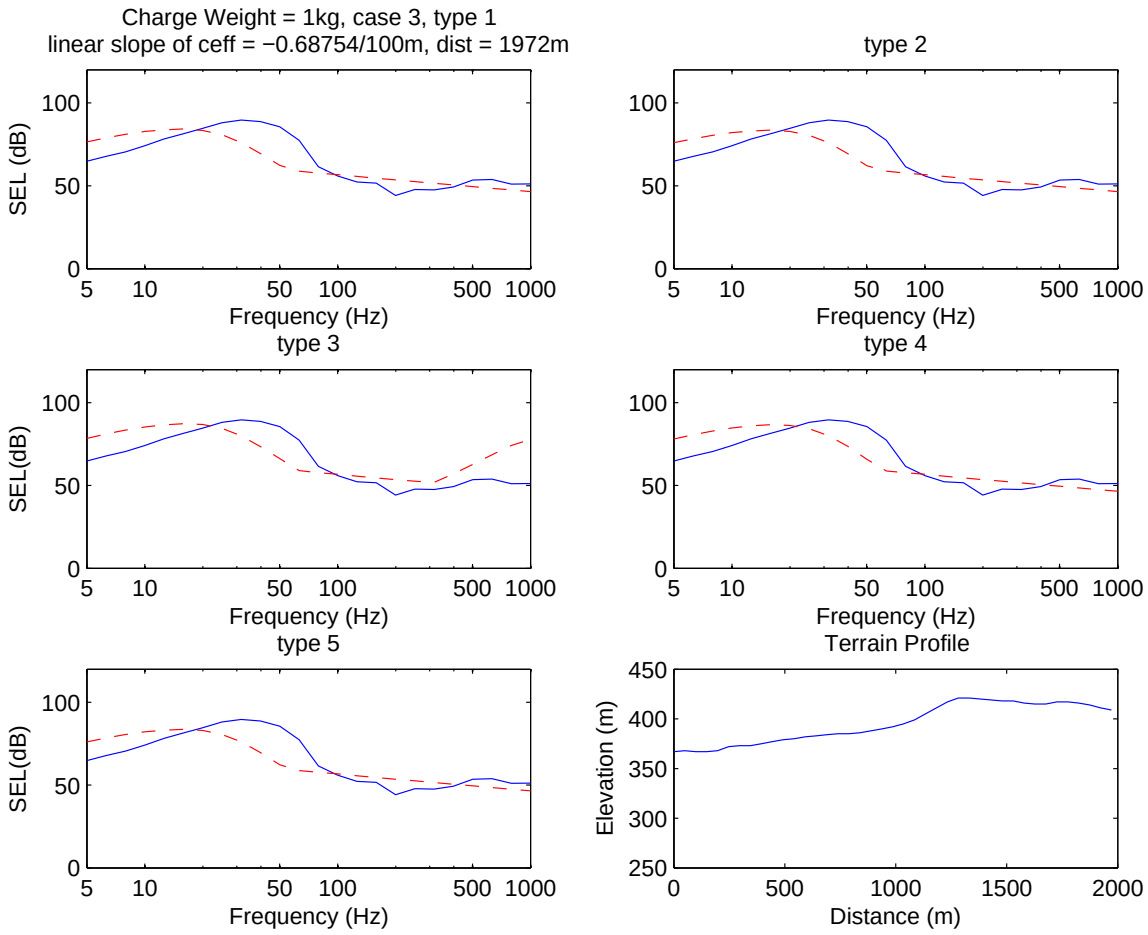
Charge Weight = 1kg, case 3, type 1
linear slope of ceff = −0.68754/100m, dist = 1972m
SEL (dB)
Frequency (Hz)
type 2
type 3
SEL(dB)
type 4
type 5
Terrain Profile
Elevation (m)
Distance (m)

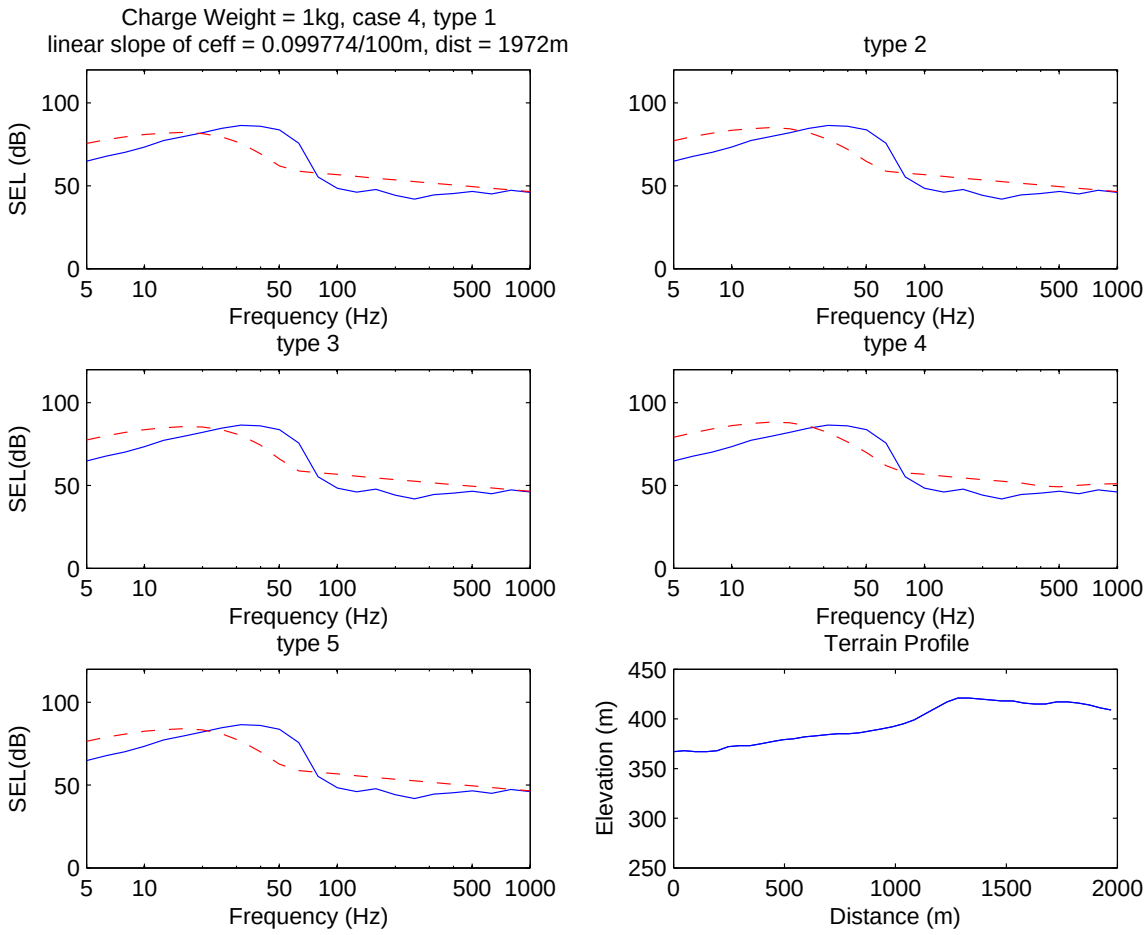
Charge Weight = 1kg, case 4, type 1
linear slope of ceff = 0.099774/100m, dist = 1972m
SEL (dB)
Frequency (Hz)
type 2
type 3
SEL(dB)
type 4
type 5
Terrain Profile
Elevation (m)
Distance (m)

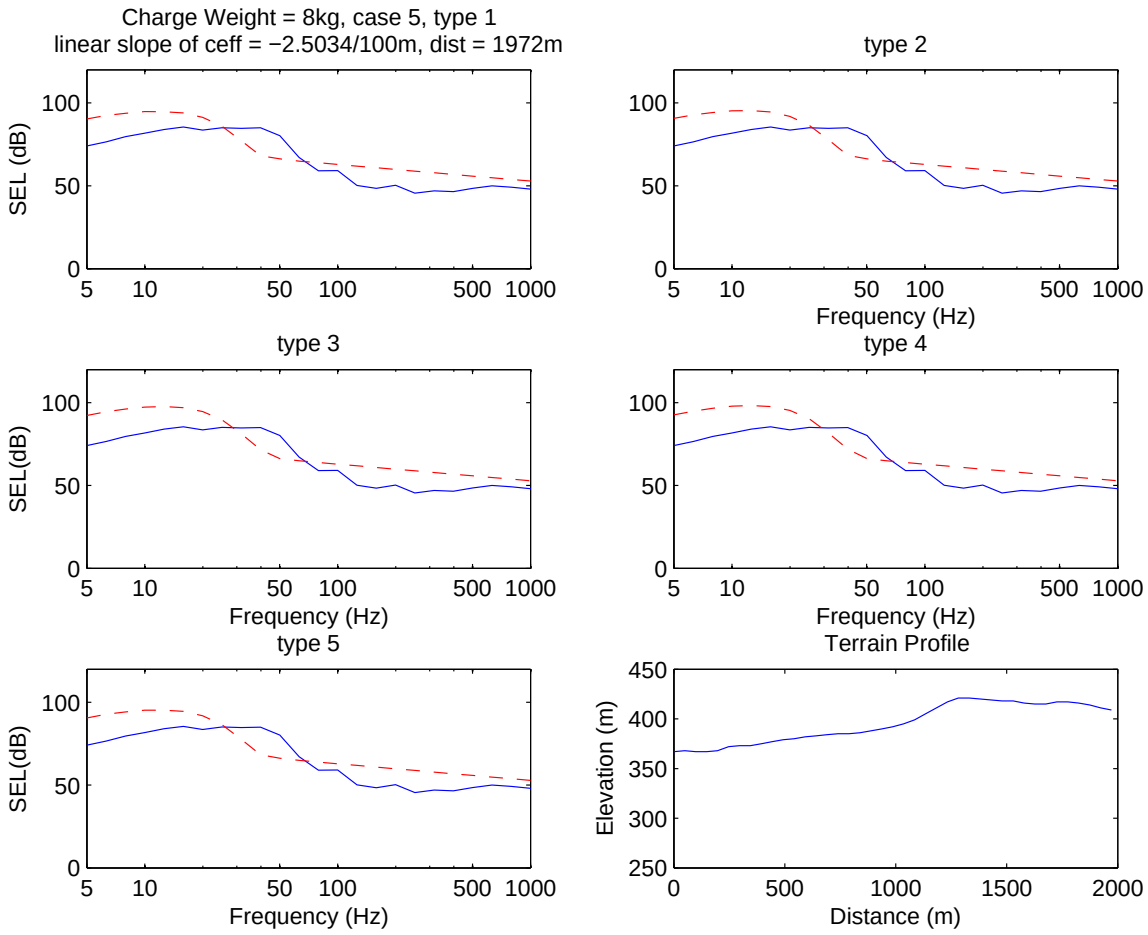
Charge Weight = 8kg, case 5, type 1
linear slope of ceff = −2.5034/100m, dist = 1972m
SEL (dB)
type 2
type 3
SEL(dB)
Frequency (Hz)
type 4
type 5
Terrain Profile
Elevation (m)
Distance (m)

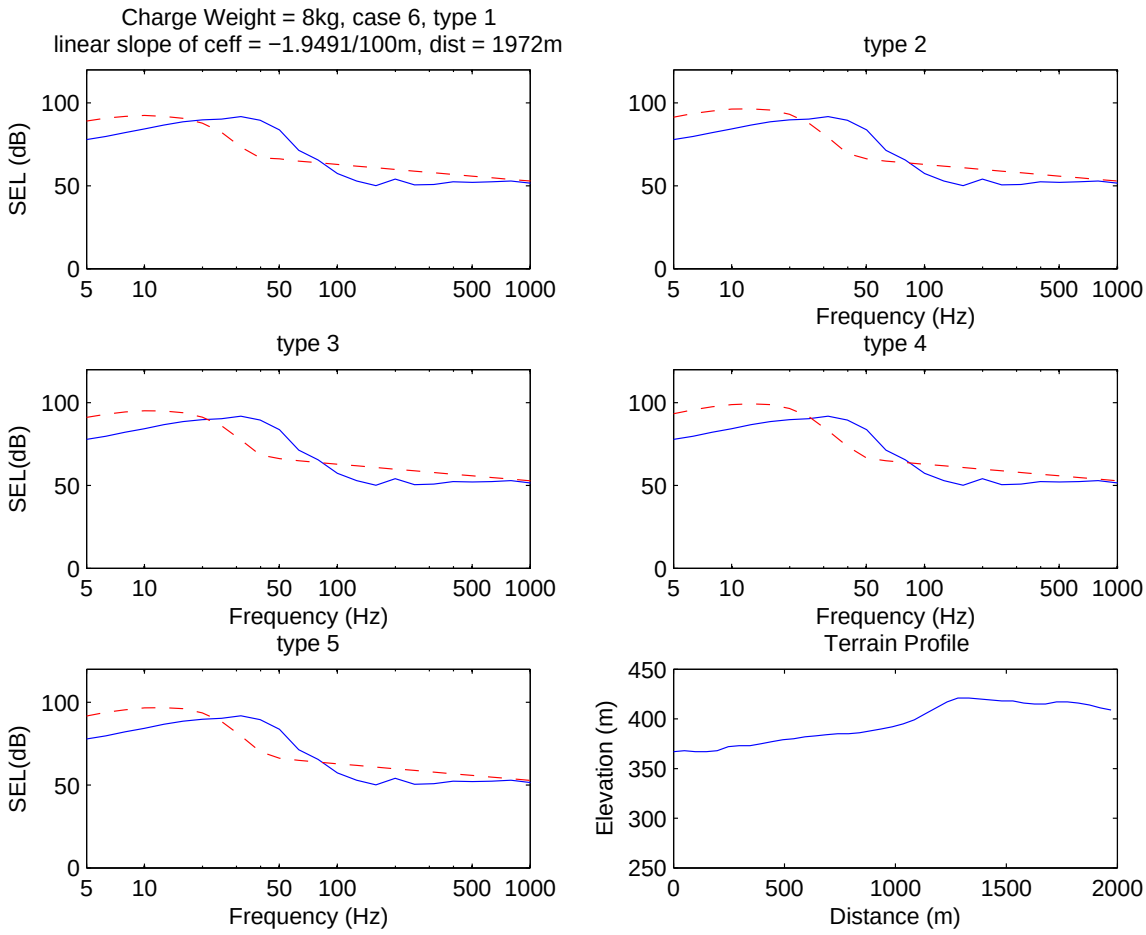
Charge Weight = 8kg, case 6, type 1
linear slope of ceff = −1.9491/100m, dist = 1972m
SEL (dB)
type 2
type 3
SEL(dB)
Frequency (Hz)
type 4
type 5
Terrain Profile
Elevation (m)
Distance (m)

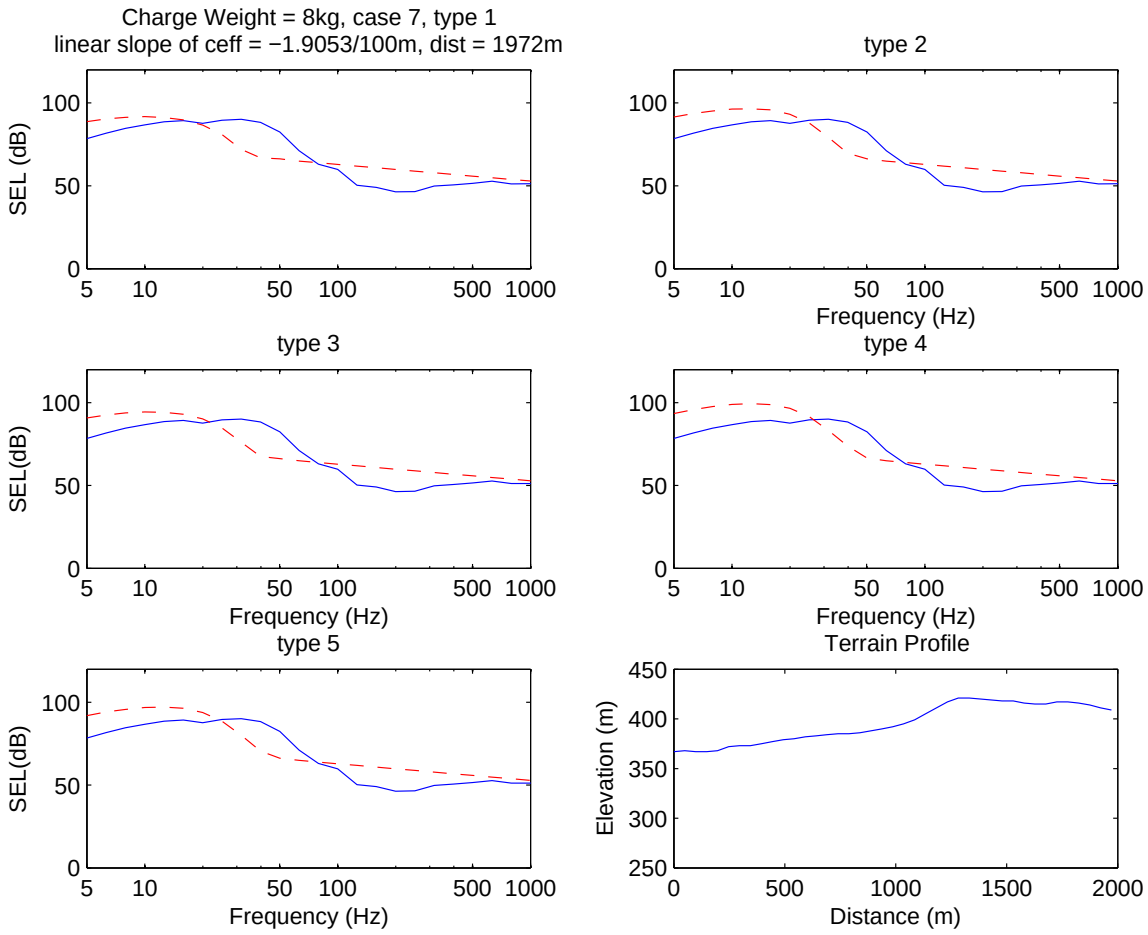
Charge Weight = 8kg, case 7, type 1
linear slope of ceff = −1.9053/100m, dist = 1972m
SEL (dB)
type 2
type 3
SEL(dB)
Frequency (Hz)
type 4
type 5
Terrain Profile
Elevation (m)
Distance (m)

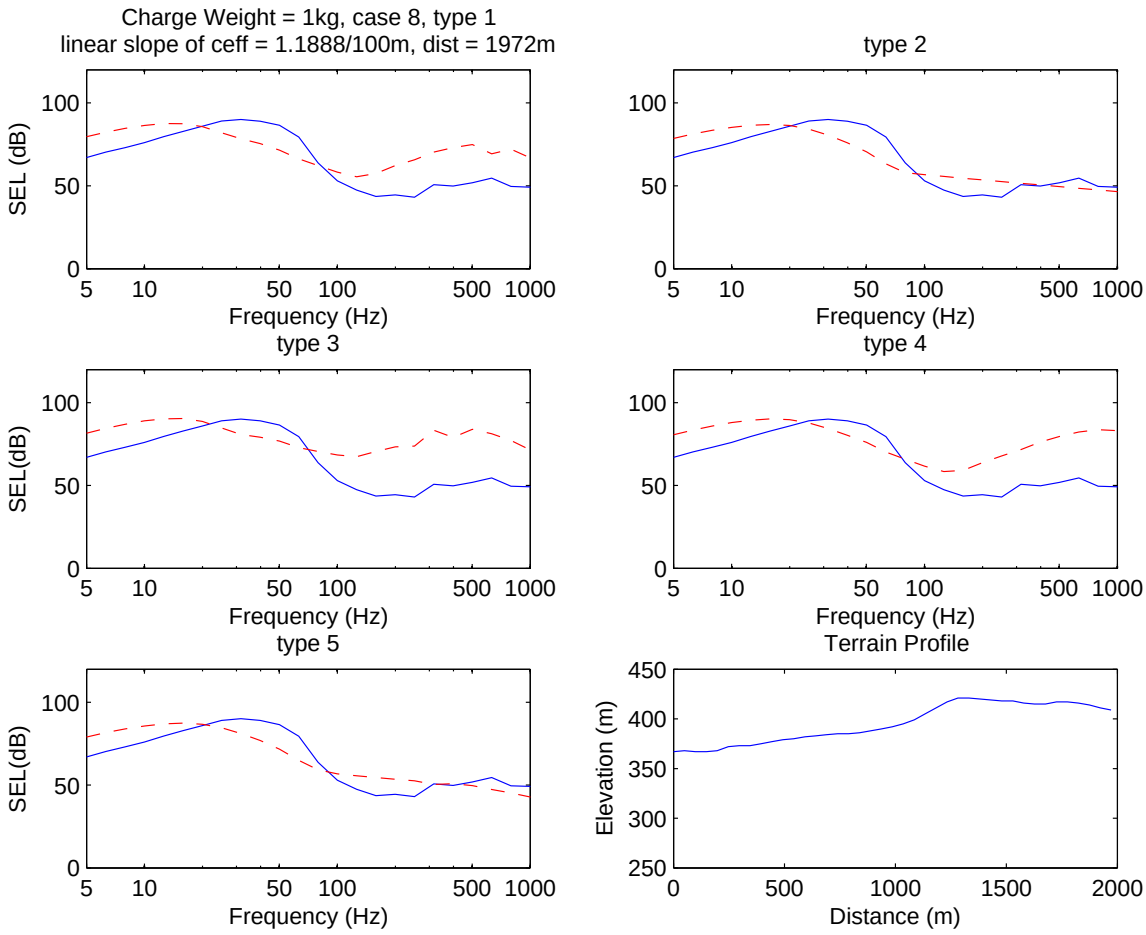
Charge Weight = 1kg, case 8, type 1
linear slope of ceff = 1.1888/100m, dist = 1972m
SEL (dB)
Frequency (Hz)
type 2
type 3
SEL(dB)
type 4
type 5
Terrain Profile
Elevation (m)
Distance (m)

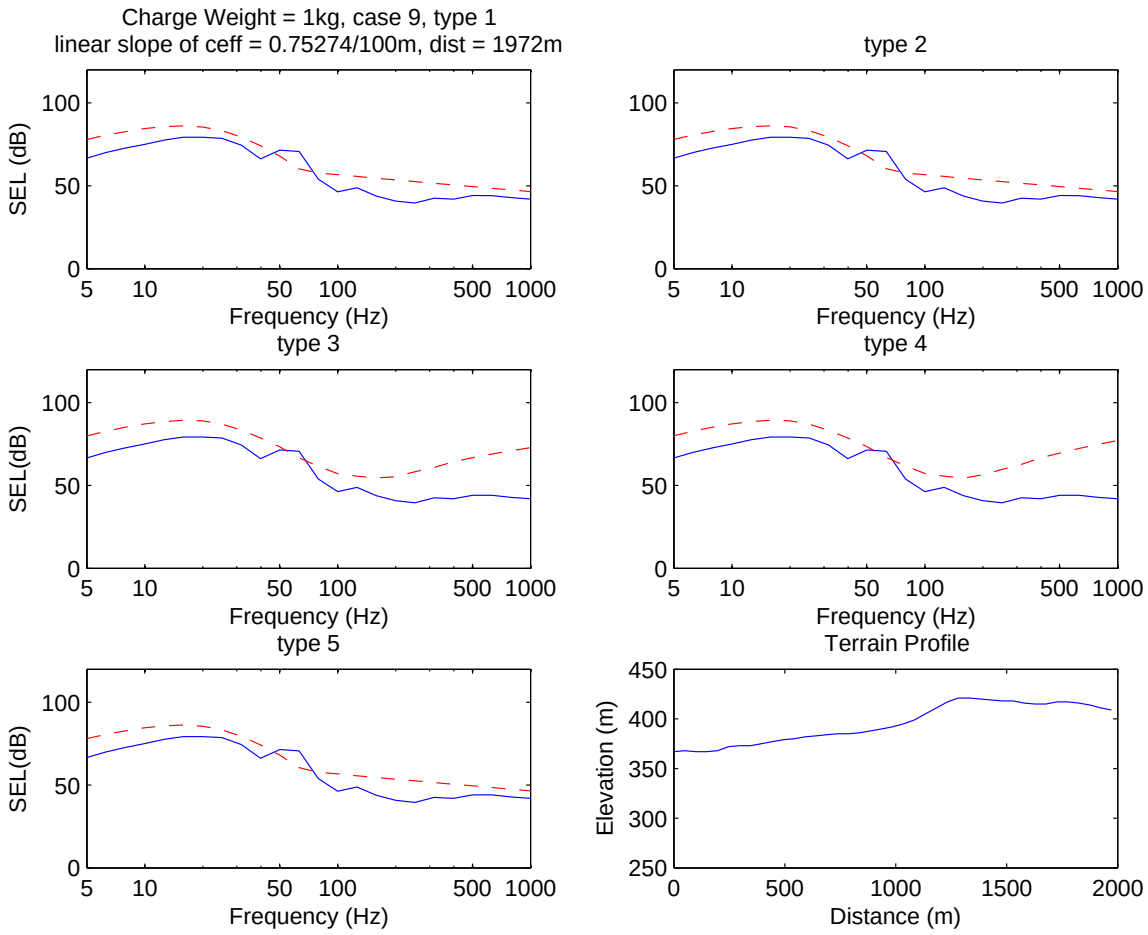
Charge Weight = 1kg, case 9, type 1
linear slope of ceff = 0.75274/100m, dist = 1972m
SEL (dB)
Frequency (Hz)
type 2
type 3
SEL(dB)
type 4
type 5
Terrain Profile
Elevation (m)
Distance (m)

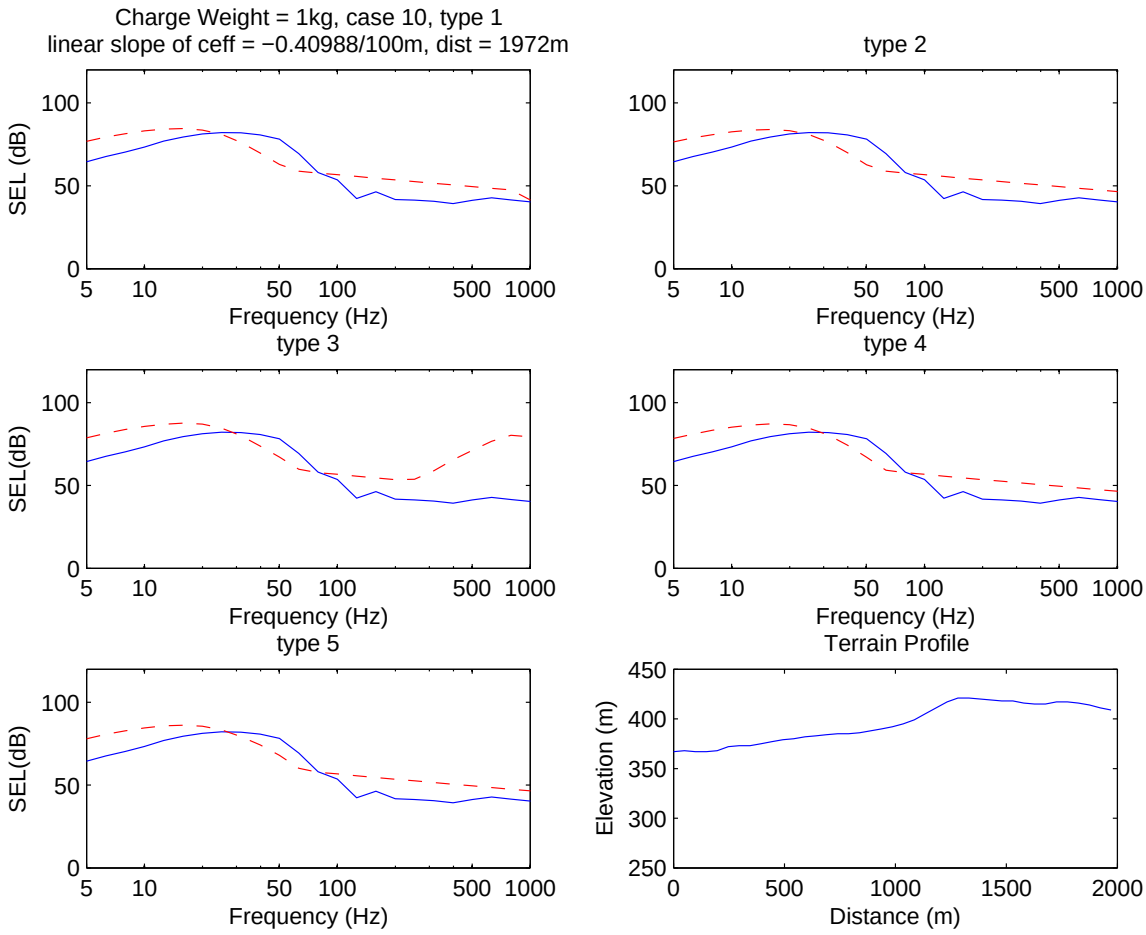
Charge Weight = 1kg, case 10, type 1
linear slope of ceff = −0.40988/100m, dist = 1972m
SEL (dB)
Frequency (Hz)
type 2
type 3
SEL(dB)
type 4
type 5
Terrain Profile
Elevation (m)
Distance (m)

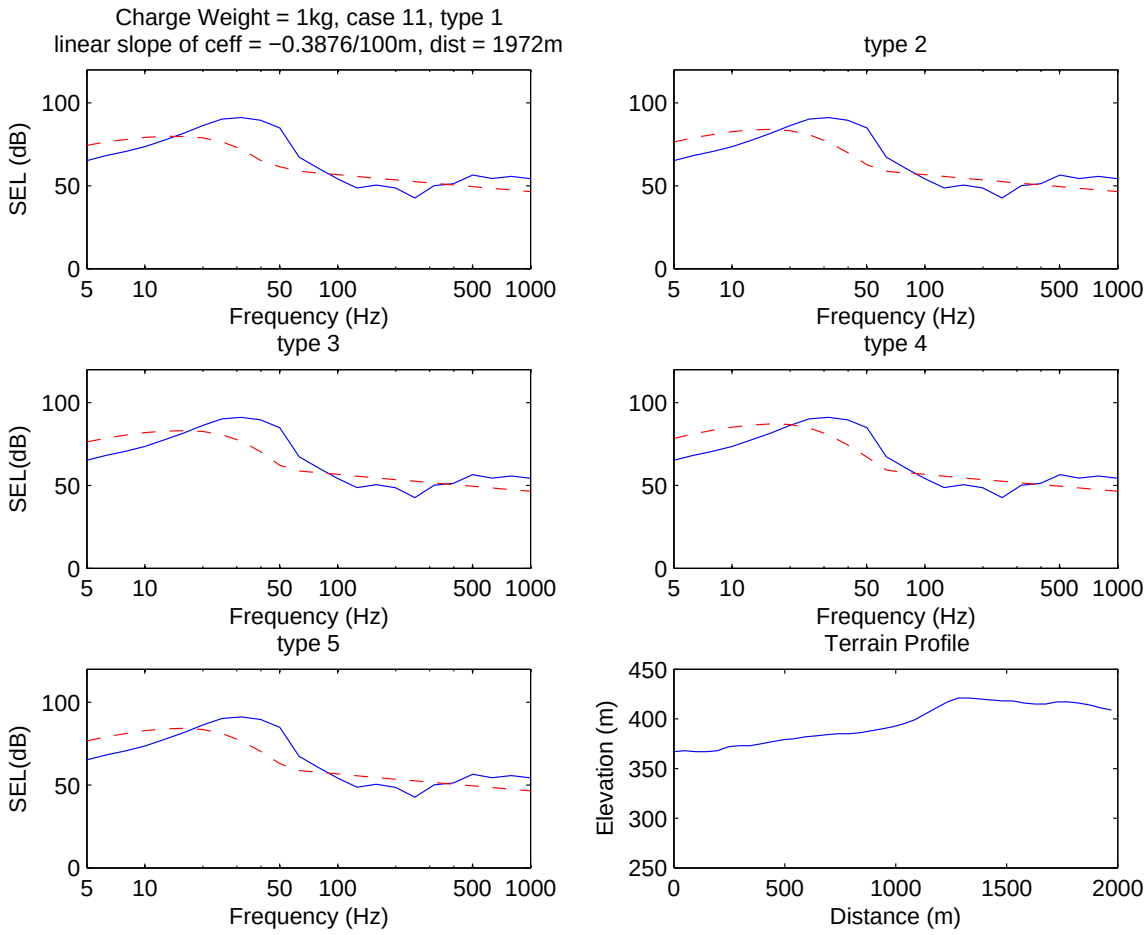
Charge Weight = 1kg, case 11, type 1
linear slope of ceff = −0.3876/100m, dist = 1972m
SEL (dB)
Frequency (Hz)
type 2
type 3
type 4
type 5
Terrain Profile
Elevation (m)
Distance (m)

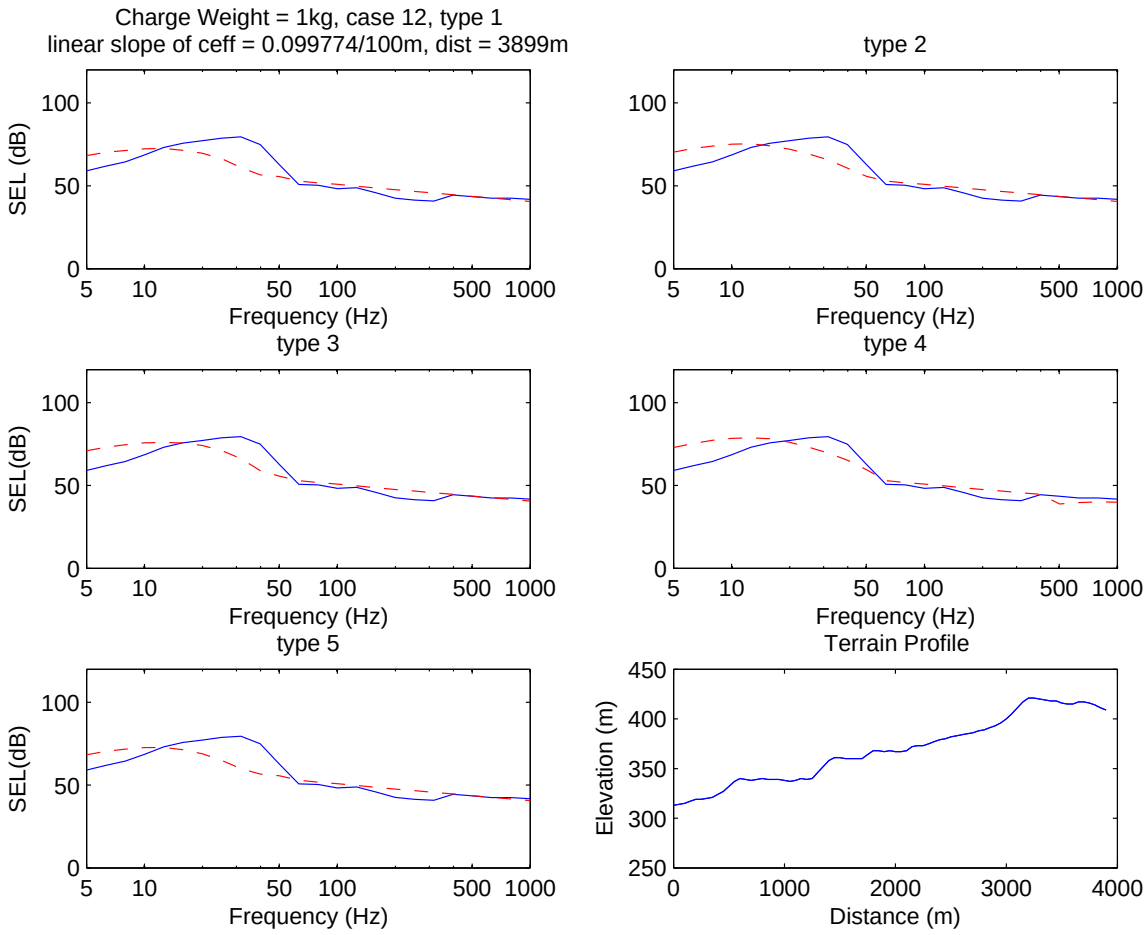
Charge Weight = 1kg, case 12, type 1
linear slope of ceff = 0.099774/100m, dist = 3899m
SEL (dB)
Frequency (Hz)
type 2
type 3
SEL(dB)
type 4
type 5
Terrain Profile
Elevation (m)
Distance (m)

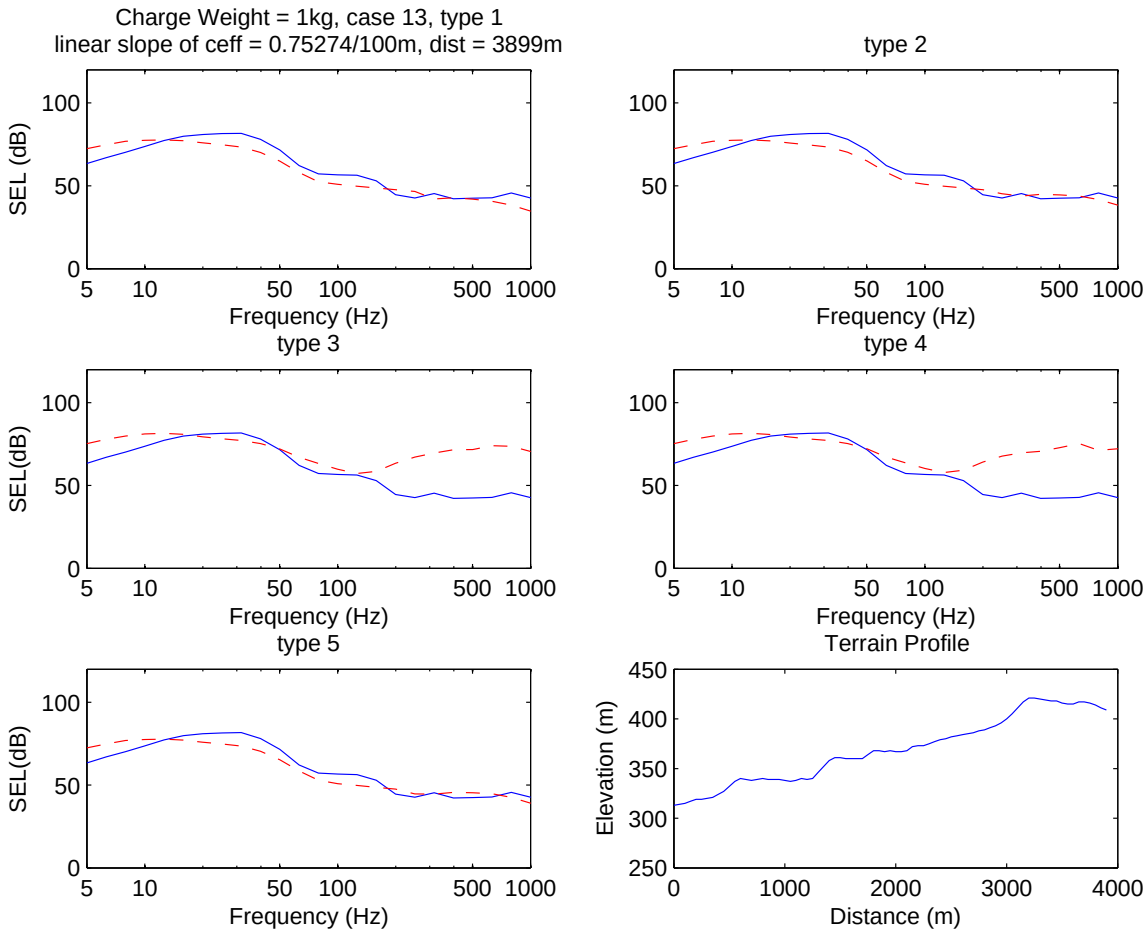
Charge Weight = 1kg, case 13, type 1
linear slope of ceff = 0.75274/100m, dist = 3899m
SEL (dB)
Frequency (Hz)
type 2
type 3
SEL(dB)
type 4
type 5
Terrain Profile
Elevation (m)
Distance (m)

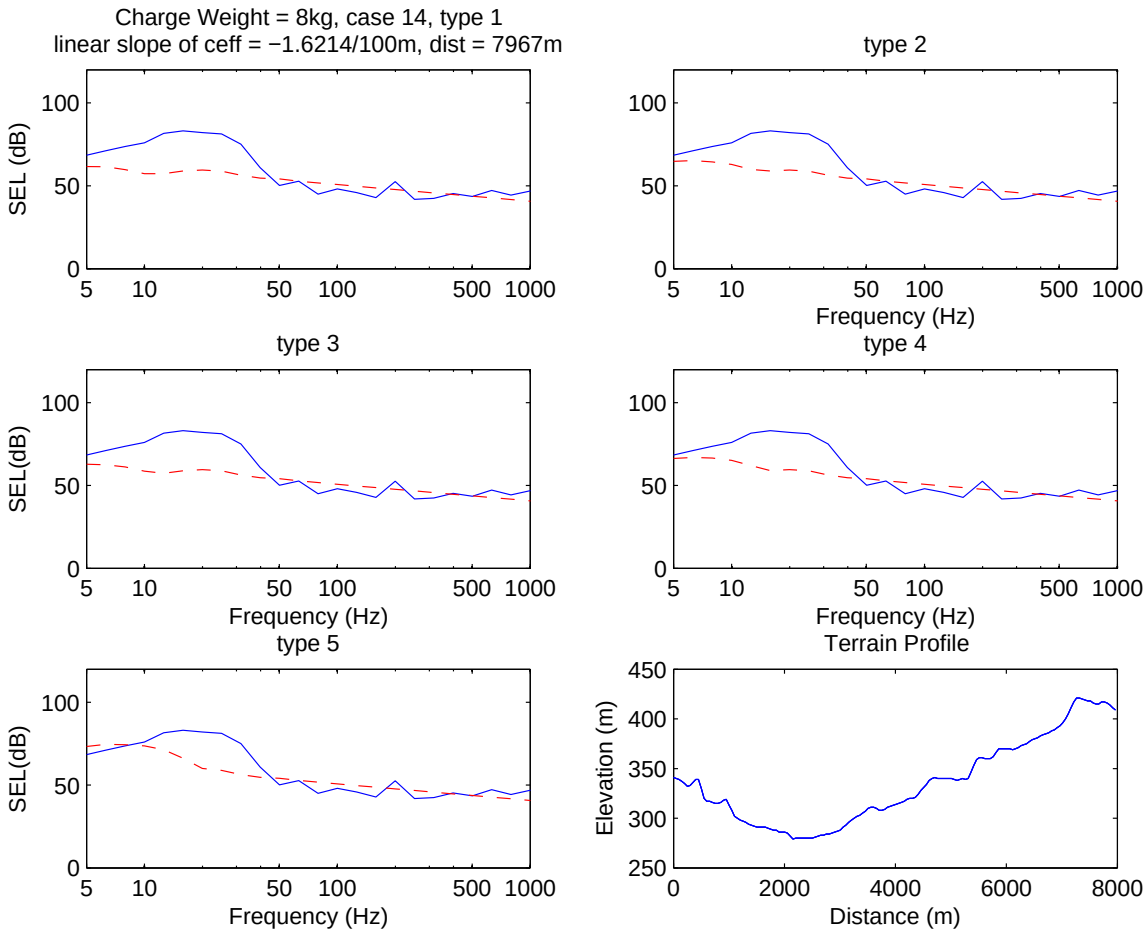
Charge Weight = 8kg, case 14, type 1
linear slope of ceff = −1.6214/100m, dist = 7967m
SEL (dB)
type 2
type 3
SEL(dB)
Frequency (Hz)
type 4
type 5
Terrain Profile
Elevation (m)
Distance (m)

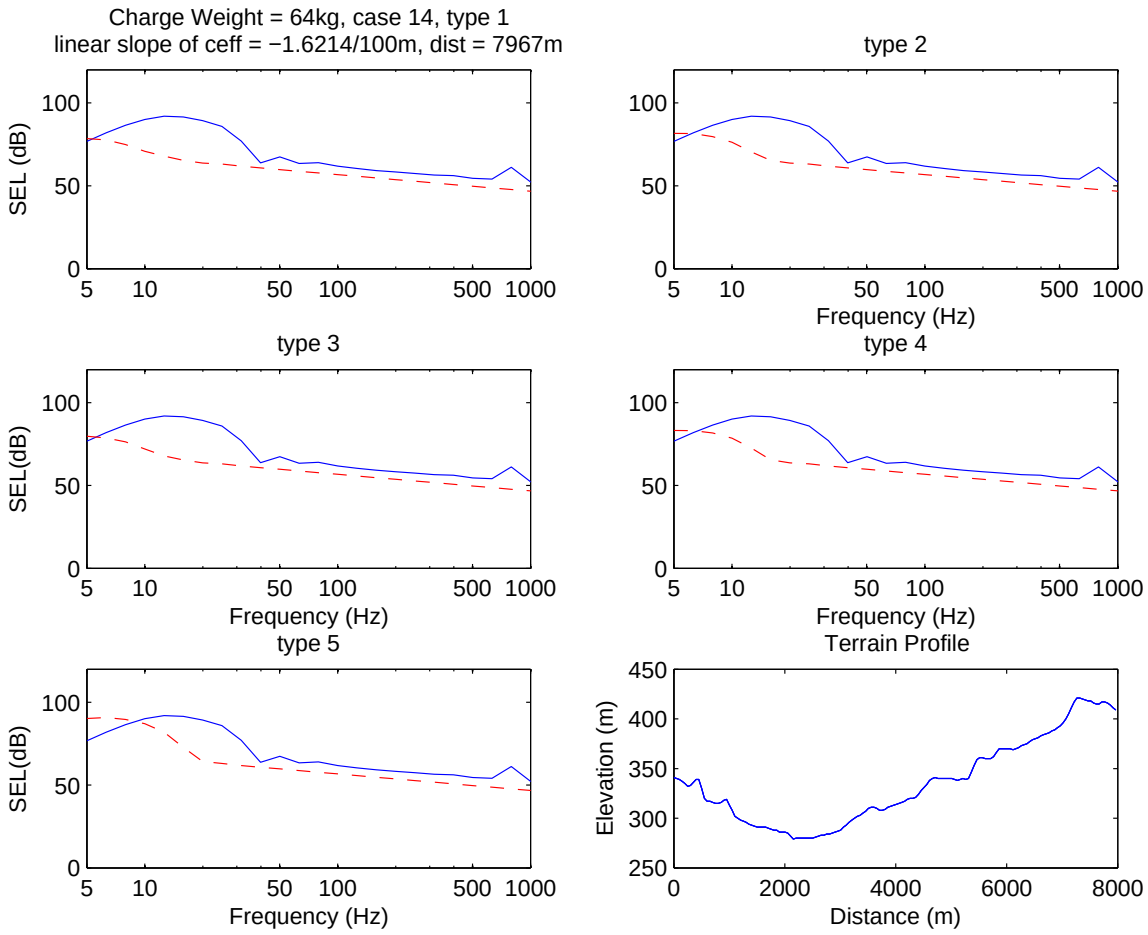
Charge Weight = 64kg, case 14, type 1
linear slope of ceff = −1.6214/100m, dist = 7967m
SEL (dB)
type 2
type 3
SEL(dB)
Frequency (Hz)
type 4
type 5
Terrain Profile
Elevation (m)
Distance (m)

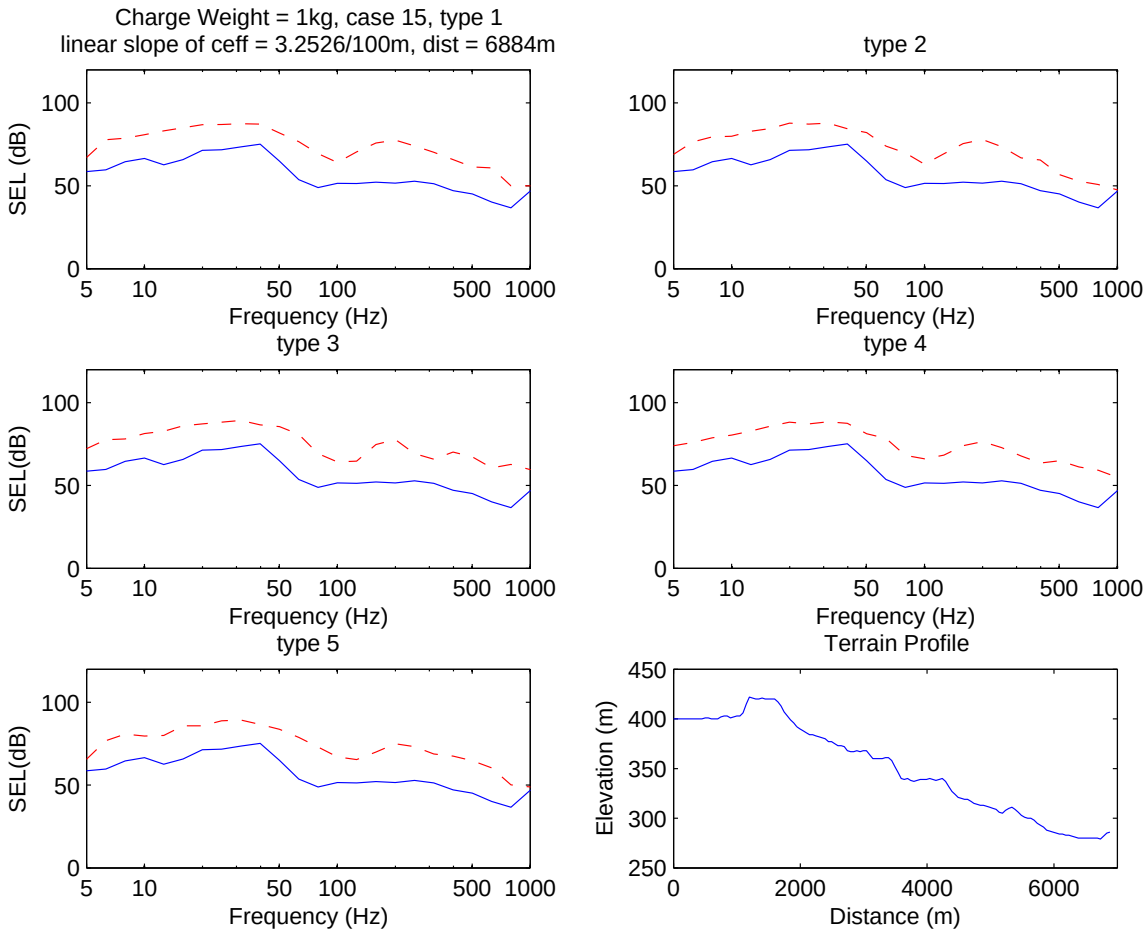
Charge Weight = 1kg, case 15, type 1
linear slope of ceff = 3.2526/100m, dist = 6884m
SEL (dB)
Frequency (Hz)
type 2
type 3
SEL(dB)
type 4
type 5
Terrain Profile
Elevation (m)
Distance (m)

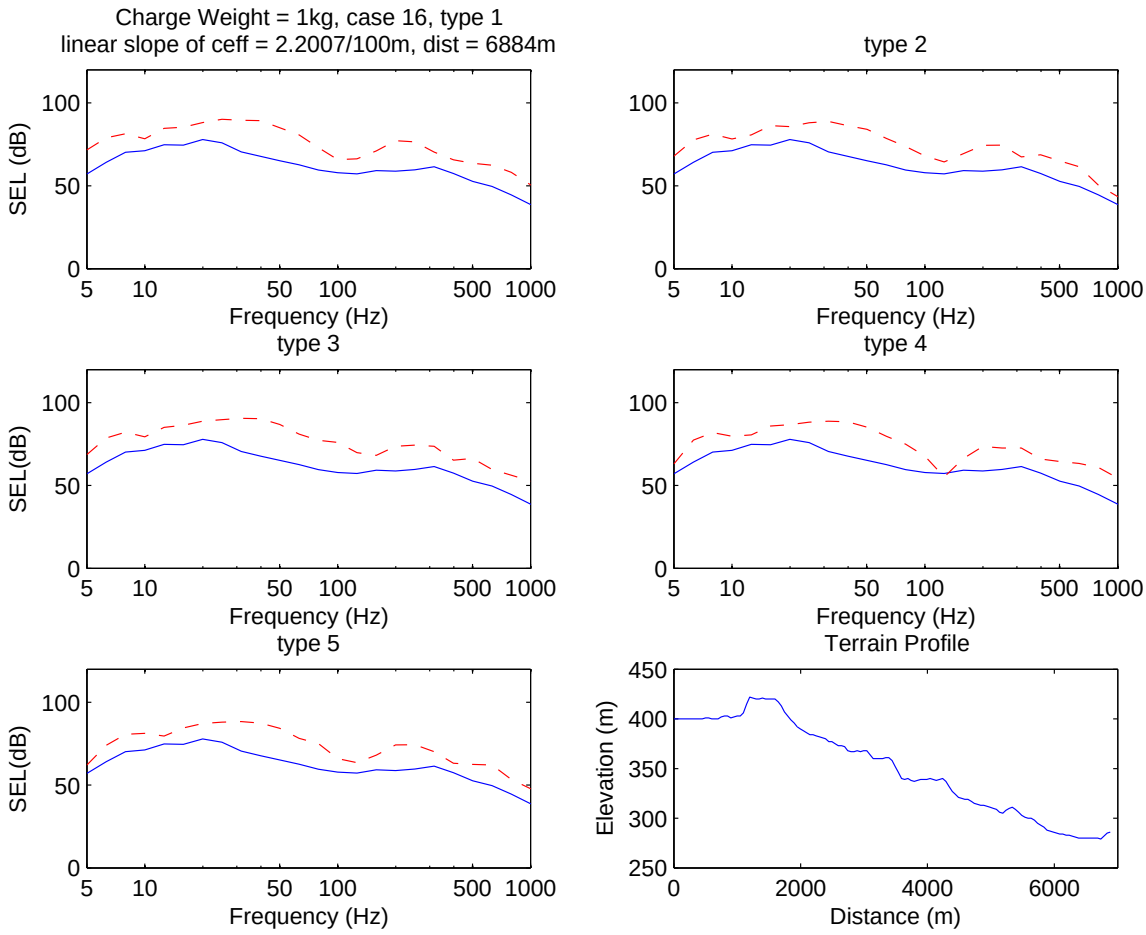
Charge Weight = 1kg, case 16, type 1
linear slope of ceff = 2.2007/100m, dist = 6884m
SEL (dB)
Frequency (Hz)
type 2
type 3
SEL(dB)
type 4
type 5
Terrain Profile
Elevation (m)
Distance (m)

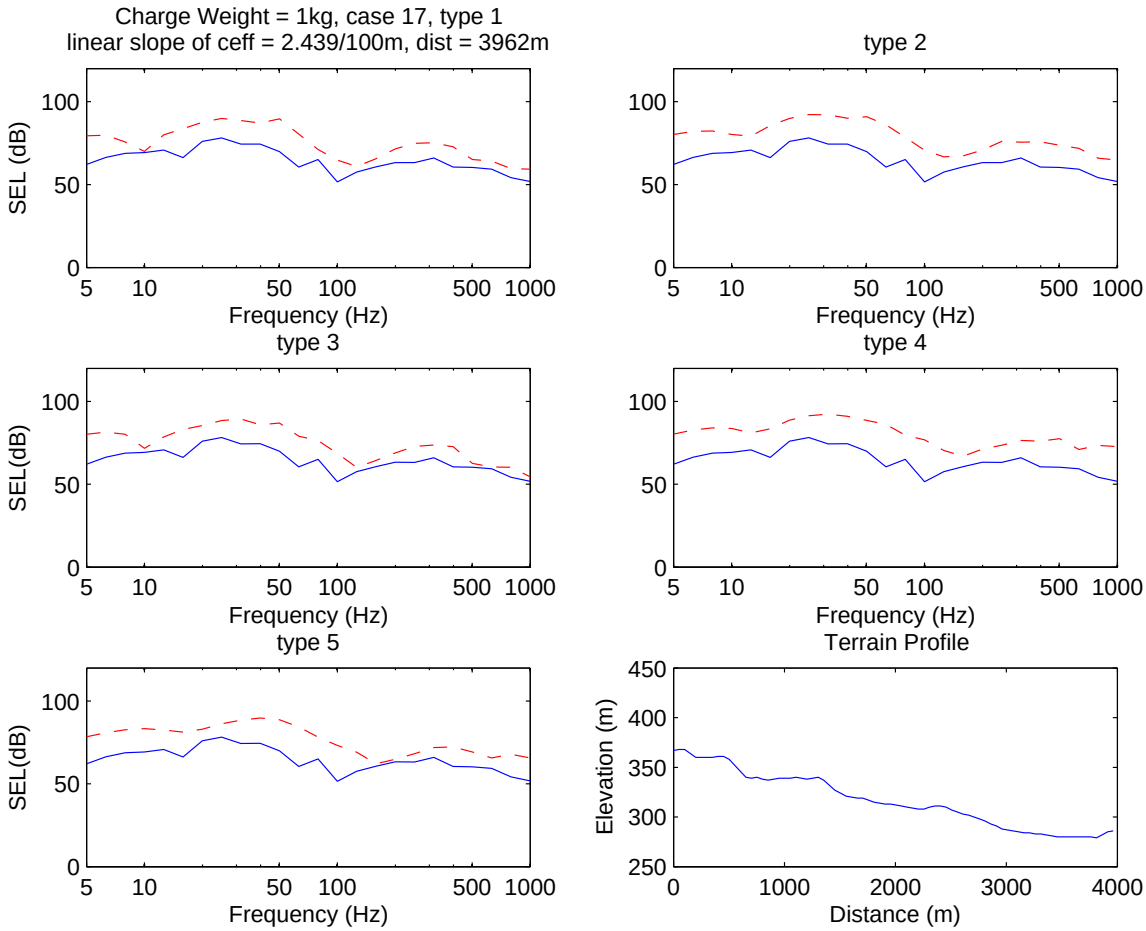
Charge Weight = 1kg, case 17, type 1
linear slope of ceff = 2.439/100m, dist = 3962m
SEL (dB)
Frequency (Hz)
type 2
type 3
SEL(dB)
type 4
type 5
Terrain Profile
Elevation (m)
Distance (m)

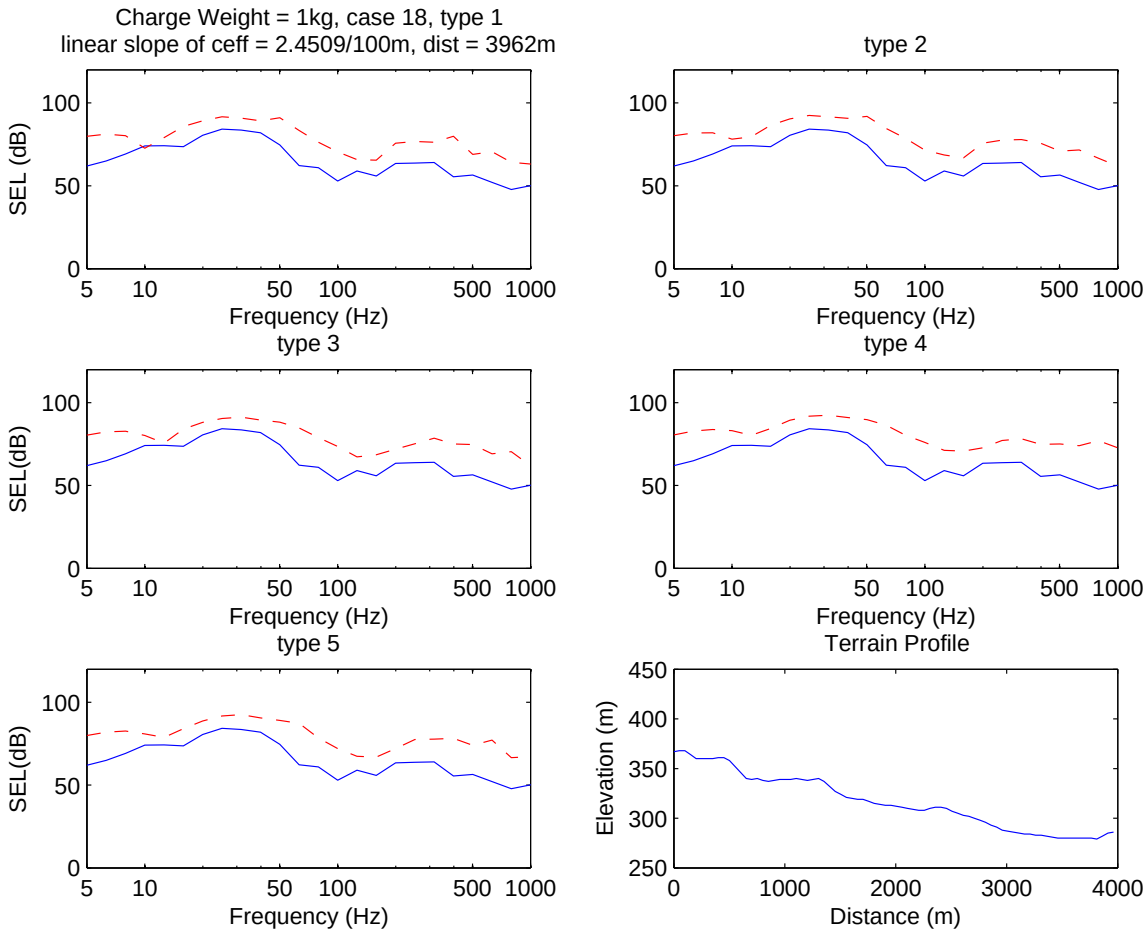
Charge Weight = 1kg, case 18, type 1
linear slope of ceff = 2.4509/100m, dist = 3962m
SEL (dB)
Frequency (Hz)
type 2
type 3
SEL(dB)
type 4
type 5
Terrain Profile
Elevation (m)
Distance (m)

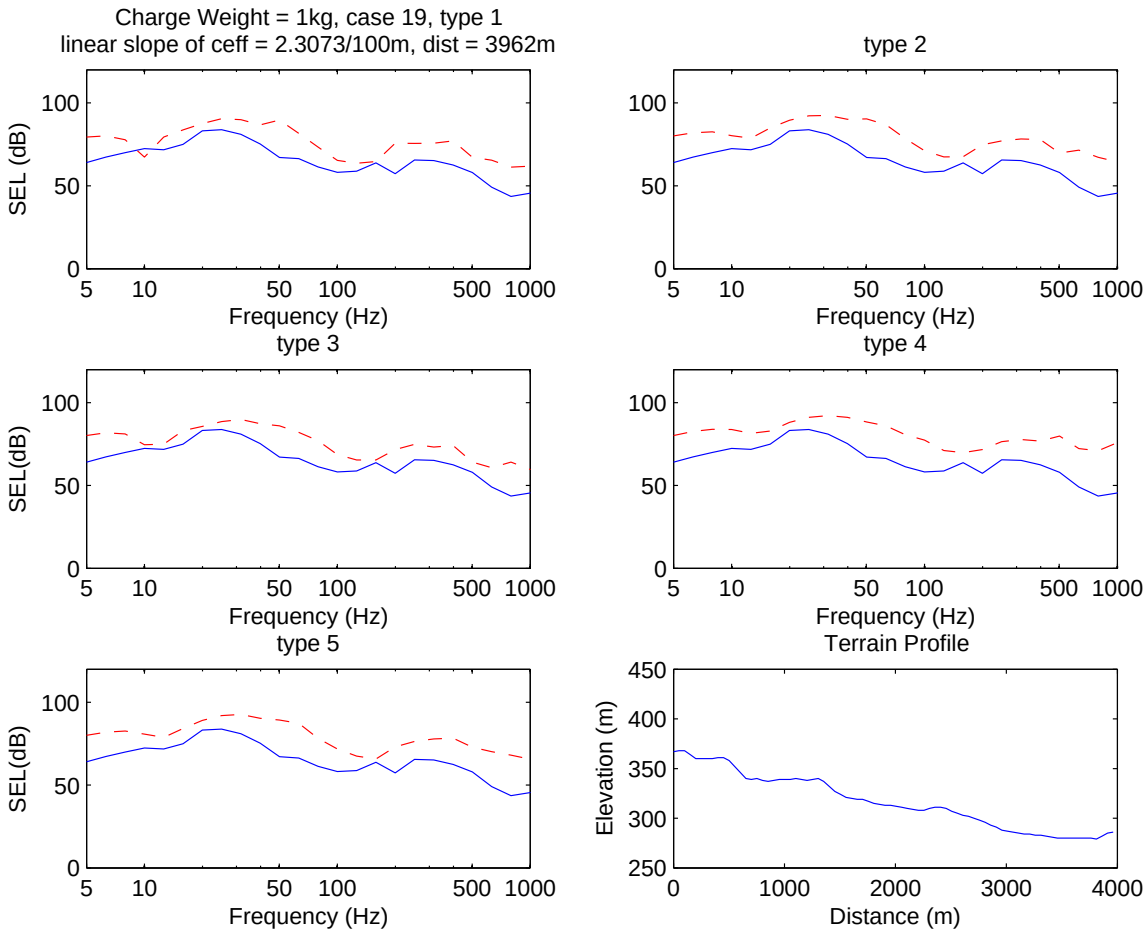
Charge Weight = 1kg, case 19, type 1
linear slope of ceff = 2.3073/100m, dist = 3962m
SEL (dB)
Frequency (Hz)
type 2
type 3
SEL(dB)
type 4
type 5
Terrain Profile
Elevation (m)
Distance (m)

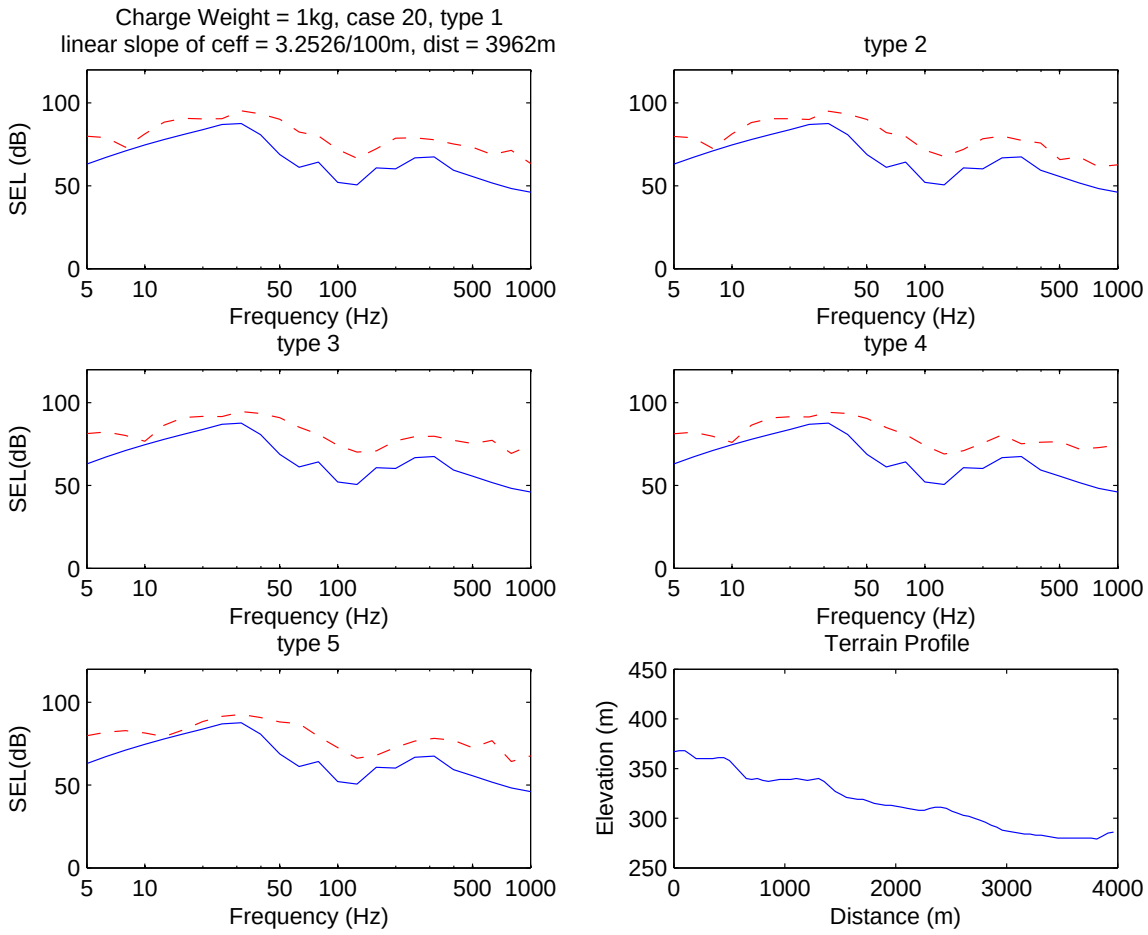
Charge Weight = 1kg, case 20, type 1
linear slope of ceff = 3.2526/100m, dist = 3962m
SEL (dB)
Frequency (Hz)
type 2
type 3
type 4
type 5
SEL(dB)
Terrain Profile
Elevation (m)
Distance (m)

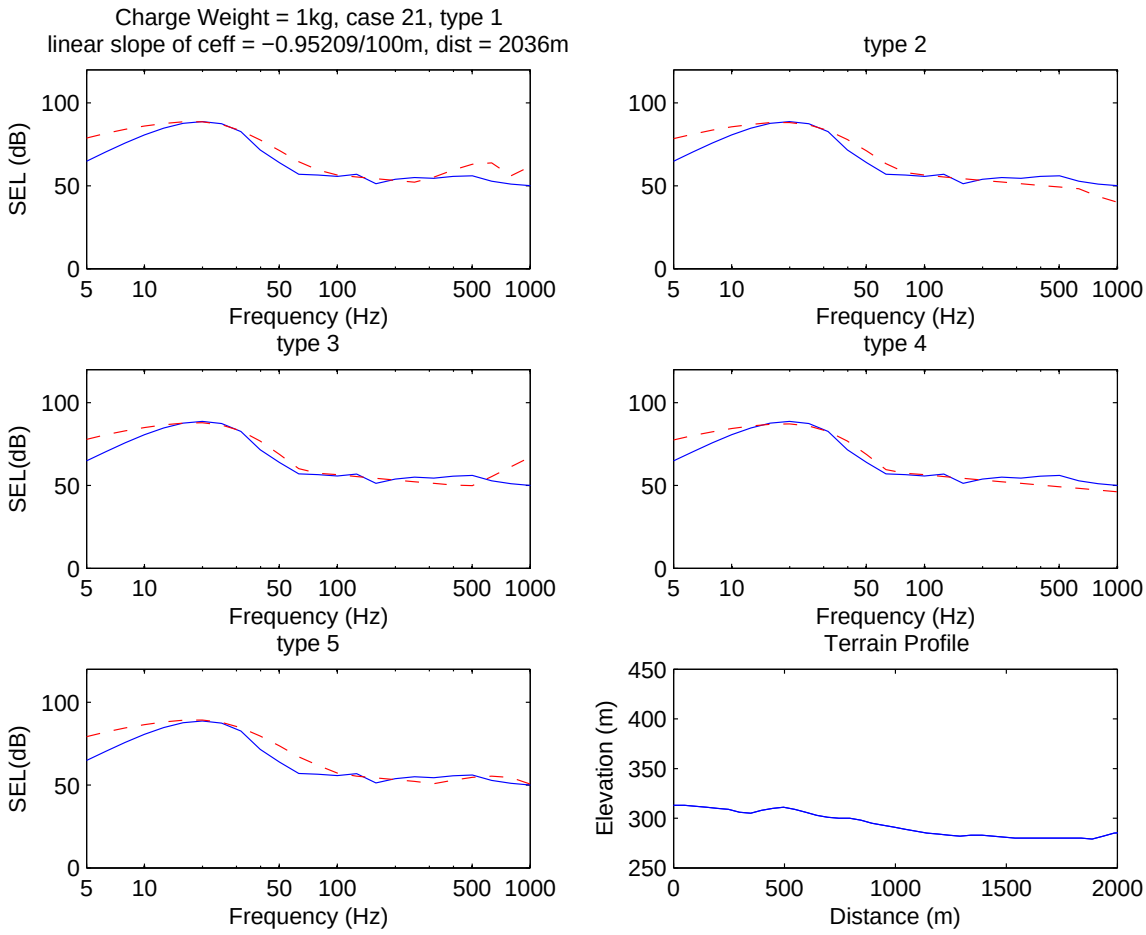
Charge Weight = 1kg, case 21, type 1
linear slope of ceff = −0.95209/100m, dist = 2036m
SEL (dB)
Frequency (Hz)
type 2
type 3
SEL(dB)
type 4
type 5
Terrain Profile
Elevation (m)
Distance (m)

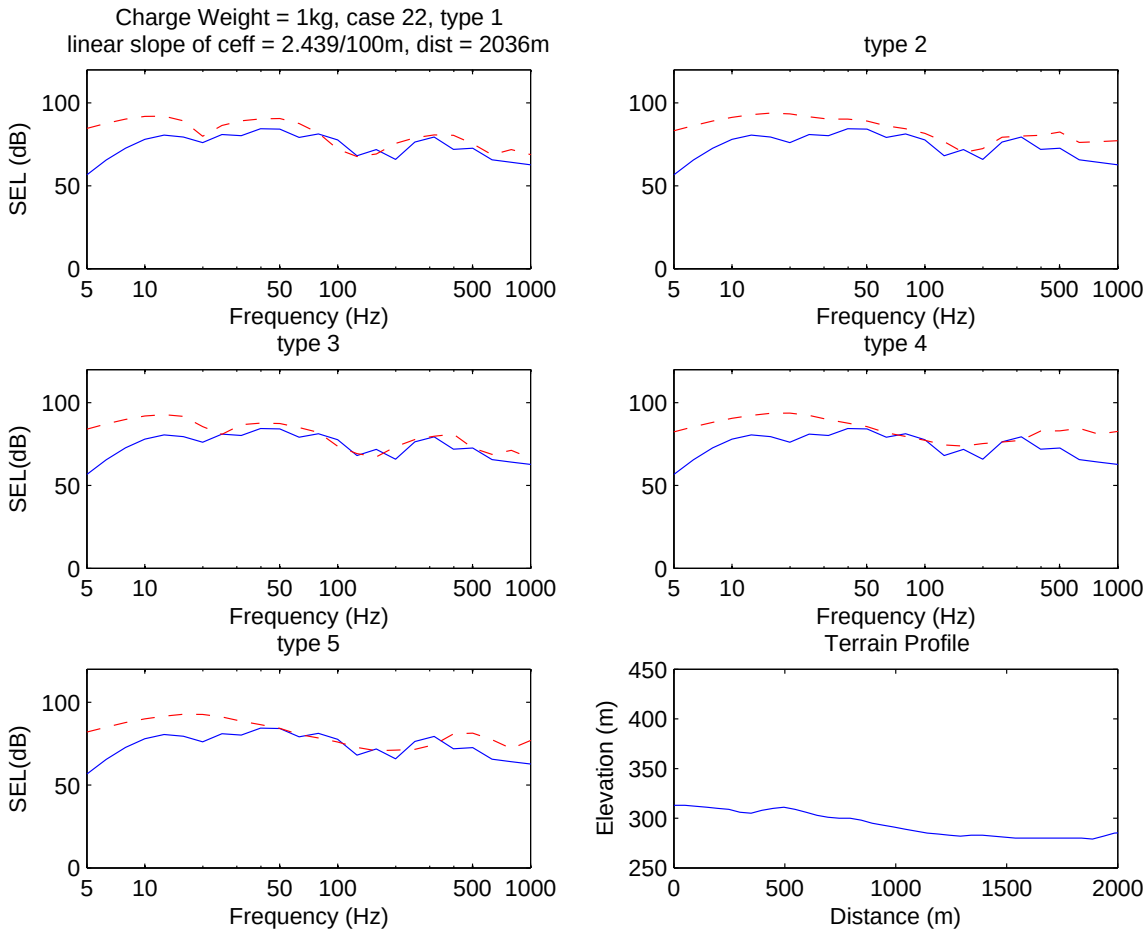
Charge Weight = 1kg, case 22, type 1
linear slope of ceff = 2.439/100m, dist = 2036m
SEL (dB)
Frequency (Hz)
type 2
type 3
SEL(dB)
type 4
type 5
Terrain Profile
Elevation (m)
Distance (m)

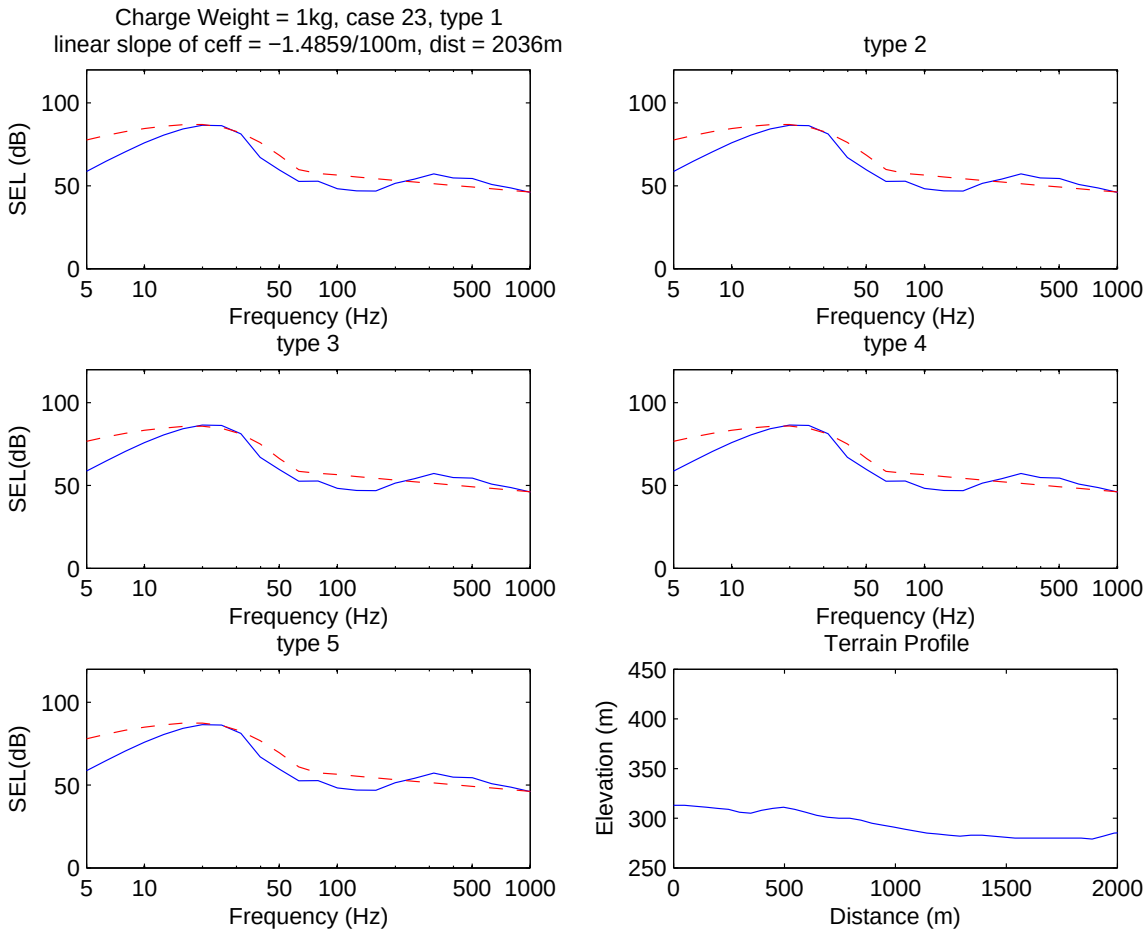
Charge Weight = 1kg, case 23, type 1
linear slope of ceff = −1.4859/100m, dist = 2036m
SEL (dB)
Frequency (Hz)
type 2
type 3
SEL(dB)
type 4
type 5
Terrain Profile
Elevation (m)
Distance (m)

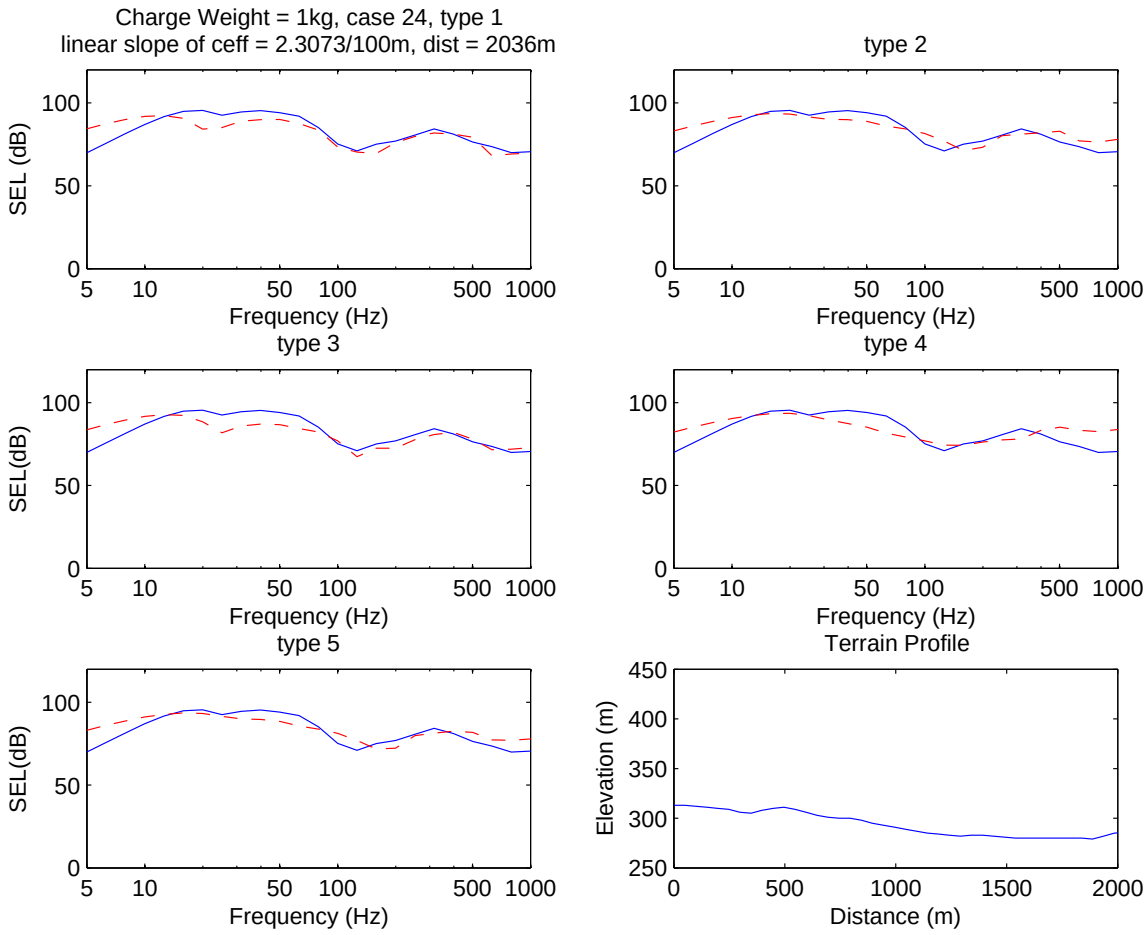
Charge Weight = 1kg, case 24, type 1
linear slope of ceff = 2.3073/100m, dist = 2036m
SEL (dB)
Frequency (Hz)
type 2
type 3
SEL(dB)
type 4
type 5
Terrain Profile
Elevation (m)
Distance (m)

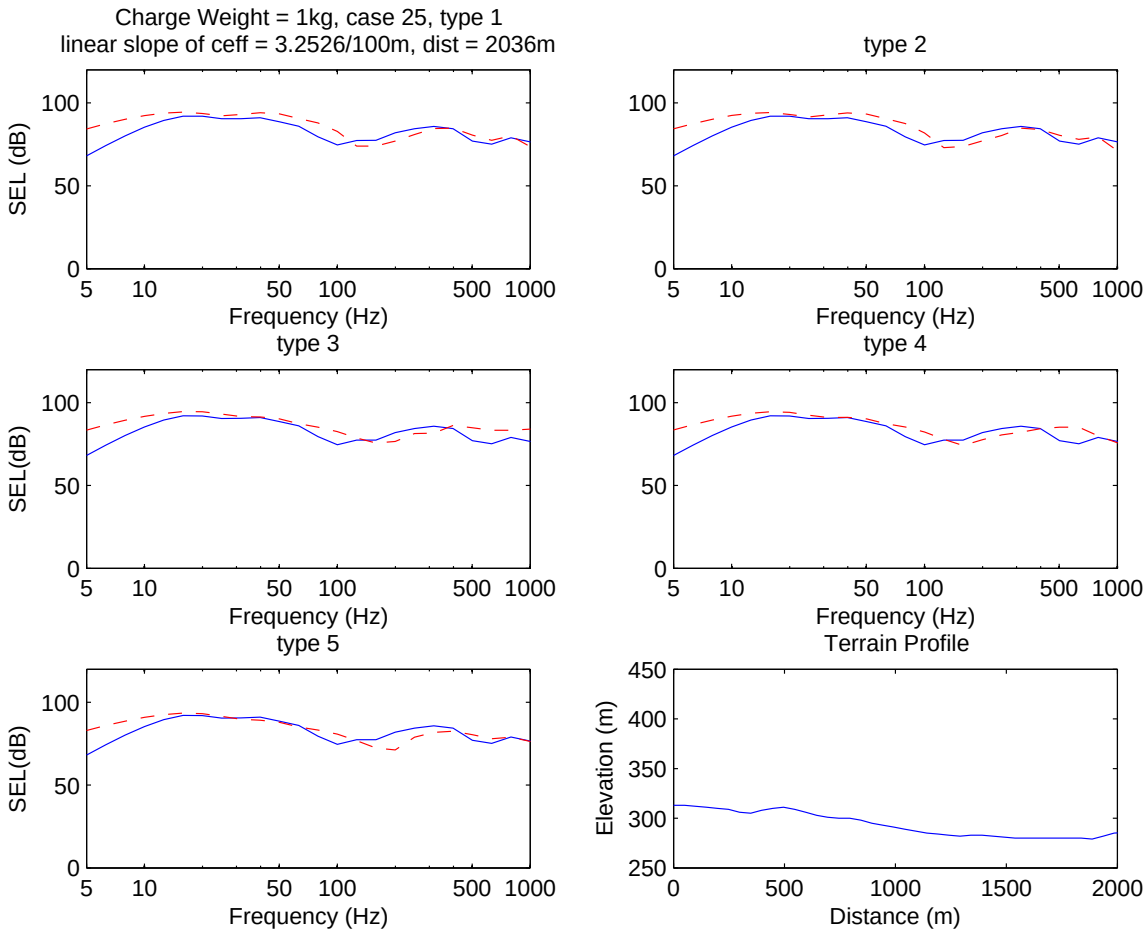
Charge Weight = 1kg, case 25, type 1
linear slope of ceff = 3.2526/100m, dist = 2036m
SEL (dB)
Frequency (Hz)
type 2
type 3
SEL(dB)
type 4
type 5
Terrain Profile
Elevation (m)
Distance (m)

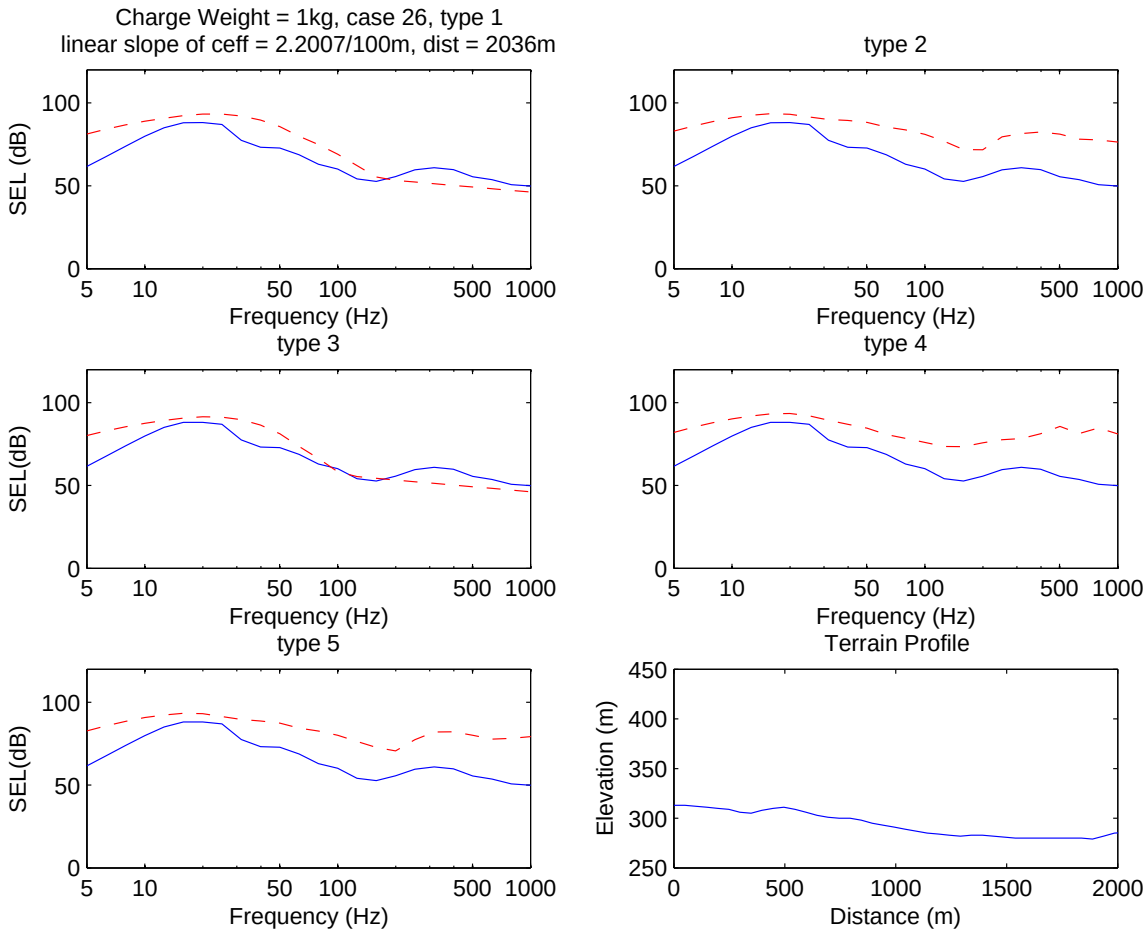
Charge Weight = 1kg, case 26, type 1
linear slope of ceff = 2.2007/100m, dist = 2036m
SEL (dB)
Frequency (Hz)
type 2
type 3
SEL(dB)
type 4
type 5
Terrain Profile
Elevation (m)
Distance (m)

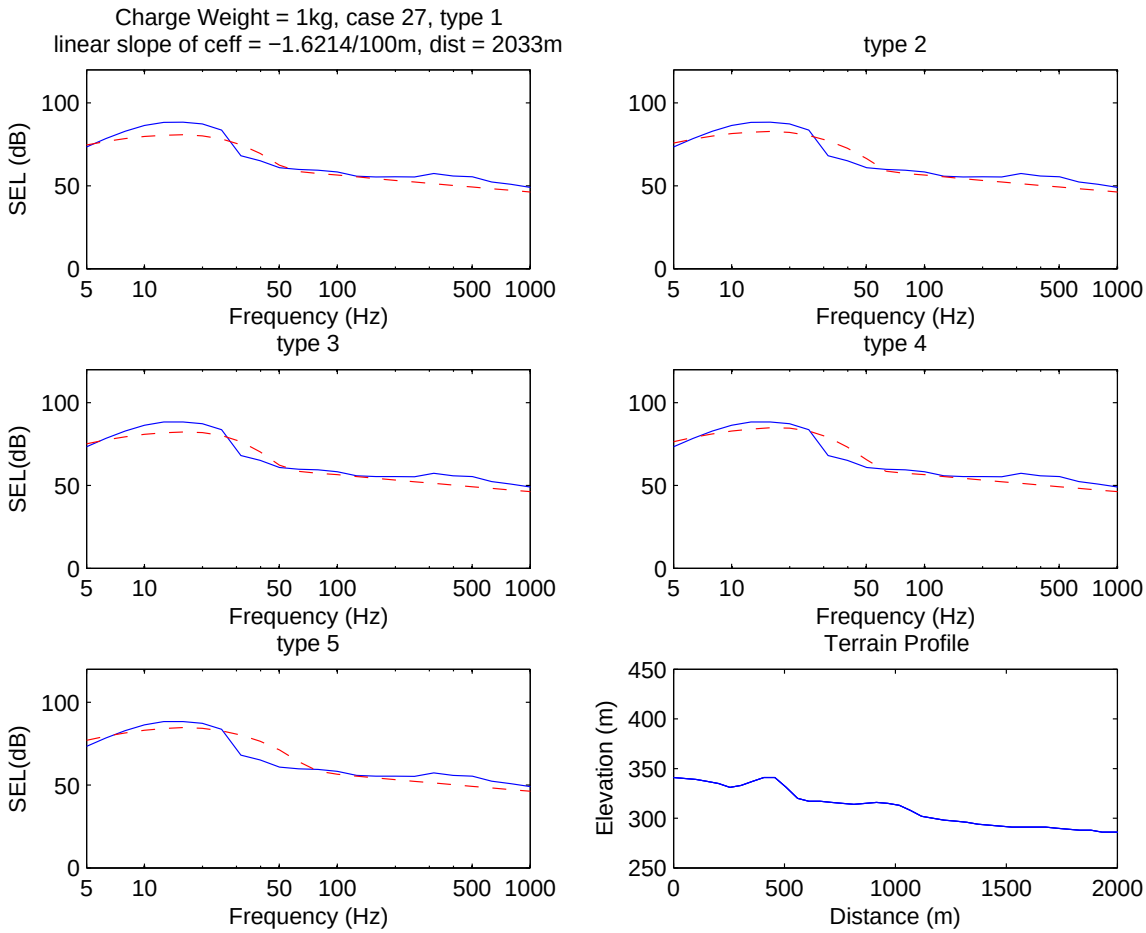
Charge Weight = 1kg, case 27, type 1
linear slope of ceff = −1.6214/100m, dist = 2033m
SEL (dB)
Frequency (Hz)
type 2
type 3
SEL(dB)
type 4
type 5
Terrain Profile
Elevation (m)
Distance (m)

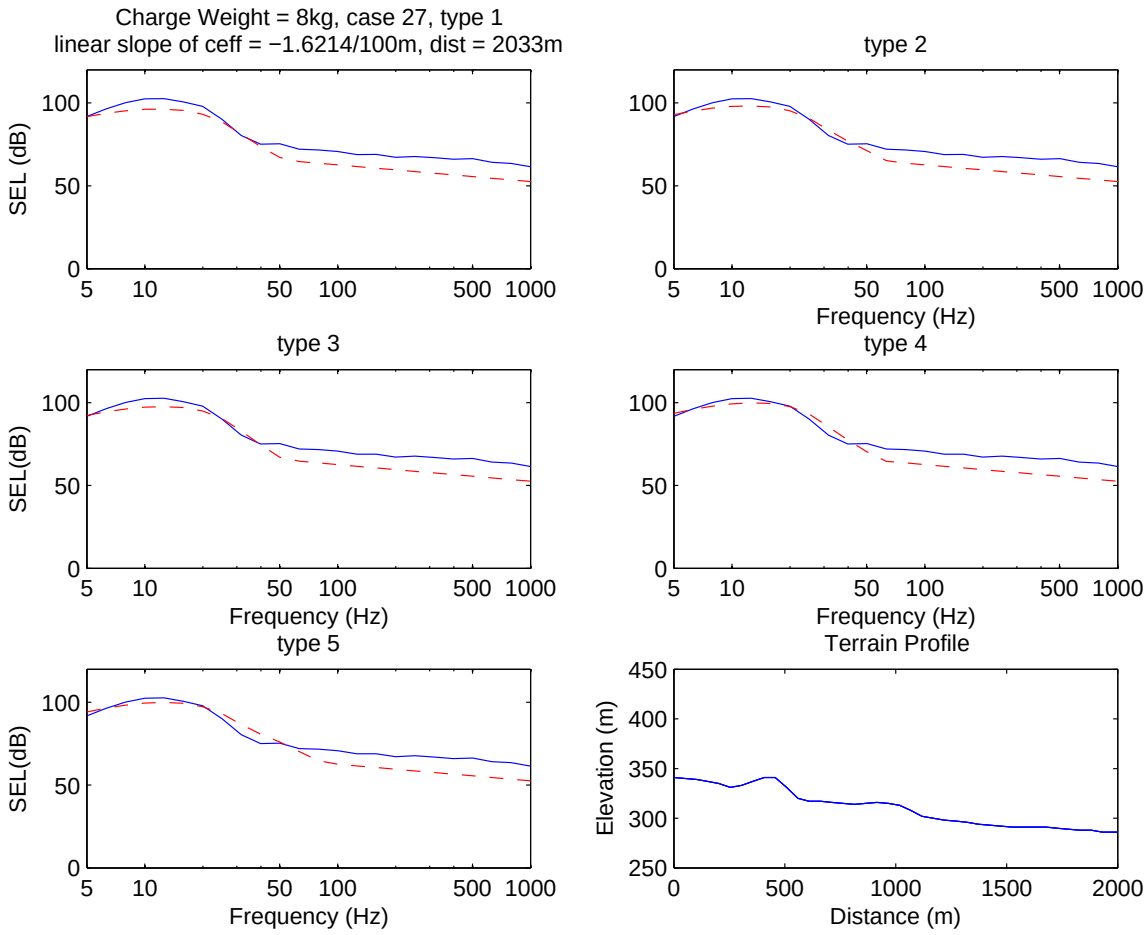
Charge Weight = 8kg, case 27, type 1
linear slope of ceff = −1.6214/100m, dist = 2033m
SEL (dB)
type 2
type 3
SEL(dB)
Frequency (Hz)
type 4
type 5
Terrain Profile
Elevation (m)
Distance (m)

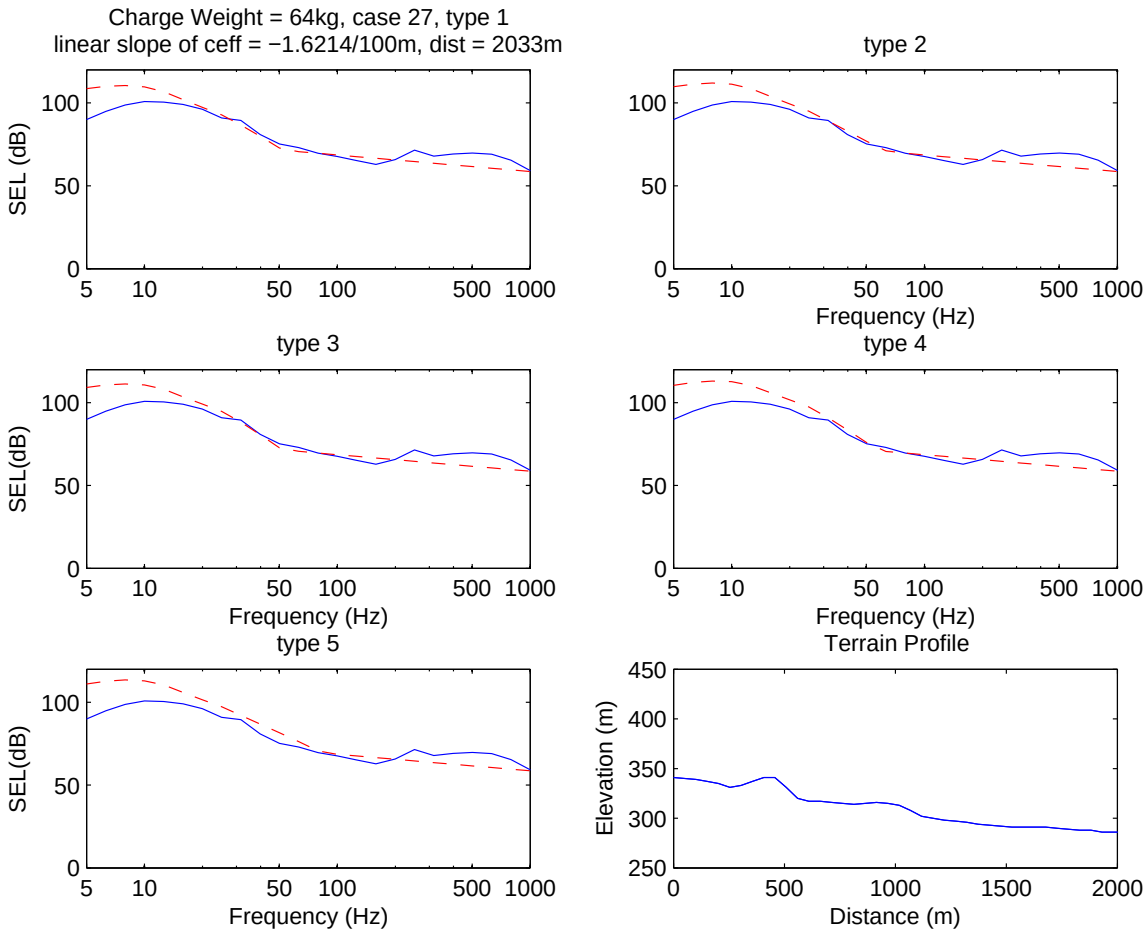
Charge Weight = 64kg, case 27, type 1
linear slope of ceff = −1.6214/100m, dist = 2033m
SEL (dB)
type 2
type 3
SEL(dB)
Frequency (Hz)
type 4
type 5
Terrain Profile
Elevation (m)
Distance (m)

References

[1] B. Plovsing and J. Kragh. Nord2000. Comprehensive outdoor sound propagation model. Part 1: Propagation in an atmosphere without significant refraction. DELTA Acoustica & vibration report AV 1849/00, 2001.

[2] B. Plovsing and J. Kragh. Nord2000. Comprehensive outdoor sound propagation model. Part 1: Propagation in an atmosphere with refraction. DELTA Acoustica & vibration report AV 1851/00, 2001.

[3] M. Huseby. A selection of data from measurements of C4 detonations at Finnskogen in 1994, test case C1. FFI-rapport 2007/00528, Norwegian Defence Research Establishment, 2007.

[4] R. Rahimi and M. Huseby. Innledende testing av utviklingsversjon av MILSTØY II: Testutvalg C1 fra NORTRIAL. FFI-notat 2007/00766, Norwegian Defence Research Establishment, 2007.

[5] R. Rahimi and M. Huseby. Innledende testing av utviklingsversjon av MILSTØY II: Testutvalg C2 fra NORTRIAL. FFI-notat 2007/01867, Norwegian Defence Research Establishment, 2007.

[6] M. Huseby, R. Rahimi, J. A. Teland, I Dyrdal, H. Fykse, B. Hugsted, C. E. Wasberg, E. Aker, R. Cleave, F. Løvholt, C. Madshus, K. Rothschild, H. Olsen, S. Storeheier, and G. Taraldsen. Final report: Improvement of the computational methods of the Norwegian Defence Estates Agency for computing noise from the Norwegian defence training ranges. FFI-rapport 2007/02602, Joint report by: Norwegian Defence Research Establishment (FFI), Norwegian Geotechnical Institute (NGI) and SINTEF ICT, 2008.

[7] B. L. Andersson, A. Cederholm, M. Huseby, I. Karasalo, and U. Tengzelius. Validation of a ray-tracer for long range noise-prediction using noise measurements from Finnskogen available in the NORTRIAL database. In R. Korneliussen, editor, *Proceedings 30th Scandinavian Symposium on Physical Acoustics*, Ustaoset, Norway, 28–31 Jan, 2007. ISBN 978-82-8123-002-6.

[8] From a series of confidential contractor reports made for ERDC-CERL detailing development and testing of BNoise, produced between 1998 and 2003.

[9] C. M. Madshus, E. Aker, F. Løvholt, R. Cleave, and N. I. Nilsen. NORTRIAL database on long range low frequency sound and vibration propagation. INTER-NOISE 2006, December 2006.

[10] IEC 61672-1. Electroacoustics – sound level meters – part 1: Specifications, 2002.

[11] M. Huseby, B. Hugsted, I. Dyrdal, H. Fykse, and A. Jordet. Målinger av lydtrykket nær lette våpen, Terningmoen, revidert utgave. FFI/RAPPORT - 2006/00260, Norwegian Defence Research Establishment, 2006.

[12] ANSI S1.11. Specification for octave-band and fractional-octave-band analog and digital filters, 2004.

[13] R. A. Sack and M. West. A parabolic equation for sound propagation in two dimensions over any smooth terrain profile: The Generalised Terrain Parabolic Equation [GT-PE. *Applied Acoustics*, 45:113–129, 1995.

[14] N. A. Kampanis, D. A. Mitsoudis, and M. C. Dracopoulos. Benchmarking two simulation models for underwater and atmospheric sound propagation. *Environmental Modelling & Software*, 22:308–314, 2007.

[15] E. M. Salomons. *Computational Atmospheric Acoustics*. Kluwer academic publishers, 2001.

[16] M.E. Delany and E.N. Bazley. Acoustical properties of fibrous absorbent materials. *Applied Acoustics*, 3:105–116, 1970.

[17] G. Taraldsen. The Delany-Bazley impedance model and Darcy's Law. *Acta Acustica united with Acustica*, 91:41–50, 2005.

[18] Xiao Di and Kenneth E. Gilbert. An exact Laplace transform formulation for a point source above a ground surface. *J. Acoust. Soc. Am.*, 93(2):714–720, 1993.

[19] B. L. Madsen, J. Andersen, and E. A. Andersen. Dokumentasjon av beregningsprogrammet FOFTlyd version 0.4. Technical Report FOFT M-45/1997, Forsvarets Forskningstjeneste, Danmark, 1997.

[20] W. E. Baker. *Explosions in air*. Austin, University of Texas Press, first edition, 1973. ISBN 0–292–72003–3.

[21] J. W. Reed. Atmospheric attenuation of explosion waves. *J. Acoust. Soc. Am.*, 61(1):39–47, 1977.